MASTERARBEIT | MASTER'S THESIS

Titel | Title

Towards a Proposal for a Network Nonlocal and Detection-Loophole-Free Experiment in the Triangle Network

verfasst von | submitted by

Martin Kerschbaumer BSc BSc

angestrebter akademischer Grad | in partial fulfilment of the requirements for the degree of

Master of Science (MSc)

Wien | Vienna, 2025

Studienkennzahl lt. Studienblatt | Degree programme code as it appears on the student record sheet:	UA 066 876
Studienrichtung lt. Studienblatt | Degree programme as it appears on the student record sheet:	Masterstudium Physics
Betreut von | Supervisor:	Mag. Dr. Beatrix Hiesmayr Privatdoz.

Acknowledgements

I would like to express my sincere gratitude to the following institutions and individuals for their support throughout the course of my Master's Thesis:
First and foremost, I thank the University of Vienna and the Erasmus+ program for providing the funding and the opportunity to study abroad, as well as the European Union for supporting this initiative. I am also grateful to the Gesellschaft für Forschungsförderung Niederösterreich m.b.H. for their financial support during my stay abroad. Additionally, I extend my thanks to ICFO - Institute of Photonic Sciences for funding and supporting my research and for fostering such a welcoming and vibrant community.
I am deeply indebted to Prof. Dr. Antonio Acín for giving me the opportunity to work in his group at ICFO for nearly a year, for his guidance, and for enabling my participation in an international conference. The excellent working environment in his group greatly enriched my experience in research.
I also very thankful to Prof. Dr. Beatrix Hiesmayr for her continuous support and availability as well as for supervising my work throughout my studies.
Finally, I am especially grateful to Dr. Tamás Kriváchy, who, although it was formally not possible to include him as a co-supervisor, supervised my research before, during, and after my stay at ICFO, providing excellent collaboration, mentorship, and a supportive working atmosphere. Also, due to his and Prof. Acín's efforts it was possible for me to carry out my research at ICFO in Spain, for which I am truly thankful.

Abstract

This Master's thesis investigates the robustness of quantum nonlocality in the triangle network—a scenario without input choices—focusing on photonic implementations using generalized N00N states. We demonstrate that even for $N = 2$, these states exhibit high resistance to photon loss, with certified robustness up to 10.3% under realistic conditions. Additionally, we identify and address experimental challenges, not only including single- and full-photon loss, but also source imperfection and the challenge those imperfections pose for reliably generating the desired quantum state. Using heralded SPDC sources, we propose an experimental scheme that generates the desired state while avoiding global post-selection, thereby closing the detection loophole in the triangle configuration. Our results lay the groundwork for a practical realization of network nonlocality in photonic systems.

Kurzfassung

Diese Masterarbeit untersucht die Robustheit nichtlokaler Korrelationen im Triangle Network, mit Fokus auf photonische Implementierungen basierend auf verallgemeinerten N00N-Zuständen. Wir zeigen, dass bereits für $N = 2$ eine hohe Widerstandsfähigkeit gegenüber Photonenverlust erreicht wird, mit nachgewiesener Robustheit bis zu 10,3% unter realistischen Bedingungen. Neben dem Einfluss von Einzel- und Totalverlust von Photonen analysieren wir auch die Imperfektionen der Quellen und die damit verbundene Schwierigkeit einen gewünschten Quantenzustand zu erzeugen. Durch den Einsatz von SPDC-Quellen schlagen wir ein experimentelles Konzept vor, welches den gewünschten Zustand generiert, und das sogleich ohne globaler Selektion. Somit schließt sich die Detektionslücke in dieser Konfiguration. Unsere Ergebnisse ebnen den Weg für eine realistische, experimentelle Umsetzung von Nichtlokalität in photonischen Systemen.

Contents

1 Introduction

Bell's theorem[1], established in 1964, marks an important moment in quantum theory, showing that local and realistic hidden variables alone do not fully explain quantum predictions. Research on Bell's nonlocality surged over decades, driven by curiosity and advances in quantum information science. Initially focused on simple experiments like the Einstein-Podolsky-Rosen paradox[2], recent years experienced a shift towards studying Bell's nonlocality in multi-party scenarios, reflecting interconnected independent sources. This exploration, known as Bell's nonlocality in quantum networks, offers a broader understanding of nonlocality, aiding comprehension of quantum theory's relation to other physical models and facilitating quantum information processing, especially within scalable quantum networks.

In the following, we give an introduction to locality versus non-locality in the standard Bell scenario (see section 1.1) and beyond the conventional Bell framework (see section 1.2). We also briefly discuss the motivation for conducting research in this field, introduce the topology of the triangle network (see section 1.3) and discuss advancements made concerning triangle network nonlocality (see section 1.4).

1.1 The Standard Bell Scenario

For the purpose of comprehension and convenience, we consider the bipartite scenario. The parties Alice and Bob independently choose measurements x and y, obtaining outcomes a and b. The local-hidden-variable theory states that the outcomes of measurements are determined exclusively by the inputs and local hidden variables, which determine the observed correlations. This local hidden variable λ depends on some unknown probability density $p(\lambda)$. The correlations admit a local model if they can be written as

$$p(a,b|x,y) = \int d\lambda\, p(\lambda)\, p(a|x,\lambda) \cdot p(b|y,\lambda), \quad \text{with} \quad \int d\lambda p(\lambda) = 1. \tag{1.1}$$

Note that Alice's and Bob's choices of settings (x, y) are independent from the local hidden variable λ. Any correlation consistent with the no-signaling principle (stating that information cannot be transmitted faster than light) that does not admit a local model is nonlocal[3].
In general, the local scenario is described by a finite set $P = \{p(ab|xy)\}$. The set of points P that allows a decomposition of the form (1.1) corresponds to a local polytope. A polytope for a standard Bell scenario is a geometric object that is both compact and convex, characterized by having a finite number of extreme points, known as vertices.

Hereby, convex refers to a shape where any line segment connecting two points within the shape lies entirely within the shape. The polytope is bounded by a finite set of hyperplanes, also addressed as facets[4]. Those facets of a local polytope delimit the local region from the non-local one, meaning they coincide to linear inequalities

$$\sum_{ab}\sum_{xy} z_{abxy}\, p(a,b|x,y) \leq C, \tag{1.2}$$

with C arising from the maximum classical correlation between measurements and z_{abxy} is associated with specific combinations of measurement outcomes (a and b) and settings (x and y). Those inequalities are called Bell inequalities. A well-known Bell inequality is, e.g., the Clauser-Horne-Shimony-Holt (CHSH) Bell inequality[5]. In summary, the local polytope is the convex hull of these vertices, allowing the determination of nonlocal correlations by checking Bell inequalities.
In addition to a local polytope, there exists another category known as the no-signaling polytope, which ensures that no information can be transmitted between parties[4]. In summary, Bell's Theorem and subsequent experiments demonstrate that quantum theory cannot be fully explained by any local hidden variable model. This means that the entangled particles exhibit correlations that defy classical intuition about locality and realism, highlighting the fundamentally non-local nature of quantum mechanics

1.2 Expanding beyond the conventional Bell Framework - Quantum Networks

Recently the interest has grown how the effects of the "Standard Bell scenarios" change when considering Bell scenarios in quantum networks. The definition of a quantum network is as follows:

Definition 1.2.1 (Quantum Network)**.** *A quantum network in the context of Bell's nonlocality is a structured arrangement of m independent (quantum) sources that distribute entangled states or other (quantum) states to a set of n parties, referred to as nodes.*

Unlike the theory of traditional Bell tests, quantum networks generalize nonlocality by exploring scenarios with complex interconnections and dependencies, such as multipartite entanglement or nonlocality across independent sources. Also, Bell scenarios in networks come with a crucial difference: They attribute more than one source. Each source is assumed to be independent from the rest of the network. This independence is the key feature, which differentiate it from standard multipartite scenarios. Additionally, it causes a more complex structure than it is the case for the usual local polytope. Hereby, the most crucial properties of this local set in networks are[6,7]:

1. As in the Standard Bell scenario, the local set is contained in a local polytope.
2. It is **not** convex.

3. It is closed and connected by a finite number of **polynomial** inequalities.

We will not provide a proof for these statements, but rather discuss them briefly. For a proof, the reader is referred to Tavakoli et al.[3]. The first point is intuitive as it arises from loosening the constraint of source independence in equation (1.3), reflected in the structure of the local polytope

$$p(a_1, ..., a_n|x_1, ..., x_n) = \int d\lambda_1\, q(\lambda_1)... \int d\lambda_m\, q(\lambda_m)\, p(a_1|x_1, \widetilde{\lambda_1}) \cdot ... \cdot p(a_n|x_n, \widetilde{\lambda_n}). \quad (1.3)$$

Note that equation (1.3) represents the local model for a network, with m sources, n parties. $\widetilde{\lambda_i}$ denotes the collection of local variables received by the party i, with $i \in \{1, ..., n\}$. The other two properties are fundamentally different from the standard Bell scenario, but can be intuitively understood when constructing the local polytope for networks, see figure 1.1. Non-convexity can be seen when studying the local sets of networks, see figure 1.1 (right). Due to this non-convexity, the network Bell inequality is not linear, but polynomial[3].

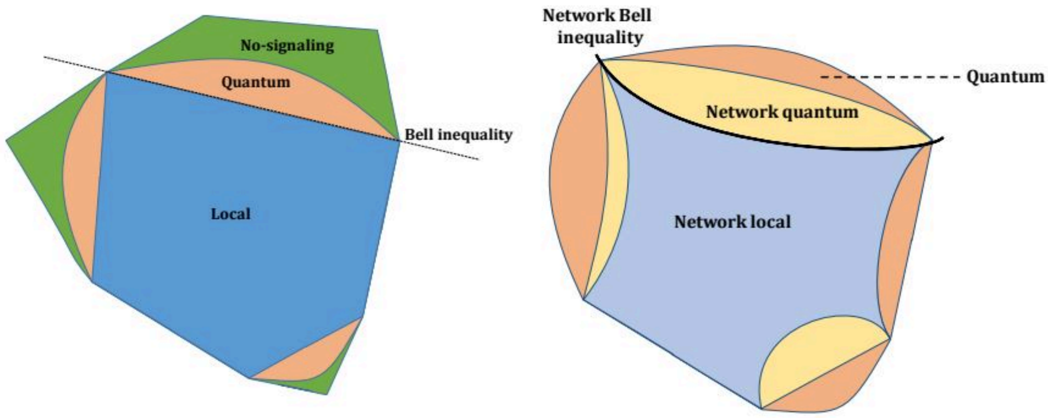

Figure 1.1: (left) An illustration depicting the local polytope, the convex quantum set of correlations, and the no-signaling polytope. Bell inequalities are represented as hyperplanes corresponding to a facet of the local polytope. (right) Network local correlations are within network quantum correlations, nested in quantum correlations without independent sources[3].

Due to these changes of properties (2. and 3.), the task of characterizing the correlations in networks is much more challenging than in the "Standard Bell scenarios". Applying the conventional framework, by using linear Bell inequalities, gives an incomplete characterization of a problem due to the second property. Violating a Bell-like inequality in a quantum network context carries two distinct interpretations: it could signify the use of non-classical resources (such as entanglement or other quantum phenomena) if

the assumed network structure is correct. Alternatively, it might indicate that the assumed network structure itself is incorrect, highlighting the need to carefully consider the underlying assumptions about the network configuration[3].
To describe network correlations by utilizing quantum models, the Born rule

$$p_Q(a_1, ..., a_n|x_1, ..., x_n) = Tr\Big[(\rho_1 \otimes ... \otimes \rho_m)(A^{(1)}_{a_1|x_1} \otimes ... \otimes A^{(n)}_{a_n|x_n})\Big] \tag{1.4}$$

is used. Due to the independence of each source, one can associate to each source an independent, (perhaps even entangled) quantum state $\rho_i, i \in \{1, ..., m\}$. Each of the parties performs a measurement $A^{(j)}_{a_j|x_j}, j \in \{1, ..., n\}$, depending on the connection to their respective sources. Note that the network quantum set is, as the network local set, non-convex and closed[3].
Exploring Bell's nonlocality in networks bridges foundational quantum theory and practical quantum information science. On a fundamental level, it deepens our understanding of quantum mechanics by extending Bell's theorem to more complex scenarios. Practically, it holds promise for advancing information processing through scalable quantum networks and the development of a quantum internet. Theoretical interest is complemented by experimental efforts to tackle the unique challenges of networked nonlocality, offering new avenues for both scientific inquiry and technological innovation[3].

1.3 The Topology of the Triangle Network

In this section, we provide an overview of the fundamental aspects and topology of the triangle network. A more detailed mathematical formulation will follow in chapter 2.

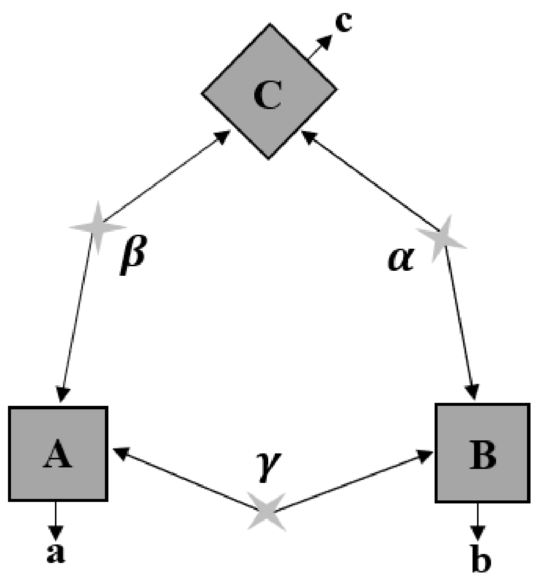

Figure 1.2: Topology of the triangle network, with three parties A, B and C and three sources α, β and γ

The triangle network, a minimal yet powerful model, serves as a foundational framework for exploring quantum correlations in complex quantum networks. This network comprises three nodes or "parties" — typically labeled A, B, and C, often addressed as Alice, Bob and Charlie — interconnected by three independent sources. Each source transmits a bipartite state shared between two parties. Specifically, source α connects B and C, source β links A and C, and source γ links A and B. Unlike traditional Bell setups, the triangle network functions without external inputs for each party, making it distinct and inherently challenging[3].

In studying triangle networks without input, the notion of Bell's locality is mathematically the same as in equation (1.3), but only $m = n = 3$. A distribution $p(a, b, c)$ in the triangle network is thus *local* if it can be expressed in a form reflecting classical causal constraints:

$$p(a,b,c) = \int d\alpha d\beta d\gamma \; p_A(a|\beta\gamma)\, p_B(b|\gamma\alpha)\, p_C(c|\alpha\beta)\, p_\alpha(\alpha)\, p_\beta(\beta)\, p_\gamma(\gamma), \tag{1.5}$$

where the variables α, β, and γ represent hidden classical states distributed by each source $p_i, i \in \{\alpha, \beta, \gamma\}$, and each party's response function $p_X, X \in \{A, B, C\}$ depends only on its locally received information. In contrast, *nonlocality* is observed when a distribution $p(a, b, c)$ cannot be decomposed into such a form. Quantum mechanics allows for such nonlocal correlations, which can be modeled by replacing classical distributions with quantum states ρ_α, ρ_β, and ρ_γ, and response functions with measurements in the form of Positive Operator-Valued Measures (POVMs). For a quantum model, the probability distribution is given by:

$$p_Q(a,b,c) = \mathrm{Tr}\left(\rho_\alpha \otimes \rho_\beta \otimes \rho_\gamma \cdot \Pi_A^{(a)} \otimes \Pi_B^{(b)} \otimes \Pi_C^{(c)}\right), \tag{1.6}$$

where $\Pi_X^{(x)}$ denotes the measurement operator for the outcome x at party $X \in \{A, B, C\}$ with the properties $\sum_x \Pi_X^{(x)} = \mathbb{I}_{\mathbb{X}}$ and $\Pi_X^{(x)} \geq 0, \forall x$. In equation (1.6), we slightly simplify the notation by omitting explicit references to the distinct Hilbert spaces where the operators act, as these are evident from figure 1.2[3].

Throughout this thesis, we explore network nonlocality not by constructing polynomial Bell inequalities, but by using an alternative approach namely through logical contradictions. This concept is examined in depth in the following chapter.

1.4 Progress Toward Noise-Robust and Experimentally Implementable Triangle Network Nonlocality

In recent years, significant progress has been made in the field of nonlocality within the triangle network. Nine key milestones in this development are illustrated in figure 1.3 below.

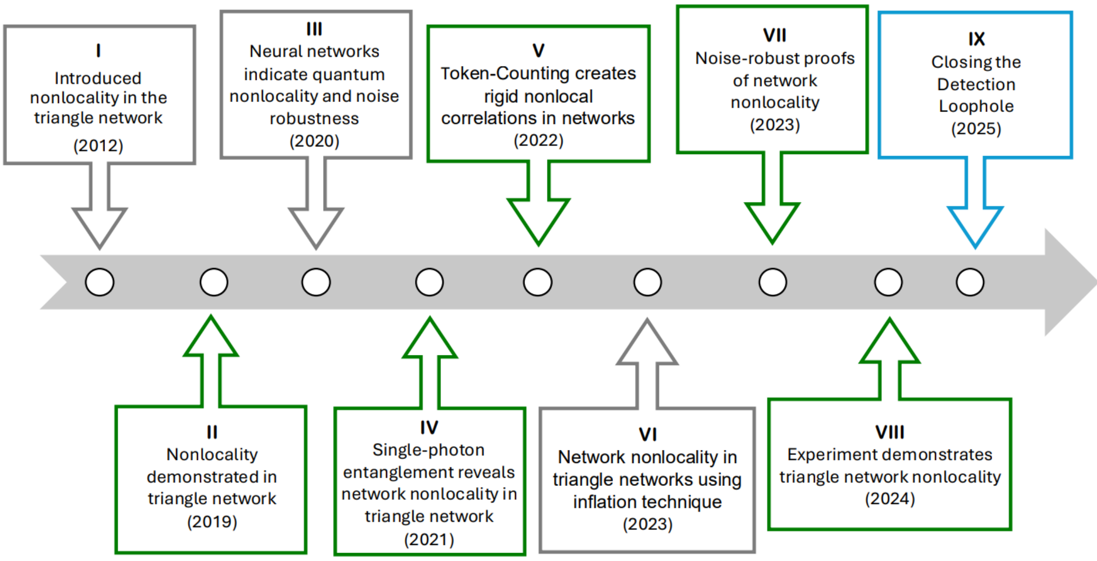

Figure 1.3: Advancements in Triangle Network Nonlocality

Our timeline represents the milestones by boxes of different colors. The green colored boxes highlight crucial contributions, each of which will be discussed in detail in dedicated sections later in the next chapter. However, the three uncolored boxes, which also represent foundational developments, will be briefly addressed here to provide a complete overview, but will not be discussed in detail later. This approach ensures that the reader gains the necessary background while avoiding unnecessary repetition. By following this structure, we aim to establish a clear narrative that ties together the theoretical and experimental advancements in the field, setting the stage for a deeper exploration of the concepts and methodologies that define this area of research. The blue colored box represents our contribution.

1.4.1 Range of Nonlocality

Over the past 15 years, the concept of *Network Nonlocality* has garnered significant attention. In the publication by Branciard et al.[6], one of the earliest uses of network configurations was presented to demonstrate entanglement swapping. In the work by Fritz[7], the author expanded on this work by exploring scenarios involving multiple sources but no measurement choices, with a focus on identifying quantum nonlocality and posing several open questions. In particular, he investigated the triangle scenario, emphasizing its symmetry, monogamy properties, classical correlation constraints, and the presence of non-classical quantum correlations (see figure 1.3, Box I).
A significant advancement in the understanding of non-local correlations has been made in 2019 by Renou et al.[8], who demonstrated quantum nonlocality with entangled sources and measurements in the triangle network using joint statistics of local measurements. Two of the measurement projectors in their study are defined by the parameter $u^2 \in [0, 1]$,

which represents the degree of entanglement in the measurement basis. For balanced quantum states, they proved the presence of nonlocal correlations for $u^2 \in (0, 0.21551)$ and $u^2 \in (0.78499, 1)$, using logical contradictions rather than Bell inequalities. The results will be thoroughly discussed in section 2.2 (see figure 1.3, Box II).
In 2023, the study of Pozas-Kerstjens et al.[9] extends the investigation of nonlocality in quantum networks, proving that certain quantum triangle distributions do not admit triangle-local models beyond the range initially established. By reducing the distributions to binary outcomes and applying the inflation technique[10], the authors additionally demonstrate network nonlocality for $u^2 \in (0.56250, 0.65626)$ using balanced Bell states, while also creating a set of network Bell inequalities for the triangle scenario that are of broader interest (see figure 1.3, Box VI).
The main result of those two publications is shown in figure 1.4.

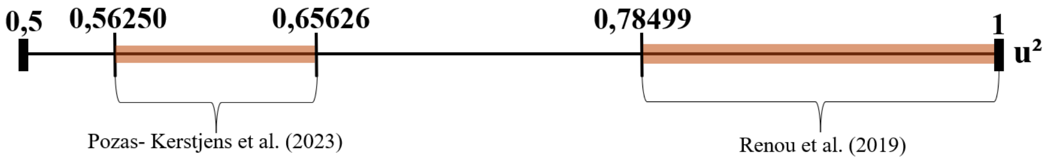

Figure 1.4: Range of Nonlocality of the RGB4 distribution for balanced quantum states

Note that the range of nonlocality is symmetric around 0.5, thus only the interval $[0.5, 1]$ in figure 1.4 is shown.
Lastly, it is important to note that both studies utilized the RGB4-distribution, which was introduced by Renou et al.[8]. This specific distribution is a token-counting (TC) distribution[11], meaning that a fixed number of tokens are distributed by the sources (see figure 1.3, Box V). We will also discuss this type of distributions in detail later in section 2.1.

1.4.2 Indicating Network Nonlocality

A powerful method for studying network nonlocality, developed by Kriváchy et al.[12], involves training neural networks to replicate observed probability distributions. The key idea is that if a distribution can be accurately learned by the network, it is likely classical. The approach works by minimizing the Euclidean distance between the network's predicted distribution and the actual observed distribution. A larger Euclidean distance suggests that the distribution cannot be reproduced by classical means, indicating the presence of quantum nonlocality. In other words, when the neural network struggles to approximate the distribution (i.e., when the Euclidean distance is large), it points to the likelihood of quantum nonlocal correlations.
The researchers applied this technique to several examples within the triangle network configuration, providing strong evidence that certain distributions exhibit nonlocal correlations. There, they also explored the previously mentioned RGB4-distribution proposed by Renou et al.[8], using the neural network approach to further conjecture nonlocality.

The study also offers estimates on the noise robustness, shedding light on the resilience of quantum correlations in the presence of noise (see figure 1.3, Box III). In figure 1.5, the conjectured nonlocality of the RGB4 distribution in the noiseless case is illustrated, predicting nonlocality throughout almost the entire interval $u^2 \in (0.5, 1)$.

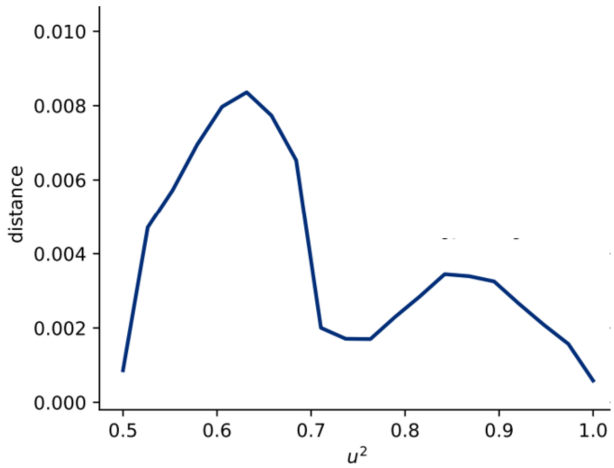

Figure 1.5: Indication of network nonlocality for the RGB4-distribution [12].

1.4.3 Advancing to Experimental Realizations

We now shift the focus to its experimental realization. In 2021, Abiuso, Kriváchy et al. published an interpretation of the RGB4 distribution [8], introducing spatially entangled photons and providing a theoretical blueprint for an experimental setup to eventually prove nonlocality with [13]. This proposed setup relies exclusively on passive optical elements.
Nonlocality with passive tools, such as beamsplitters and photodetectors, is often regarded as unattainable since these elements fail to preserve the quantum uncertainty essential for nonlocal behavior. Passive measurements reveal whether a photon reached a given party, collapsing the quantum superposition into classical-like certainty. Active techniques, e.g. adding local photons, are conventionally deemed necessary to probe entanglement and demonstrate nonlocality.
This work challenges that notion, showing that nonlocality can indeed be revealed using only passive measurements. Furthermore, it addresses crucial aspects of experimental feasibility, including the handling of noise—such as photon loss, as well as source and detector inefficiency. Numerical evidence presented by the authors highlights the setup's robustness to noise sources (see figure 1.3, Box IV).
While numerical evidence for noise-robust nonlocality in the triangle network exists, an analytical proof remains elusive. In 2023, Boreiri, Ulu et al. made significant progress toward this goal [14]. They introduced a novel approach, here referred to as the Party Token-Counting (PTC) method, which provides an analytical proof of noise robustness for a more generalized version of the RGB4 distribution, tolerating up to 0.48% loss.

This method represents a crucial step in understanding the analytical foundations of noise-robust nonlocality. A detailed discussion of the PTC method and its implications will be presented in a later section of this chapter (see figure 1.3, Box VII).
Experimental realizations of network nonlocality without inputs remain limited, but in 2024 Wang et al.[15] successfully demonstrated genuine quantum nonlocality in the triangle network. Instead of utilizing a TC distribution, their work employed the Elegant distribution[16] with an experimental setup consisting exclusively of entangled photon sources and Elegant Joint Measurements (EJM). Nonlocality was confirmed through inequality violations and neural network analysis, establishing that the observed distribution lies outside the local set. However, the approach introduces loopholes as it presents reliance on global postprocessing of outcomes and data renormalization (see figure 1.3, Box VIII). We also address this problem in a later section.

1.4.4 Closing the Detection Loophole in the Triangle Network

This Master's thesis was prepared simultaneously with the publication by Krivachy et al. (2025), *Closing the Detection Loophole in the Triangle Network with High-Dimensional Photonic States*[17]. As such, the majority of the results presented here align with those in the referenced publication, with deviations occurring only in section 4.1. In this section, we present a distinct proof, as the paper provides a generalization and adopts a different approach.
In this work, we investigate triangle network nonlocality across both the single-photon and multi-photon regimes by constructing a local hidden variable model for generalized NOON states. We demonstrate nonlocality for $N = 2$ photons, showing an expansion of the nonlocality range within the interval $u^2 \in (0.761, 0.785]$ for balanced quantum states. Furthermore, we examine the dominant noise source in the transmission channels—single-photon loss—and achieve robustness up to 10.3%. Although our initial approach to addressing full photon loss was unsuccessful. A second approach appears promising, as it yields results; however, these results are incorrect.
Additionally, we explore the detection loophole in relation to state generation and photon loss in transmission channels. We successfully resolve the state generation issue and provide a generalization for a J-party ring network. Moreover, we propose an experimental setup for generating spatially entangled quantum states via heralded SPDC-based entanglement. This approach eliminates the need for global post-processing by utilizing failure bits to certify unsuccessful photon generation, thus ensuring the validity of nonlocality proofs even in the presence of photon loss.
Ultimately, our goal is to propose a detection loophole-free and feasible experimental implementation of network nonlocality in the triangle network.

2 Methodological Approaches for analyzing Triangle Networks

This chapter provides a comprehensive and detailed exploration of the fundamental concepts and developments essential for understanding the discussions in the subsequent chapters. To establish a clear framework, we orient ourselves based on the previously introduced timeline, beginning with the concept of a token-counting distribution. We then outline the methodological approach used in this thesis to demonstrate triangle network nonlocality. Subsequently, we introduce the concept of a passive optical setup that preserves nonlocality within the triangle network. Finally, we address realistic experimental conditions, such as photon loss and the detection loophole, along with the associated challenges they present.

2.1 Token Counting Distributions

This section solely focuses on main aspects of the token-counting (TC) approach as presented in the publication *Network Nonlocality via Rigidity of Token-Counting and Color-Matching*[11]. Emphasis is placed on the TC method's role in generating nonlocal correlations across network structures.

2.1.1 Mathematical Framework for Network Subspaces

A network N is constructed of I sources $S_1, \ldots, S_I$ and J parties $A_1, \ldots, A_J$, where each source connects to a certain number of parties, further denoted as $S_i \to A_j$. Without inputs, each party measures the received subsystems, yielding a joint output distribution $P = \{P(a_1, \ldots, a_J)\}$.

In the context of a network N, the focus lies on the set of probability distributions generated when sources transmit either classical or quantum signals to the parties involved. To provide greater clarity and precision for the subsequent definitions and theorems, the classical and quantum strategies are presented with more detailed mathematical formulation.

In a classical strategy, each source S_i sends classical information by selecting a value $s_i \in S_i$ with probability $p(s_i)$. Each party A_j then receives values $\{s_i : S_i \to A_j\}$ from connected sources and provides an output a_j based on a probabilistic function $p(a_j|\{s_i : S_i \to A_j\})$. The joint distribution of outputs is expressed as

$$p_C(a_1, \ldots, a_J) = \sum_{s_1,\ldots,s_I} \prod_i p(s_i) \cdot \prod_j p(a_j|\{s_i : S_i \to A_j\}).$$

In a quantum strategy, sources distribute quantum states, with parties performing projective measurements. Here, each source S_i distributes a quantum state $|\psi_i\rangle$ in the Hilbert space $H_i = \bigotimes_{j:i\to j} H_{i,j}$, where $H_{i,j}$ contains the part sent to party A_j by S_i. The arrows represent the flow of quantum information between the different parties, each associated with its own Hilbert space. Thus, each party A_j performs a projective measurement $\{\Pi_{a_j} : a_j\}$ on the Hilbert space $H_j = \bigotimes_{i:i\to j} H_{i,j}$. The resulting joint distribution of outputs is given by

$$p_Q(a_1, \ldots, a_J) = \mathrm{Tr}\left(\bigotimes_i |\psi_i\rangle\langle\psi_i| \cdot \bigotimes_j \Pi_{a_j}\right).$$

2.1.2 Concept of Token-Counting Strategies

The concept involves each source S_i distributing η_i tokens to its connected parties. Each party A_j counts the number of tokens received and may additionally measure other degrees of freedom.

Definition 2.1.1 (TC Strategy)**.** *A strategy in network N is termed TC if: (i) Each source S_i distributes a fixed number of tokens η_i to connected parties, possibly along with additional information. (ii) Each party A_j counts the total tokens n_j received and outputs $a_j = (n_j, \alpha_j)$, where α_j represents any additional information. The resulting distribution is referred to as a TC distribution $P = \{P((n_1, \alpha_1), \ldots, (n_J, \alpha_J))\}$.*

Note that not accounting for α_j, leaves the token-count marginal distribution P_{token}. Such a TC distribution can always be classically simulated by a TC strategy. Not accounting additional information α_j, can be understood as coarse-graining outcomes.
Additionally to the definition above, we define the notion of a No-Double-Common-Source network.

Definition 2.1.2 (No Double Common-Source (NDCS) Networks)**.** *A network N is called a NDCS network if each pair of parties do not share more than one common source.*

This essentially means that there do not exist distinct sources $S_i \neq S_{i'}$ such that $S_i \to A_j, A_{j'}$ and $S_{i'} \to A_j, A_{j'}$.

2.1.3 Rigidity of Token-Counting Strategies

When speaking of rigidity, we hereby refer to the ability to demonstrate that certain distributions can only be explained by one unique local hidden variable model. In the following, we will discuss the rigidity of TC strategies.

Theorem 2.1.3 (Token Counting)**.** *Let N be a NDCS network consisting of J parties and I sources. Consider a strategy where source S_i distributes η_i tokens, leading to the corresponding TC distribution $P = \{P((n_1, \alpha_1), \ldots, (n_J, \alpha_J))\}$.*
For any possible token distribution t_i^j with the condition that $\sum_{j:S_i \to A_j} t_i^j = \eta_i$, define the probability $q_i(t_i^j)$ that the source S_i distributes $\{t_i^j\}_{j:S_i \to A_j}$ tokens to the connected parties $\{A_j\}_{j:S_i \to A_j}$.
When considering another strategy that simulates $P = \{P((n_1, \alpha_1), \ldots, (n_J, \alpha_J))\}$ on N, this strategy will also be a TC strategy with the same distribution of tokens. Essentially, for any strategy that simulates P, there exist functions $T_i^j : S_i \to \mathbb{Z}_{\geq 0}$ for all $S_i \to A_j$ satisfying the following conditions:
1.

$$\sum_{j:S_i \to A_j} T_i^j(s_i) = \eta_i, \tag{2.1}$$

2.

$$\sum_{i:S_i \to A_j} T_i^j(s_i) = n_j. \tag{2.2}$$

3. For any source S_i and any t_i^j satisfying $\sum_{j:S_i \to A_j} t_i^j = \eta_i$, the following holds:

$$\Pr_{s_i}[T_i^j(s_i) = t_i^j] = q_i(t_i^j) \tag{2.3}$$

The theorem argues that any strategy simulating a TC distribution must itself be TC. This means that there exist functions T_j^i that determine the token allocation, satisfying three conditions: Firstly, the total number of tokens distributed, equals η_i. The second condition establishes that the total number of tokens received by party A_j from the connected sources is equal to n_j. The third condition relates to the probability that source S_i distributes a specific token configuration t_i^j while maintaining the total token allocation η_i. It implies that for any token distribution satisfying this condition, the likelihood of achieving that distribution must align with the probability $q_i(t_i^j)$. This condition ensures consistency in the probabilistic framework governing the simulation of the token distributions across the network.
Additionally, we need to emphasis that the total number of tokens is fixed, such that

$$\sum_j n_j = \sum_i \eta_i, \text{ if } P_{token} > 0.$$

For a triangle network distribution $p(a, b, c)$, this implies that $a + b + c$ is constant.
For a comprehensive understanding of the proof, readers are encouraged to study the publication on TC strategy for detailed insights[11].
Specific TC distributions will not be addressed in this section, as they will be covered later.

2.2 Network Nonlocality by logical Contradictions (RGB4-Method)

This section examines network nonlocality using logical contradictions (RGB4-method) introduced in *Genuine Quantum Nonlocality in the Triangle Network*[8] by Renou et al. Named after the initials of its authors, the RGB4 method demonstrates a novel form of quantum nonlocality in input-free networks, exemplified in the triangle network using entangled states and joint entangled measurements. The resulting quantum distribution is classified as TC distribution.

A key challenge in analyzing the triangle network is characterizing the set of distributions $p(a,b,c)$ that arise from independent sources. This independence results in a non-convex set, making traditional tools such as linear Bell inequalities ineffective. To overcome this, the authors employ a logical contradiction approach. They construct a family of quantum distributions $p_Q(a,b,c)$ and prove that no local hidden variable model, can reproduce these distributions. This is achieved by identifying a set of conditions required for any local model and demonstrating that these conditions cannot be satisfied simultaneously. We will discuss the derivations in the following sections.

Also, while the approach of investigating network nonlocality through non-linear Bell inequalities has certain limitations, it has been employed in several studies, e.g. by Bibak et al.[18].

2.2.1 RGB4-Distribution

The first step in order to prove nonlocality, is to construct the distribution $p_Q(a,b,c)$. Each party, Alice, Bob and Charlie share a two-qubit pure entangled state

$$|\psi\rangle = s\,|01\rangle + r\,|10\rangle\,, \tag{2.4}$$

where $s, r \in \mathbb{R}$ and $s^2 + r^2 = 1$. Additionally, each party A, B and C perform a projective measurement. The basis is given by

$$\begin{aligned}
|2\rangle &= |11\rangle\,, \quad |\chi_0\rangle = u_0\,|01\rangle + v_0\,|10\rangle\,,\\
|0\rangle &= |00\rangle\,, \quad |\chi_1\rangle = u_1\,|01\rangle - v_1\,|10\rangle\,,
\end{aligned} \tag{2.5}$$

with $u \equiv u_0 = -v_1, v \equiv u_1 = v_0$, $u, v \in \mathbb{R}$ and $u^2 + v^2 = 1$. The projective measurement is labeled by $|\phi_i\rangle$ for $\phi_i = \{2, 0, \chi_0, \chi_1\}$, $i \in \{a, b, c\}$. The statistic is given by

$$p_Q(a,b,c) = |\,\langle \phi_a \phi_b \phi_c | \Psi\rangle\,|^2. \tag{2.6}$$

$|\Psi\rangle$ is the global state shared by the parties and is given by

$$\begin{aligned}
|\Psi\rangle &= s^3\,|101010\rangle + r^3\,|010101\rangle + s^2 r(|101100\rangle + |001011\rangle + |110010\rangle) + sr^2(|110100\rangle\\
&+|010011\rangle + |001101\rangle) = s^3(u\,|\chi_0\rangle + v\,|\chi_1\rangle)^{\otimes 3} + r^3(v\,|\chi_0\rangle - u\,|\chi_1\rangle)^{\otimes 3} + s^2 r\,(u(|02\chi_0\rangle + |2\chi_0 0\rangle\\
&+|\chi_0 02\rangle) + v(|02\chi_1\rangle + |2\chi_1 0\rangle + |\chi_1 02\rangle)) + sr^2\,(v(|02\chi_0\rangle + |2\chi_0 0\rangle + |\chi_0 02\rangle) - u(|02\chi_1\rangle + |2\chi_1 0\rangle + |\chi_1 02\rangle))\,.
\end{aligned}$$

Note that the state $|\Psi\rangle$ is permuted, as the last qubit is permuted to the first. Applying equation (2.6) to certain projective measurements $\{|\phi_i\rangle\}$, properties of $p_Q(a,b,c)$ are obtained, such as

$$p_Q(2,2,c) = p_Q(0,0,c) = 0, \, \forall c \tag{2.7}$$

$$p_Q(0,2,c) = p_Q(a,0,2) = s^4 r^2, \, p_Q(0,b,2) = s^2 r^4. \tag{2.8}$$

By permuting the parties, the results stay equivalent. Other crucial properties of $P_Q(a,b,c)$ are

$$p_Q(\chi_i, 2, 0) = s^4 r^2 u_i^2, \, p_Q(\chi_i, 0, 2) = s^2 r^4 v_i^2 \tag{2.9}$$

$$p_Q(\chi_i, \chi_j, \chi_k) = (s^3 u_i u_j u_k + r^3 v_i v_j v_k)^2. \tag{2.10}$$

2.2.2 Theorem of RGB4

Utilizing the quantum distributions $p_Q(a,b,c)$, the theorem regarding the proof of non-locality can be formulated.

Theorem 2.2.1 (RGB4)**.** *The quantum distribution $p_Q(a,b,c)$ cannot be reproduced by any local model whenever $u^2_{max}(s) < u^2 < 1$, where $u_{max}(s)$ is defined by the following constraint*

$$3(s^3u^2v - r^3uv^2)^2 - 3u^2(s^6 + r^6) + 2(s^6 + (s^3u^3 + r^3v^3)^2) + s^6 + (s^3v^3 - r^3u^3)^2 \geq 0.$$

For the following proof of theorem 2.2.1, we start by stating a lemma about the fact that coarse graining $(\{2, 0, \chi = \{\chi_0, \chi_1\}\})$ determines the outputs based on local variable subsets. Using this approach, another distribution q is defined, which is related to p_Q. From this, marginals are derived to analytically establish a bound for $u_{\max}$; values above this are deemed incompatible with the local model and are classified as nonlocal.

Lemma 1 (Coarse Graining Local Variable Outputs)**.** *The source sets can be partitioned into two subsets $X = X_0 \coprod X_1$, $Y = Y_0 \coprod Y_1$, $Z = Z_0 \coprod Z_1$ with $p(X_0) = p(Y_0) = p(Z_0) = s^2$ and $p(X_1) = p(Y_1) = p(Z_1) = r^2$. The local variables α, β, γ determine the outputs.*

$$\begin{aligned} p(a=0, b=2) &= p(X_0)p(Y_0)p(Z_1), \\ p(c=2, a=0) &= p(X_1)p(Y_0)p(Z_1), \\ p(b=0, c=2) &= p(X_1)p(Y_0)p(Z_0). \end{aligned} \tag{2.11}$$

Since a similar idea will be explored in the next section, only a sketch of the proof is provided here.

Proof. *(Sketch)* The approach involves defining specific sets, namely X_0, X'_0, X_1, X'_1, along with analogous sets for Y and Z, where each set corresponds to particular outcomes (0 or 2) associated with the variables α, β, and γ. By using equations (2.7),(2.8), (2.9) and (2.10), in conjunction with logical contradictions, we are able to assign particular outcomes to the relevant sets. Specifically, the following conditions hold:

$$\begin{aligned}
a(\beta,\gamma) &= 0 \quad \text{if and only if} \quad \beta \in Y_0 = Y'_0, \gamma \in Z_1 = Z'_1,\\
a(\beta,\gamma) &= 2 \quad \text{if and only if} \quad \beta \in Y_1 = Y'_1, \gamma \in Z_0 = Z'_0,\\
b(\gamma,\alpha) &= 0 \quad \text{if and only if} \quad \gamma \in Z_0 = Z'_0, \alpha \in X_1 = X'_1,\\
b(\gamma,\alpha) &= 2 \quad \text{if and only if} \quad \gamma \in Z_1 = Z'_1, \alpha \in X_0 = X'_0,\\
c(\alpha,\beta) &= 0 \quad \text{if and only if} \quad \alpha \in X_0 = X'_0, \beta \in Y_1 = Y'_1,\\
c(\alpha,\beta) &= 2 \quad \text{if and only if} \quad \alpha \in X_1 = X'_1, \beta \in Y_0 = Y'_0.
\end{aligned}$$

From these relationships, we can directly deduce the equations (2.11). □

Figure 2.1 illustrates an example of how the parties' outputs are determined given the defined sets.

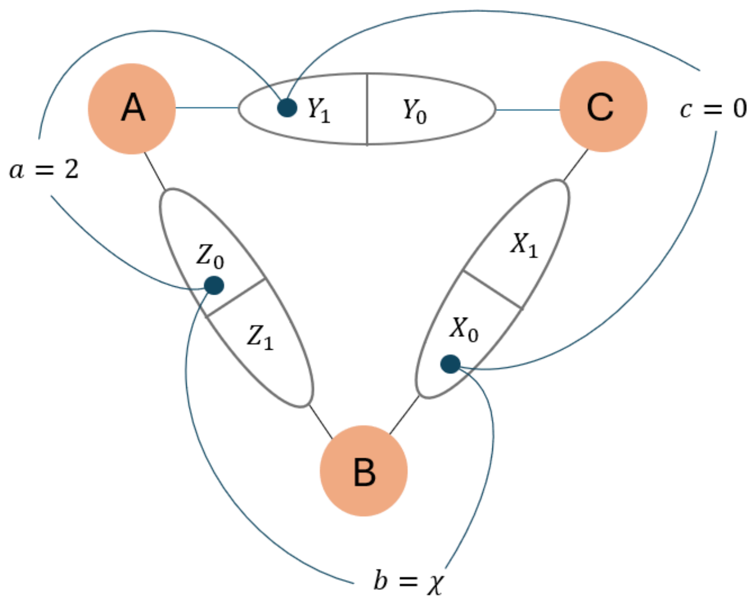

Figure 2.1: For each source, the classical variable set is divided into two equal-weight, disjoint subsets, where the subsets encode all output information based on the coarse-grained distribution $\chi = \{\chi_0, \chi_1\}$, grouping two outputs, with outputs $a = 2$ for Alice, $b = \chi$ for Bob, and $c = 0$ for Charlie, maintaining an important ordering.

Note that when fine-graining χ, it could be that these sets are not enough to describe the whole distribution, leading to a nonlocal model. As discussed in the section 2.1, this fine-graining provides the additional information required to reveal potential nonlocality. Armed with the lemma 1, we now prove theorem 2.2.1.

Proof. (*RGB4*) We start by introducing a new distribution

$$q(i,j,k,\mathrm{o}) :=$$

$$p(a=\chi_i,\, b=\chi_j,\, c=\chi_k,\, \zeta\in X_\mathrm{O}\times Y_\mathrm{O}\times Z_\mathrm{O}\,|\,\zeta\in(X_0\times Y_0\times Z_0)\cup(X_1\times Y_1\times Z_1)),$$

with $\zeta=(\alpha,\beta,\gamma)$. The distribution $q(i,j,k,\mathrm{o})$ represents a probability distribution in which all parties must output χ, with i,j,k specifying whether χ_0 or χ_1 is the outcome. Note that we constraint q to be normalized and semi-positive.
According to Lemma 1, the outcome (χ,χ,χ) is possible if and only if neither $\beta\in Y_0,\gamma\in Z_1$ nor $\beta\in Y_1,\gamma\in Z_0$ apply for the output a, and equivalent for b and c. Consequently, the only valid sets for the outcome (χ,χ,χ) are $X_0\times Y_0\times Z_0$ or $X_1\times Y_1\times Z_1$.
From here we can derive marginal distributions of $q(i,j,k,\mathrm{o})$. First, we simplify the expression for q. To achieve this, we utilize the concept of conditional probability along with the fact that $p(X_0)=p(Y_0)=p(Z_0)=s^2$ and $p(X_1)=p(Y_1)=p(Z_1)=r^2$. Consequently, we obtain

$$q(i,j,k,\mathrm{o})=\frac{1}{s^6+r^6}\cdot p(a=\chi_i,\, b=\chi_j,\, c=\chi_k,\, \zeta\in X_\mathrm{O}\times Y_\mathrm{O}\times Z_\mathrm{O}). \tag{2.12}$$

When summing over o, we use (2.10) to attain

$$q(i,j,k)=\sum_\mathrm{o} q(i,j,k,\mathrm{o})=\frac{1}{s^6+r^6}\cdot p(a=\chi_i,\, b=\chi_j,\, c=\chi_k)=\frac{(s^3u_iu_ju_k+r^3v_iv_jv_k)^2}{s^6+r^6}. \tag{2.13}$$

When summing alternately over i, j, and k, we get

$$\begin{aligned}
q(i,\mathrm{o}=0)&=\frac{s^6}{s^6+r^6}\cdot u_i^2, & q(i,\mathrm{o}=1)&=\frac{r^6}{s^6+r^6}\cdot v_i^2,\\
q(j,\mathrm{o}=0)&=\frac{s^6}{s^6+r^6}\cdot u_j^2, & q(j,\mathrm{o}=1)&=\frac{r^6}{s^6+r^6}\cdot v_j^2,\\
q(k,\mathrm{o}=0)&=\frac{s^6}{s^6+r^6}\cdot u_k^2, & q(k,\mathrm{o}=1)&=\frac{r^6}{s^6+r^6}\cdot v_k^2.
\end{aligned} \tag{2.14}$$

We can derive these marginals directly from equation (2.12). We also use the fact that Alice's answer is independent of the value α and similar for Bob and Charlie.

$$\begin{aligned}
q(i,\mathrm{o}=0)&=\frac{1}{s^6+r^6}p\left(a=\chi_i,\zeta\in(X_0,Y_0,Z_0)\right)\\
&=\frac{1}{s^6+r^6}\frac{P(X_0)}{P(X_1)}p\left(a=\chi_i,\zeta\in(X_1,Y_0,Z_0)\right)=\frac{s^6}{s^6+r^6}\cdot u_i^2
\end{aligned} \tag{2.15}$$

In the last step we use equation (2.9) as well as Lemma 1, since for (X_1,Y_0,Z_0) we get $b=0$ and $c=2$. We compute the other five marginals in a similar way.

It is important to note that for any local distribution, there must exist a q that satisfies the constraints in (2.13) and (2.14). This set of linear constraints can be solved via a linear program (LP). However, it can also be solved analytically, as we demonstrate below. We now introduce a new probability distribution $\tilde{q}$, in order to achieve symmetrization of q over i, j, k,

$$\tilde{q} = \frac{1}{6}\big(q(i,j,k,\mathrm{o})+q(j,k,i,\mathrm{o})+q(k,i,j,\mathrm{o})+q(i,k,j,\mathrm{o})+q(k,j,i,\mathrm{o})+q(j,i,k,\mathrm{o})\big). \tag{2.16}$$

$\tilde{q}$ satisfies the same constraints as q. We then define a new variable

$$\xi_{ijk} := \tilde{q}(i,j,k,\mathrm{o}=0) - \tilde{q}(i,j,k,\mathrm{o}=1).$$

in order to relate ξ with the derived constraints. We can write

$$\tilde{q}(i,j,k,\mathrm{o}=0) = \frac{1}{2}\left(\tilde{q}(i,j,k)+\xi_{ijk}\right), \quad \tilde{q}(i,j,k,\mathrm{o}=1) = \frac{1}{2}\left(\tilde{q}(i,j,k)-\xi_{ijk}\right).$$

Due to the symmetry, we define $\xi_0 := \xi_{000},\ \xi_1 := \xi_{100} = \xi_{010} = \xi_{001},\ \xi_2 := \xi_{110} = \xi_{101} = \xi_{011},\ \xi_3 := \xi_{111}$. Considering equation (2.13), we can write the marginals

$$\sum_{i,j}\tilde{q}(i,j,k,\mathrm{o}=0) = \tilde{q}(k,\mathrm{o}=0) = \frac{1}{2}\sum_{i,j}\left(\frac{\left(s^3u_iu_ju_k + r^3v_iv_jv_k\right)^2}{s^6+r^6} + \xi_{ijk}\right),$$

$$\sum_{i,j}\tilde{q}(i,j,k,\mathrm{o}=1) = \tilde{q}(k,\mathrm{o}=1) = \frac{1}{2}\sum_{i,j}\left(\frac{\left(s^3u_iu_ju_k + r^3v_iv_jv_k\right)^2}{s^6+r^6} - \xi_{ijk}\right).$$

We calculated

$$\sum_{i,j}\left(s^3u_iu_ju_k + r^3v_iv_jv_k\right)^2 = \sum_{i,j}(s^3u_iu_ju_k)^2 + \sum_{i,j}(r^3v_iv_jv_k)^2 + \sum_{i,j}2\cdot s^3r^3u_iu_ju_kv_iv_jv_k.$$

Recall section 2.3.1, in which we introduced $u_0 = -v_1 = u, v_0 = u_1 = v$, thus obtaining $\sum_{i,j}u_i^2u_j^2 = \sum_{i,j}v_i^2v_j^2 = 1$ and $\sum_{i,j}u_iu_jv_iv_j = 0$. Therefore, we write

$$\tilde{q}(k,\mathrm{o}=0) = \frac{1}{2}\left(\frac{s^6u_k^2+r^6v_k^2}{s^6+r^6} + \sum_{i,j}\xi_{ijk}\right),$$

$$\tilde{q}(k,\mathrm{o}=1) = \frac{1}{2}\left(\frac{\left(s^6u_k^2+r^6v_k^2\right)}{s^6+r^6} - \sum_{i,j}\xi_{ijk}\right).$$

Now, we choose values for k such that the following equations $\sum_{i,j}\xi_{ijk} = \xi_0+2\xi_1+\xi_2$ and $\sum_{i,j}\xi_{ij1} = \xi_1+2\xi_2+\xi_3$. hold. Using the given marginals of $\tilde{q}(k,\mathrm{o}=0)$ and $\tilde{q}(k,\mathrm{o}=1)$ from above (see equations (2.14)), we then deduce the corresponding relationships.

$$\xi_0 = \frac{s^6u^2-r^6v^2}{s^6+r^6} - 2\xi_1 - \xi_2 = u^2 - \frac{r^6}{s^6+r^6} - 2\xi_1 - 2\xi_2,$$

$$\xi_3 = \frac{s^6v^2 - r^6u^2}{s^6+r^6} - \xi_1 - 2\xi_2 = \frac{r^6}{s^6+r^6} - u^2 - \xi_1 - 2\xi_2.$$

Using the positivity conditions and two specific values of $\tilde{q}$, we write

$$0 \leq \tilde{q}(0,0,0,1) = \frac{(s^3u^3+r^3v^3)^2}{2(s^6+r^6)} - \frac{\xi_0}{2}, \quad 0 \leq \tilde{q}(1,1,1,0) = \frac{(s^3v^3-r^3u^3)^2}{2(s^6+r^6)} + \frac{\xi_3}{2},$$

hence

$$\xi_2 \geq u^2 - \frac{r^6+(s^3u^3+r^3v^3)^2}{2(s^6+r^6)} - 2\xi_1, \quad \xi_2 \leq \frac{s^6+(s^3u^3+r^3v^3)^2}{2(s^6+r^6)} - \frac{u^2}{2} - \frac{\xi_1}{2}.$$

These two inequalities lead to

$$\xi_1 \geq u^2 - \frac{2\left(r^6+\left(s^3v^3-r^3u^3\right)^2\right)+s^6+\left(s^3v^3-r^3u^3\right)^2}{3\left(s^6+r^6\right)}.$$

Finally, we again use the positivity condition

$$0 \leq \tilde{q}(0,0,1,1) = \frac{(s^3u^2v-r^3uv^2)^2}{2(s^6+r^6)} - \frac{\xi_1}{2}$$

to get

$$3(s^3u^2v-r^3uv^2)^2 - 3u^2(s^6+r^6) + 2(r^6+(s^3u^3+r^3v^3)^2) + r^6 + (s^3v^3-r^3u^3)^2 \geq 0.$$

This last inequality defines $u_{\max}(s)$. Every value of $u > u_{\max}(s)$ is considered nonlocal. The result is plotted in figure 2.2.

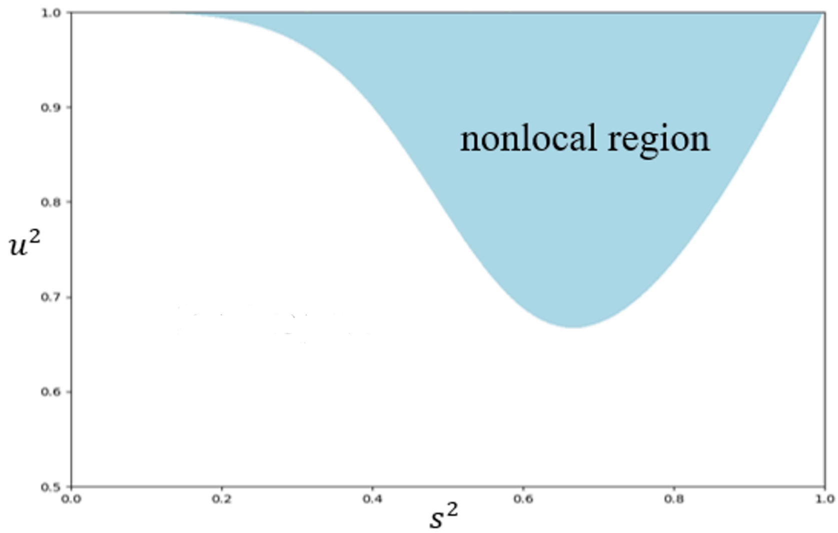

Figure 2.2: Nonlocal and local regions defined by measurement parameter u^2 and degree of entanglement s^2

As discussed in section 1.4.1, the range of nonlocality exhibits symmetrical behavior around $u^2 = 0.5$. $\square$

Emphasis is payed to the nonlocality range for balanced quantum states, thus $s^2 = r^2 = \frac{1}{2}$. Here we have nonlocal correlations for $u^2 \in (0.78499, 1)$.
But one natural question arises: Is the distribution p_Q local when $u^2 \leq u^2_{\max}$? Not necessarily. By utilizing different methods, one might discover a larger range of nonlocality, as Pozas-Kerstjens et al.[9] did in their study, demonstrating network nonlocality for $u^2 \in (0.56250, 0.65626)$.

2.3 Single-Photon Nonlocality

So far, we have discussed the existence of a range of nonlocality, but these findings remain purely theoretical. To advance toward experimentally feasible setups and analyses, it is essential to introduce configurations that are more practical for implementation in the laboratory. A common and promising platform in this context is photonic setups, which are frequently used in quantum communication protocols. With such setups in mind, we require a method to verify whether network nonlocality can be demonstrated using photonic states. This section focuses on discussing such methods. All derivations and information presented in this section are based on the work by Abiuso, Kriváchy, et al.[13].

2.3.1 Setup with passive Optical Elements

In figure 2.3, the basic setup for the experimental setup is shown.

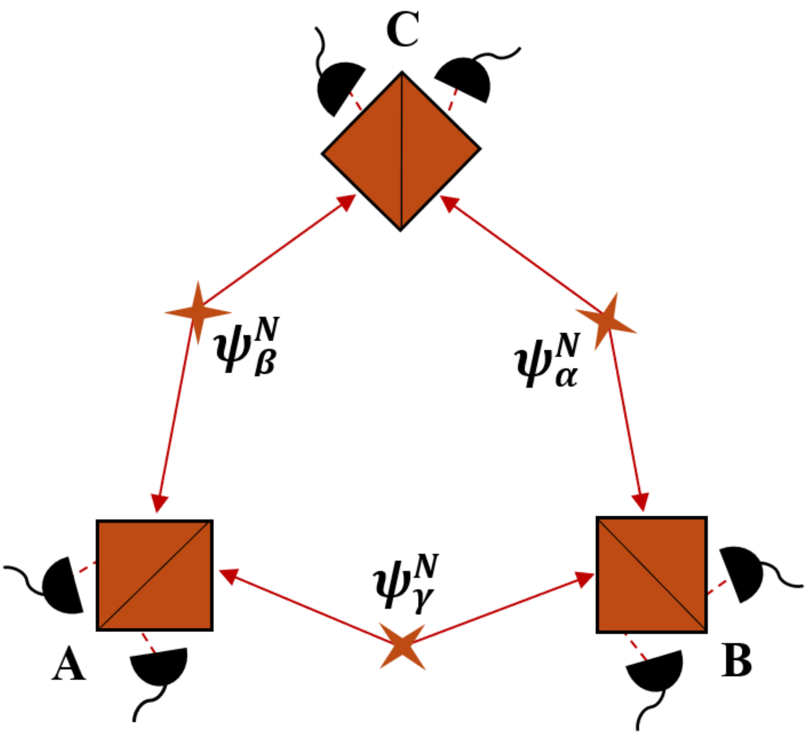

Figure 2.3: The proposed quantum optical experiment involves the parties A, B, and C sharing single-photon entangled states $|\psi\rangle$ prepared by the sources α, β and γ. Each party receives two optical modes, which are mixed using a beamsplitter. The output modes are measured by photodetectors[17].

For this setup, only balanced quantum states are considered, in particular, single-photon entanglement, denoted as

$$|\psi\rangle = \frac{1}{\sqrt{2}}\big(\,|01\rangle + |10\rangle\,\big). \tag{2.17}$$

The three parties share three states, one state from each source. The initial state of the entire network is thus given by

$$|\psi\rangle_{A_2B_1} \otimes |\psi\rangle_{B_2C_1} \otimes |\psi\rangle_{C_2A_1} = |\Psi\rangle_{A_1A_2B_1B_2C_1C_2}\,.$$

Attention must be given to ensure that the corresponding Hilbert spaces are correctly matched, see section 2.1.1.

Furthermore, each party receives two optical input modes, which are processed using a beamsplitter. The beamsplitter applies a unitary transformation, $U_{X_1,X_2}(t,\phi)$ with $X_1, X_2 \in \{A, B, C\}$, characterized by its transmissivity t and phase ϕ. For simplicity, all parties use the same transmissivity and phase. After the photons pass through the beamsplitters, they are detected by photodetectors. For each mode, the detection process is described by operators corresponding to photodetectors with 100% efficiency. These operators include $D^{\square}_{X_i} = |0\rangle\langle 0|_{X_i}$ (no detection) and its complement $D^{\blacksquare}_{X_i} = \mathbb{I}_{X_i} - |0\rangle\langle 0|_{X_i}$ (detector is firing). It is assumed that the detectors can only resolve the presence of photons, but cannot count them. The resulting measurement, combining the beamsplitter's action and the photodetectors, is expressed as a Positive Operator-Valued Measure Π for each party, where $U = U_{X_1X_2}(t,\phi)$,

$$\begin{aligned}
\Pi^0_X &= U^\dagger(D^{\square} \otimes D^{\square})U, \\
\Pi^R_X &= U^\dagger(D^{\square} \otimes D^{\blacksquare})U, \\
\Pi^L_X &= U^\dagger(D^{\blacksquare} \otimes D^{\square})U, \\
\Pi^2_X &= U^\dagger(D^{\blacksquare} \otimes D^{\blacksquare})U.
\end{aligned} \tag{2.18}$$

The notation of the measurement $\Pi^x_X (x \in \{0, L, R, 2\})$ labels at which detector a photon has been resolved, for 0 both detectors do not fire, for L only the left, for R only the right and for 2 both, left and right detector is detecting photons. The output distribution is thus given by

$$p(a,b,c) = Tr\big(\,|\Psi\rangle\,\langle\Psi| \cdot (\Pi^a_A \otimes \Pi^b_B \otimes \Pi^c_C)\big). \tag{2.19}$$

The detailed procedure for calculating the output distribution is outlined in section 6.1. It is important to note that this distribution is a coarse-grained version of the previously utilized RGB4 distribution. We explain this fact in section 2.3.3.

The method for proving nonlocality is conceptually similar to the RGB4-method but is conducted numerically rather than analytically, including an enhanced visualization of the Local Hidden Variable (LHV) model. In the triangle network, classical strategies are simplified by assuming deterministic local response functions, while indeterminacy is assigned to uniformly distributed classical sources. Strict constraints, derived from cyclic symmetry, null components, and photon-number conservation, are expressed as linear equations on response functions, parametrized by t and ϕ. The feasibility of a linear program (LP) determines the existence of classical models. If infeasibility occurs for specific t and ϕ values, the absence of a valid Local Hidden Variable (LHV) model confirms nonlocal correlations.

2.3.2 Deriving a LHV Model for the triangle network with passive optical elements having click/no-click detectors

The approach to proving nonlocality involves identifying constraints that any LHV model must satisfy. Here, we start with an explicit derivation of the LHV model. This process is conceptually similar to Lemma 1. The classical shared variables $\{\alpha, \beta, \gamma\}$ can be assumed as real numbers uniformly distributed in the interval $[0, 1]$. By arranging them orthogonally, a cubic structure with a unit volume is formed. Additionally, all randomness in the local statistical responses can be absorbed into the distribution of $\{\alpha, \beta, \gamma\}$, allowing the local response functions to be considered deterministic. Let X, Y, and Z represent the sets of possible values for α, β, and γ, respectively. We define

$$\begin{aligned}
X_0^B &= \{\alpha \mid \exists\gamma : b(\gamma,\alpha) = 0\}, & X_2^B &= \{\alpha \mid \exists\gamma : b(\gamma,\alpha) = 2\},\\
X_0^C &= \{\alpha \mid \exists\beta : c(\alpha,\beta) = 0\}, & X_2^C &= \{\alpha \mid \exists\beta : c(\alpha,\beta) = 2\},\\
Y_0^C &= \{\beta \mid \exists\alpha : c(\alpha,\beta) = 0\}, & Y_2^C &= \{\beta \mid \exists\alpha : c(\alpha,\beta) = 2\},\\
Y_0^A &= \{\beta \mid \exists\gamma : a(\beta,\gamma) = 0\}, & Y_2^A &= \{\beta \mid \exists\gamma : a(\beta,\gamma) = 2\},\\
Z_0^A &= \{\gamma \mid \exists\beta : a(\beta,\gamma) = 0\}, & Z_2^A &= \{\gamma \mid \exists\beta : a(\beta,\gamma) = 2\},\\
Z_0^B &= \{\gamma \mid \exists\alpha : b(\gamma,\alpha) = 0\}, & Z_2^B &= \{\gamma \mid \exists\alpha : b(\gamma,\alpha) = 2\}.
\end{aligned} \tag{2.20}$$

The sets X_i^P, Y_i^P, and Z_i^P represent values of α, β, and γ for which party P can achieve outcome $i \in \{0, 2\}$. The outcomes L and R are coarse-grained as χ such that the possible outcomes reduces to $a, b, c \in \{0, \chi, 2\}$, reducing the model to a purely local one. Constrained by photon conservation and photodetector limits, the possible outcomes with nonzero probability in this setup are, up to permutations,

$$abc \in \{0\chi\chi, 02\chi, \chi\chi\chi\}. \tag{2.21}$$

By using these fundamental properties of these sets, we derive four additional properties, which enable the construction of the LHV model.

1.Property: $X_2^B \cap X_2^C = \emptyset, \quad X_0^B \cap X_0^B = \emptyset$

Proof. These properties directly follow from equation (2.21). Since it is impossible to have four (or zero) photons among two parties. □

2.Property: $X_0^B \cup X_0^C = X$

Proof. The proof goes by contradiction. Assume $\exists\alpha' \in X \backslash (X_0^B \cup X_0^C) : b(\gamma, \alpha'), c(\alpha', \beta) \in \{\chi, 2\}, \forall\beta, \gamma$, since α' lies outside of $X_0^B \cup X_0^C$, not allowing b and c to output 0.
But this means, Alice is never allowed to output $a = 2$. This, however leads to a contradiction, since $p(a = 2) \neq 0$ is possible. □

3.Property: $X_0^B \cap X_2^B = \emptyset, \quad X_0^C \cap X_2^C = \emptyset$

Proof. The proof goes by contradiction. Assume $\exists \alpha' \in X_0^B \cap X_2^B$, then $\exists \gamma_1, \gamma_2$ s.t. $b(\gamma_1, \alpha') = 0$ and $b(\gamma_2, \alpha') = 2$.
Since Charlies does not know γ and since χ is the only output consistent with 0 and 2, it follows that $c(\alpha', \beta) = \chi$, $\forall \beta$.
Assume $\gamma = \gamma_2$. Since Alice does not know whether $\alpha = \alpha'$ or not, her response function must be consistent with $\alpha = \alpha'$. Having $\forall \beta, c(\alpha', \beta) = \chi$ leads to $a(\beta, \gamma_2) = 0, \forall \beta$. This, consequently, means that $Y = Y_0^A$. But, due to properties 1 and 2, this would imply that $Y_0^C = \emptyset$. This, however, is impossible, since $p(c = 0) \neq 0$. □

4.Property: All sets X_0^P, Y_0^P, Z_0^P have a probability of 50%

Proof. Since balanced quantum states at the sources are considered, the probability for one party to output 0 is 25% (e.g. Alice does not receive a photon neither from source β nor from γ). Additionally, due to the statistical independence of the hidden variables, we write

$$\frac{1}{4} = p(a = 0) \leq p(\beta \in Y_0^A, \gamma \in Z_0^A) = p(\beta \in Y_0^A) p(\gamma \in Z_0^A). \tag{2.22}$$

Utilizing the inequality $xy \leq \frac{(x+y)^2}{4}$, we can write

$$p(Y_0^A)p(Y_0^C) \leq \frac{(\overbrace{p(Y_0^A) + p(Y_0^C)}^{=1,\text{ due to } \mathbf{1.} \text{ and } \mathbf{2.}})^2}{4} = \frac{1}{4}. \tag{2.23}$$

When combining equations (2.22) and (2.23), we obtain $p(Y_0^C) \leq p(Z_0^A)$. We can repeat this process cyclically for the other parties, then obtaining $p(Y_0^C) \leq p(Z_0^A) \leq p(X_0^B) \leq p(Y_0^C)$, implying that all those probabilities are in fact equal. Using equation (2.22), we notice that all $p(\Sigma_0^P)$, with $\Sigma \in \{X, Y, Z\}$, are equal to $\frac{1}{2}$. □

It is important to note that all the stated properties are valid for the sets $\{Y_i^P\}$ and $\{Z_i^P\}$. With this information, we can construct the LHV model (see figure 2.4).

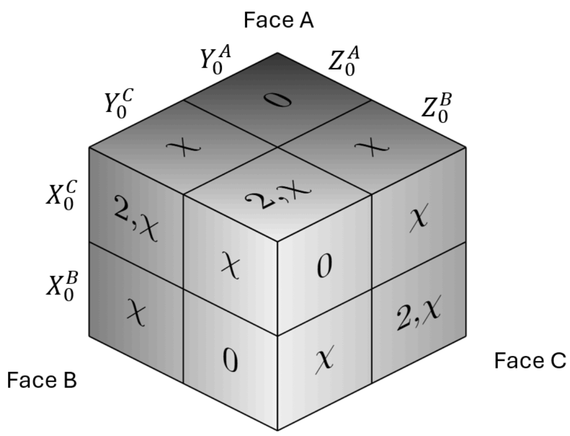

Figure 2.4: LHV Model for one photon per source, beamsplitters and click/no-click detectors

Since each of hidden variables is distributed on the interval $[0,1]$, the edges of the cube representation of the LHV model have equal length. As seen in the 4. property, $p(\Sigma_0^P) = \frac{1}{2}, \forall\Sigma, P$. The labels on the faces are the possible response function of each party. For example, if we have the sets Y_0^A and Z_0^A, we obtain for Alice the output $a = 0$. Similar for any other output. Moreover, the subset labeled $2, \chi$, e.g. on the face B can be further decomposed using the components X_2^B and Z_2^B.
It is important to note that each face of the cube is not merely divided into four subfaces but instead consists of $n^3 - n$ subfaces[19], where n represents the number of possible outcomes. In this case, with $n = 4$, each local hidden variable is divided into 60 parts if discrete random variables are used. Thus, each face contains 3600 subrectangles.
Due to the statistical independence of the local hidden variables, it is possible to rearrange slices of the cube while preserving the structure of the LHV model.
As an example, consider leaving face B unchanged. Along the edge corresponding to the hidden variable β, one might select its associated subfaces with respect to faces A and C. This entire slice can then be relocated elsewhere within the LHV model. However, it is crucial to note that subcuboids themselves cannot be rearranged arbitrarily, otherwise, the consistency of the LHV model would be violated.

2.3.3 Proving Nonlocality with Linear Programming

Now, we add additional information to the problem by fine-graining χ again into $\{L, R\}$. The idea is the following, if there exists a local model as derived in the previous section for the probability distribution $p(a, b, c)$, then there should exist a distribution $q(1_i, 1_j, 1_k, \mathrm{o})$ that reproduces the parties collective response function for $i, j, k = L, R$, when the hidden variables come from $S_0 = X_0^C \times Y_0^A \times Z_0^B$ ($\mathrm{o} = 0$) or $S_1 = X_0^B \times Y_0^C \times Z_0^A$ ($\mathrm{o} = 1$).
To achieve this, we derive the marginals of q and relate them to $p(a, b, c)$. For certain values of transmissivity t and phase ϕ, these marginals become incompatible. Demonstrating this incompatibility allows us to conclude that no local model exists for $p(a, b, c)$ with the specified transmissivity t and phase ϕ. Now, consider the two disjoint subcubes S_0 and S_1, with $S_0 \cap S_1 = \emptyset$ (see Figure 2.4). We define the distribution

$$q(1_i, 1_j, 1_k, \mathrm{o}) := p\big(a = 1_i, b = 1_j, c = 1_k, (\alpha, \beta, \gamma) \in S_{\mathrm{O}} \mid \zeta \in S_0 \cup S_1\big), \tag{2.24}$$

where 1 stands for the number of photons, the indices i, j, k are each either L or R, the index o, for labeling the subcuboid is either 0 or 1 and $\zeta = (\alpha, \beta, \gamma)$. All (χ, χ, χ) events occur only if $\zeta \in S_0 \cup S_1$.
The definition remains consistent with that introduced in section 2.2.2. We now proceed to derive the constraints. While the constraints are derived in a similar manner, there is a key difference in the second constraint, which we will clarify during the derivation.
Due to their importance, we highlight the role of these constraints, as they will serve as a foundation for the analysis in the subsequent chapters.

1. Constraint: The event (χ, χ, χ) appears only in two disjoint subsets in the LHV model.
2. Constraint: The output of any given party cannot be influenced by a source to which it is not connected.

With these definitions in place, we now turn to the detailed derivation of the constraints. Using the definition of conditional probability and the fact that the sets S_0 and S_1 have probability $\frac{1}{8}$ for balanced quantum states, we write

$$q(1_i, 1_j, 1_k, \mathrm{o}) = 4 \cdot p(a = 1_i, b = 1_j, c = 1_k, \zeta \in S_\mathrm{O}). \tag{2.25}$$

By summing over o, we obtain the first constraint[1]

$$q(1_i, 1_j, 1_k) = 4 \cdot p(a = 1_i, b = 1_j, c = 1_k),\ \forall i, j, k. \tag{2.26}$$

By comparing equation (2.26) with equations (2.13) and (2.10) from the previous chapter, we observe that the 1. constraint is identical.
To understand why the second constraint differs from those of the RGB4 method[8], we must examine the measurement basis. Recall that the RGB4 distribution is based on token-counting and uses the following measurement basis (2.5)

$$\begin{aligned} \Pi'_0 &= |00\rangle\langle 00|, & \Pi'_R &= |\chi_r\rangle\langle\chi_r|, \\ \Pi'_L &= |\chi_l\rangle\langle\chi_l|, & \Pi'_2 &= |11\rangle\langle 11|, \end{aligned}$$

where $|\chi_r\rangle = \sqrt{t}|01\rangle - \sqrt{1-t}|10\rangle, |\chi_l\rangle = \sqrt{t}|10\rangle + \sqrt{1-t}|01\rangle$. In comparison to the previous section, we can write $\sqrt{t} \equiv u$ and $\sqrt{1-t} \equiv v$. Unfortunately, this does not conserve the number of photons, but it is necessary to account for situations where, for example, only the left detector fired while two photons were incident. Consequently, this issue must be addressed. To do so, the following measurement basis is employed:

$$\begin{aligned} \Pi_0 &= |00\rangle\langle 00|, & \Pi_R &= |\chi_r\rangle\langle\chi_r| + 2t(1-t)|11\rangle\langle 11|, \\ \Pi_L &= |\chi_l\rangle\langle\chi_l| + 2t(1-t)|11\rangle\langle 11|, & \Pi_2 &= (2t-1)^2|11\rangle\langle 11|. \end{aligned}$$

In this case, photon number is conserved, but the distribution is not token-counting. To satisfy both conditions, photon-number resolving detectors must be considered. Mathematically, this involves fine-graining the above POVMs to obtain

$$\begin{aligned} \Pi''_0 &= |00\rangle\langle 00|, & \Pi''_{R1} &= |\chi_r\rangle\langle\chi_r|, & \Pi''_{R2} &= 2t(1-t)|11\rangle\langle 11|, \\ \Pi''_{L1} &= |\chi_l\rangle\langle\chi_l|, & \Pi''_{L2} &= 2t(1-t)|11\rangle\langle 11|, & \Pi''_2 &= (2t-1)^2|11\rangle\langle 11|. \end{aligned}$$

Note that the difference between, for example, Π''_{L1} and Π''_{L2} lies in the number of photons detected: in Π''_{L1}, there is 1 photon in the left detector, whereas in Π''_{L2}, there are 2 photons in the left detector.

[1]Alongside the description of the first constraint stated in the grey box, a more intuitive explanation would be: (χ, χ, χ) occurs only when all photons travel exclusively in either the clockwise or counterclockwise direction; the first constraint only considers this event

Since Π_L and Π_R account for different numbers of photons, we can frame the problem as follows: consider, for example,

$$q(1_i, \mathrm{o} = 0) \propto p\left(a = 1_i, \zeta \in (X_0^C \times Y_0^A \times Z_0^B)\right).$$

When applying the same approach (speaking of the constraint that, e.g. Alice's answer is independent of the value α) as in the proof of the RGB4 theorem[8], as shown in equation (2.15), we encounter the issue that we end up in the two different subcuboids of the LHV model, where the probability $p(i, 0, c \in \{2, \chi\})$ arises, since click/no-click detectors are considered. Thus, another approach is needed.
To start, consider $p(1_i, 0, \chi)$. We can write

$$\sum_{k\in\{\chi,2\}} p(1_i, 0, k) = p(a = 1_i, \zeta \in X_0^B \times Y_0^A \times Z_0^B) + p(a = 1_i, \zeta \in X_0^B \times Y_0^C \times Z_0^B).$$

Similar for $p(1_i, \chi, 0)$, we write

$$\sum_{j\in\{\chi,2\}} p(1_i, j, 0) = p(a = 1_i, \zeta \in X_0^C \times Y_0^C \times Z_0^A) + p(a = 1_i, \zeta \in X_0^C \times Y_0^C \times Z_0^B).$$

Now, we subtract the second equation from the first. Additionally, it is important to note that we still can apply the approach used in (2.15). We thus write

$$\sum_{k\in\{\chi,2\}} p(1_i, 0, k) - \sum_{j\in\{\chi,2\}} p(1_i, j, 0) = \tag{2.27}$$

$$= \frac{p(X_0^B)}{p(X_0^C)} \cdot p(a = 1_i, \zeta \in X_0^C \times Y_0^A \times Z_0^B) + \underline{\frac{p(X_0^B)}{p(X_0^C)} \cdot p(a = 1_i, \zeta \in X_0^C \times Y_0^C \times Z_0^B)}$$
$$- \frac{p(X_0^C)}{p(X_0^B)} \cdot p(a = 1_i, \zeta \in X_0^B \times Y_0^C \times Z_0^A) - \underline{p(a = 1_i, \zeta \in X_0^C \times Y_0^C \times Z_0^B)}.$$

Since balanced quantum states are used (see equation (2.17)), the 4. property is used to obtain $\frac{p(X_0^C)}{p(X_0^B)} = \frac{p(X_0^B)}{p(X_0^C)} = 1$. Clearly, the two underlined terms cancel out, leaving

$$\sum_{k\in\{\chi,2\}} p(1_i, 0, k) - \sum_{j\in\{\chi,2\}} p(1_i, j, 0) = \underbrace{p(a = 1_i, \zeta \in X_0^C \times Y_0^A \times Z_0^B)}_{=\frac{1}{4}\cdot q(1_i, \mathrm{O}=0)} - \underbrace{p(a = 1_i, (\zeta \in X_0^B \times Y_0^C \times Z_0^A)}_{=\frac{1}{4}\cdot q(1_i, \mathrm{O}=1)}.$$

This procedure can similarly be applied to Bob and Charlie, yielding the second constraint,

$$\begin{aligned}
\sum_{j,k} \big(q(1_i, 1_j, 1_k, 0) - q(1_i, 1_j, 1_k, 1)\big) &= 4 \cdot \Big(\sum_{k\in\{\chi,2\}} p(1_i, 0, k) - \sum_{j\in\{\chi,2\}} p(1_i, j, 0)\Big) \ \forall i,\\
\sum_{i,k} \big(q(1_i, 1_j, 1_k, 0) - q(1_i, 1_j, 1_k, 1)\big) &= 4 \cdot \Big(\sum_{k\in\{\chi,2\}} p(0, 1_j, k) - \sum_{i\in\{\chi,2\}} p(i, 1_j, 0)\Big) \ \forall j,\\
\sum_{i,j} \big(q(1_i, 1_j, 1_k, 0) - q(1_i, 1_j, 1_k, 1)\big) &= 4 \cdot \Big(\sum_{i\in\{\chi,2\}} p(i, 0, 1_k) - \sum_{j\in\{\chi,2\}} p(0, j, 1_k)\Big) \ \forall k.
\end{aligned} \tag{2.28}$$

In addition to these two constraints, it is important to emphasize that, since q is a probability distribution, it must be normalized and non-negative,

$$q(i,j,k,\text{o}) \geq 0 \quad \forall\, i,j,k,\text{o} \quad \text{and} \quad \sum_{i,j,k,\text{o}} q(i,j,k,\text{o}) = 1. \tag{2.29}$$

The existence of $q(i,j,k,\text{o})$ is a necessary condition for the local feasibility of p. Thus, if the linear program fails to find a solution, the nonlocality of p is certified. Conversely, finding a solution does not directly confirm the locality of p. The linear program becomes infeasible for $t \in (0, 0.215) \cup (0.785, 1)$, which is the same range of nonlocality as shown in section 2.3. Hereby, the phase ϕ is set to 0. If $\phi > 0$, the range of nonlocality is decreasing.

Moreover the different distributions p, p', and p'' (labeled according to the different measurement bases) give the same range of nonlocality with respect to the parameter t. Specifically, if one of these distributions is classically reproducible in the triangle network for a given t, then all of them are. Note that this fact is only true for this LP. From a physical perspective, this indicates that perfect number-resolving photon detection does not enhance the nonlocality of the output distribution in the ideal experiment, although it could improve its robustness to noise, since photon number detectors provide more accurate information.

2.4 Noise Tolerance in the Triangle Network

To assess the robustness of nonlocality in the considered optical network, we need to analyze the effects of experimental imperfections, including state impurity Ξ, photon loss in the channels η, and detector efficiency ν. Abiuso and Kriváchy et al.[13] discuss a concept for an experimental setup under realistic conditions, for which they used a neural network to approximate local models and evaluate their deviation from the target distribution. Their results indicate nonlocality for $t \in (0.5, 0.785)$ and $t \in (0.785, 1)$, with the strongest indications at $t \approx 0.65$ and $t \approx 0.85$. However, nonlocality vanishes when $\eta, \nu \lesssim 95\%$. Although it is important to note that modern photon detectors have achieved efficiencies close to 100%[20 21 22].
Thus, apart from source imperfections, the primary challenge in practical implementations is photon loss in the channels. In 2023, a method was developed to address photon loss using an approximate parity TC rigidity approach. In the following sections, we first introduce the parity TC method (PTC method)[14]. Section 2.4.1 provides an overview of the approach, while section 2.4.2 derives the corresponding constraints for a linear program.
We identified an error in the code associated within the publication of Boreiri and Ulu et al.[14]. A detailed mathematical explanation of this issue is provided in section 2.4.2.

2.4.1 Approximate Parity TC Rigidity

The objective of this section is to implement the PTC method that serves as the foundation for demonstrating potential noise-robust network nonlocality, focusing is on parity TC distributions.
The method and constraint derivations described in this and the next section is based on the paper *Noise-robust proofs of quantum network nonlocality* by Boreiri and Ulu et al.[14]. Unless stated otherwise, the content presented here is directly taken over from this publication, with any other deviations or additional contributions explicitly indicated.
The concept is as follows: each source (α, β, γ) distributes a single token, which it sends to one of the two parties it is connected to. For example, source α sends the token to Bob with probability p_α, or to Charlie with probability $1 - p_\alpha$. Each party then outputs the parity of the total number of tokens it receives. Let us define the binary random variables $t_\alpha, t_\beta, t_\gamma \in \{0, 1\}$ as the number of tokens sent by sources α, β, and γ to Bob, Charlie, and Alice. For instance, Alice receives t_γ tokens from source γ and $t_\beta \oplus 1$ tokens from source β, where $\oplus$ denotes addition modulo 2. Alice's response function is then given by $a(\beta, \gamma) = t_\gamma \oplus t_\beta \oplus 1$, similar for Bob and Charlie.
The resulting probability distribution $p(a, b, c)$ generated by the PTC model has binary outputs ($d = 2$). By construction, any such distribution satisfies the condition

$$a \oplus b \oplus c = 1,$$

which we refer to as the PTC condition, with a, b and c defined by a token function

$$T_\zeta : \zeta \to t_\zeta \in \{0, 1\} \text{ such that } x(\zeta, \zeta') = t_\zeta \oplus t_{\zeta'} \oplus 1.$$

Now assume having a local distribution $p(a, b, c)$ for which the PTC condition only holds approximately, i.e.

$$Pr(a \oplus b \oplus c = 1) \geq 1 - \varepsilon, \tag{2.30}$$

with a set Λ, given by

$$\Lambda = \{\zeta | a(\beta, \gamma) \oplus b(\alpha, \gamma) \oplus c(\alpha, \beta) = 1\}. \tag{2.31}$$

This set contains all the values $\zeta = (\alpha, \beta, \gamma)$ for which the parity condition holds. By assumption, we have $Pr(\zeta \in \Lambda) \geq 1 - \varepsilon$.
This leads to the following question: Is there a subset, where token functions can be consistently defined to satisfy PTC, despite that condition? If so, then an approximate parity TC rigidity for local distributions is achieved. Indeed, it can be demonstrated that such a set exists.

Theorem 2.4.1 (Approximate parity TC rigidity)**.** *For any triangle local model leading to a distribution $p(a, b, c)$ that fulfills the approximate parity condition $Pr(a \oplus b \oplus c = 1) \geq 1 - \varepsilon$, there exists a subset Υ of local variable values $\zeta = (\alpha, \beta, \gamma)$ with $Pr(\zeta \in \Upsilon) \geq 1 - f(\varepsilon)$ (see equation (2.32)), on which one can define the token functions that satisfy the PTC rigidity.*

The function $f(\varepsilon)$ is given by

$$f(\varepsilon) = \begin{cases} \frac{1}{2} + \varepsilon - \frac{\sqrt{1-4\varepsilon}}{2}, & \varepsilon \leq \frac{1}{4}, \\ \frac{1}{2} + \varepsilon, & \varepsilon > \frac{1}{4}. \end{cases} \tag{2.32}$$

it is important to note that as ε increases, the function f reflects how much the rigidity weakens. Since the proof of theorem 2.4.1 and the definition of Υ are not required for the current discussion, we will focus solely on the result $\Pr(\zeta \in \Upsilon) \geq 1 - f(\varepsilon)$. For further details, interested readers are referred to Boreiri et al. [14], Appendix A. We will proceed utilizing the information provided in the theorem for our subsequent calculations.
The set Υ leads to the following subnormalized distribution $p(a, b, c, \zeta \in \Upsilon)$, which satisfies

$$\sum_{a,b,c} p(a, b, c, \zeta \in \Upsilon) \geq 1 - f(\varepsilon). \tag{2.33}$$

Assuming this bound is tight, thus we can write

$$p(a, b, c, \zeta \in \Upsilon) + f(\varepsilon) p'(a, b, c) = p(a, b, c), \tag{2.34}$$

where $p'(a, b, c)$ is some (not necessarily local) distribution. Extending the token functions to all values of the local variables not in Υ, by relabeling all outputs, e.g with a 0 (see figure 2.5), we define the new probability distribution

$$\tilde{p}(a, b, c) = \sum_{t_\alpha, t_\beta, t_\gamma} p(t_\alpha) p(t_\beta) p(t_\gamma)\, p_{\text{ptc}}(a|t_\beta, t_\gamma)\, p_{\text{ptc}}(b|t_\alpha, t_\gamma)\, p_{\text{ptc}}(c|t_\alpha, t_\beta). \tag{2.35}$$

This distribution is triangle-local and PTC, and since $p(a,b,c)$ and $\tilde{p}(a,b,c)$ agree on $\zeta \in \Upsilon$, we get

$$p(a,b,c,\zeta \in \Upsilon) + f(\varepsilon)\tilde{p}'(a,b,c) = \tilde{p}(a,b,c), \tag{2.36}$$

for some PTC distribution $\tilde{p}'(a,b,c)$. Figure 2.5 illustrates the graphical representation corresponding to equations (2.34) and (2.36). The axes in the figure represent the different values of the local variables β and γ. The lighter region represents the set Υ. On the left side, the outer region is represented by $p'(a,b,c)$, and similarly, on the right side, it is represented by $\tilde{p}'(a,b,c)$. Recall that on the right side, the token functions are extended, for example, by assigning them the value 0.

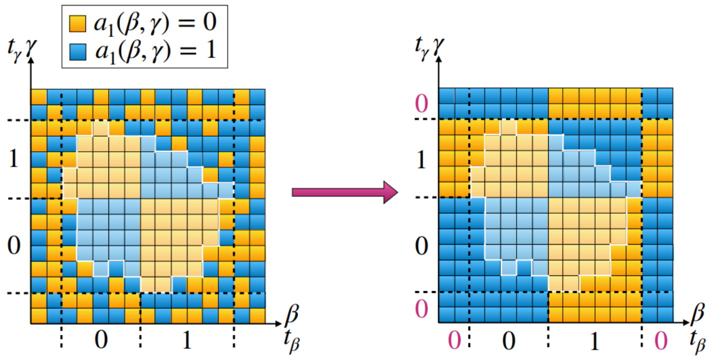

Figure 2.5: A graphical representation of the construction to explain the approximate PTC rigidity[14]

Combining the relations from equation (2.34) and (2.36), we obtain the following

$$p(a,b,c) = \tilde{p}(a,b,c) - f(\varepsilon)p'(a,b,c) + f(\varepsilon)\tilde{p}'(a,b,c), \tag{2.37}$$

which, in terms of total variation distance, leads to the inequality

$$\delta(p,\tilde{p}) = \frac{1}{2}\sum_{a,b,c} |p(a,b,c) - \tilde{p}(a,b,c)| \leq f(\varepsilon). \tag{2.38}$$

To justify the validity of the last step, the following lemma is introduced.

Lemma 2. *For probability distributions $p(x)$ and $q(x)$, the following statements are equivalent:*

(i) There exist probability distributions p' and q' such that

$$p(x) = q(x) + \epsilon p'(x) - \epsilon q'(x),$$

(ii) $\delta_{TV}(p,q) \leq \epsilon$.

Proof. (i) $\Rightarrow$ (ii):

$$\delta_{TV}(p,q) = \frac{1}{2}\sum_x |p(x) - q(x)| = \frac{\epsilon}{2}\sum_x |p'(x) - q'(x)| = \epsilon\, \delta_{TV}(p',q') \leq \epsilon,$$

since, by definition, $\delta_{TV}(p',q') \leq 1$.
(ii) $\Rightarrow$ (i): The idea is that $p'(x)$ is defined as a valid probability distribution, while $q'(x)$ is adjusted in such a way that it satisfies the equation $p(x) = q(x) + \epsilon p'(x) - \epsilon q'(x)$. Thus, let us define $r(x) = p(x) - q(x)$. Then, we have

$$\sum_x r(x) = 0 \quad \text{and} \quad \sum_x |r(x)| \leq \epsilon.$$

We define

$$p'(x) = \frac{|r(x)|}{\sum_x |r(x)|} \quad \text{and} \quad q'(x) = p'(x) - \frac{r(x)}{\epsilon},$$

which are valid probability distributions satisfying (i). □

For a noiseless distribution, note that $p(a,b,c)$ is equivalent to the distribution $\tilde{p}(a,b,c)$, as $f(\varepsilon) = 0$. This simplifies equations (2.37) to

$$p(a,b,c) = \tilde{p}(a,b,c).$$

2.4.2 Deriving Constraints for a Linear Program using PTC Method

For the observed probability distribution, which corresponds to a token-counting distribution when no noise is considered, a modification is required. Specifically, we express this as

$$p(a,b,c) \to p(a_1,a_2,b_1,b_2,c_1,c_2) \equiv p(x_1,x_2), \tag{2.39}$$

with $x_i = (a_i, b_i, c_i)$ and x_1 alone satisfying the parity condition $a_1 \oplus b_1 \oplus c_1 = 1$. Here, x_1 represents the token, while x_2 is the additional information, thus, by rigidity, there exist binary token functions for any underlying local model that explains the distribution

$$p(x_1) = \sum_t p(t)\, p_{\text{PTC}}(x_1|t) \tag{2.40}$$

with $t = (t_\alpha, t_\beta, t_\gamma)$ and $p_{\text{PTC}}(x_1|t) = p_{\text{PTC}}(a_1|t_\beta,t_\gamma)\, p_{\text{PTC}}(b_1|t_\alpha,t_\gamma)\, p_{\text{PTC}}(c_1|t_\alpha,t_\beta)$. The PTC response function is defined as follow

$$p_{PTC}(x_1|t) = \begin{cases} 1 & \text{if } a = t_\beta \oplus t_\gamma \oplus 1, b = t_\gamma \oplus t_\alpha \oplus 1, c = t_\alpha \oplus t_\beta \oplus 1, \\ 0 & \text{otherwise.} \end{cases}$$

Furthermore, we introduce the correlators $E_{a_1}, E_{b_1}, E_{c_1}$, we write

$$E_x = Pr(x=0) - Pr(x=1), \quad \forall x. \tag{2.41}$$

If $E_{a_1}, E_{b_1}, E_{c_1} \neq 0$, then the token distribution $p(t) = p_\alpha(t_\alpha)p_\beta(t_\beta)p_\gamma(t_\gamma)$ can be precisely determined using equations (2.42)

$$\begin{aligned} p_\alpha(t_\alpha = t) &= \frac{1}{2}\Big(1 + (-1)^t\sqrt{\left|\frac{E_b E_c}{E_a}\right|}\Big), \\ p_\beta(t_\beta = t) &= \frac{1}{2}\Big(1 + (-1)^t\sqrt{\left|\frac{E_a E_c}{E_b}\right|}\Big), \\ p_\gamma(t_\gamma = t) &= \frac{1}{2}\Big(1 + (-1)^t\sqrt{\left|\frac{E_b E_a}{E_c}\right|}\Big). \end{aligned} \tag{2.42}$$

The equations (2.42) are derived in the publication by Boreiri and Girardin et al.[23]
The goal is now to derive two constraints, similar to those in sections 2.3 and 2.4, that the distribution in (2.40) must satisfy.
We begin by considering a noiseless distribution to provide a baseline framework. This serves as the groundwork for subsequently adapting the analysis to a noisy distribution, using the previously stated theorem 2.4.1.
For any local model, we can define the random variable t, which represents the behavior of the tokens. Due to rigidity, we infer that x_1 is only a function of t. Applying the chain rule yields

$$p(x_1, x_2) = \sum_t p(t)\, p_{PTC}(x_1|t)\, p(x_2|t). \tag{2.43}$$

To advance the analysis of equation (2.43), we introduce a set denoted by $\mathcal{C}$,

$$\mathcal{C}(x_1) \equiv \mathcal{C}(a_1, b_1, c_1) = \{(t_\alpha, t_\beta, t_\gamma)|a_1 = t_\beta \oplus t_\gamma \oplus 1, b_1 = t_\alpha \oplus t_\beta \oplus 1, c_1 = t_\alpha \oplus t_\beta \oplus 1\}.$$

It is important to note that this set defines the non-zero output of the response function $p_{PTC}(x_1|t)$. By applying $p(t)\,p(x_2|t) = p(x_2, t)$ and conditioning on the requirement that only values of t leading to x_1 are considered, we write

$$\boxed{\sum_{(t_\alpha, t_\beta, t_\gamma)\,\in\,\mathcal{C}(x_1)} p(x_2, t) = p(x_1, x_2).} \tag{2.44}$$

Furthermore, conceptually equivalent as in the previous sections, the output of any party (e.g. a_2) cannot be influenced by sources not connected to it (i.e., by α and the token value t_α). This observation imposes the following constraints on the marginal distributions $p(a_2|t) = \sum_{b_2,c_2} p(x_2|t)$:

$$p(a_2|t_\alpha = 0, t_\beta, t_\gamma) = p(a_2|t_\alpha = 1, t_\beta, t_\gamma). \tag{2.45}$$

Here, to simplify this constraint, the definition of conditional probability and the independence of the token distributions are used, such that

$$\boxed{p_\alpha(t_\alpha = 1)\sum_{b_2,c_2} p(a_2, b_2, c_2, 0, t_\beta, t_\gamma) = p_\alpha(t_\alpha = 0)\sum_{b_2,c_2} p(a_2, b_2, c_2, 1, t_\beta, t_\gamma).} \tag{2.46}$$

Analogous constraints apply to all permutations of the parties.
When considering a noisy distribution such that $Pr(a_1 \oplus b_1 \oplus c_1 = 1) \geq 1 - \varepsilon$, note that the two distributions $p(x_1, x_2)$ and $\tilde{p}(x_1, x_2)$ coincide only on the subset Υ of the local variable values, with $Pr(\zeta \in \Upsilon) \geq 1 - f(\varepsilon)$. This condition is equivalent to the bound on the total variation distance, as stated in the previous section (see equation (2.38)).
Furthermore, by construction, $\tilde{p}(x_1, x_2)$ aligns with the original distribution $p(x_1, x_2)$ for the outcomes x_2, implying that $\tilde{p}(x_2) = p(x_2)$. Additionally, since the token functions are extended for $\tilde{p}(x_1, x_2)$, we have

$$\tilde{p}(x_1, x_2) = 0 \quad \text{for} \quad a_1 \oplus b_1 \oplus c_1 \neq 1. \tag{2.47}$$

From the previously stated lemma, we know that the condition of the total variation distance is equivalent to the existence of two probability distributions $p'(x_1, x_2)$ and $\tilde{p}'(x_1, x_2)$ fulfilling the equation (2.37). By introducing these probabilities as additional variables and by using equation (2.47) as well as the set $\mathcal{C}$, we can write the first constraint for a linear program for a noisy distribution.

$$\begin{aligned} p(x_1, x_2) = \sum_{(t_\alpha, t_\beta, t_\gamma) \in \mathcal{C}(x_1)} & p(x_2, t) - f(\varepsilon) p'(x_1, x_2) + f(\varepsilon) \tilde{p}'(x_1, x_2), \text{ with} \\ \sum_{x_1} \tilde{p}'(x_1, x_2) &= \sum_{x_1} p'(x_1, x_2), \\ \sum_{x_1, x_2} \tilde{p}'(x_1, x_2) &= \sum_{x_1, x_2} p'(x_1, x_2) = 1 \end{aligned} \tag{2.48}$$

For the second constraint, one modification is required, since $p_\alpha(t)$, $p_\beta(t)$, and $p_\gamma(t)$ correspond to the PTC distribution $\tilde{p}$, rather than the observed distribution p. Therefore, their values are unknown and are treated as additional variables. The main objective is to bound these variables using the equations in (2.42). It is important to note that, in fact, we need to bound the correlators $\tilde{E}_{x_1}$. The bound is given by

$$\left| \tilde{E}_{x_1} - E^{\Lambda}_{x_1} \right| \leq 2 f(\varepsilon) - \varepsilon, \tag{2.49}$$

where $E^{\Lambda}_{x_1} = p(x_1 = 0, a_1 \oplus b_1 \oplus c_1 = 1) - p(x_1 = 1, a_1 \oplus b_1 \oplus c_1 = 1)$ is computed from the PTC part of the observed distribution $p(x_1, x_2)$. In the following we give a proof for the inequality (2.49).

Proof. Recall the sets Λ and Υ. We can write

$$p(x_1, \zeta \in \Lambda) = p(x_1, \zeta \in \Upsilon) + (f(\varepsilon) - \varepsilon) p''(x_1). \quad (I)$$

Assuming that the bounds are tight, we have $Pr(\zeta \in \Lambda) = 1 - \varepsilon$, $Pr(\zeta \in \Upsilon) = 1 - f(\varepsilon)$ and $Pr(\zeta \in \Lambda \backslash \Upsilon) = f(\varepsilon) - \varepsilon$. Looking at equation (2.36), we write

$$\tilde{p}(x_1) = p(x_1, \zeta \in \Upsilon) + f(\varepsilon) \tilde{p}'(x_1). \quad (II)$$

Combining (I) and (II), leads to

$$\tilde{p}(x_1) = p(x_1, \zeta \in \Lambda) + f(\varepsilon)\tilde{p}'(x_1) - (f(\varepsilon) - \varepsilon)p''(x_1).$$

Using $\tilde{E}_{x_1} = \tilde{p}(x_1 = 0) - \tilde{p}(x_1 = 1)$, we obtain

$$\tilde{E}_{x_1} = E^{\Lambda}_{x_1} + f(\varepsilon)\tilde{E}^{'}_{x_1} - (f(\varepsilon) - \varepsilon)E^{''}_{x_1}.$$

The values of $\tilde{E}^{'}_{x_1}$ and $E^{''}_{x_1}$ are not known, but by definition in the interval $[-1, 1]$. Thus, the minimum and maximum of $f(\varepsilon)\tilde{E}^{'}_{x_1} - (f(\varepsilon) - \varepsilon)E^{''}_{x_1}$ is given by $\pm(2f(\varepsilon) - \varepsilon)$. This results in the following bound for $\tilde{E}_{x_1}$:

$$\left|\tilde{E}_{x_1} - E^{\Lambda}_{x_1}\right| \leq 2f(\varepsilon) - \varepsilon.$$

□

If all the correlators for the observed distribution satisfy $|E^{\Lambda}_{x_1}| \geq (2f(\varepsilon) - \varepsilon)$, the inequality (2.49) can be used to obtain

$$\begin{aligned} l_\alpha :=& \frac{1}{2}\left(1 + \sqrt{\frac{(|E^{\Lambda}_{b_1}| - (2f(\varepsilon) - \varepsilon))(|E^{\Lambda}_{c_1}| - (2f(\varepsilon) - \varepsilon))}{|E^{\Lambda}_{a_1}| + (2f(\varepsilon) - \varepsilon)}}\right) \\ &\leq p_\alpha(0) \leq \frac{1}{2}\left(1 + \sqrt{\frac{(|E^{\Lambda}_{b_1}| + (2f(\varepsilon) - \varepsilon))(|E^{\Lambda}_{c_1}| + (2f(\varepsilon) - \varepsilon))}{|E^{\Lambda}_{a_1}| - (2f(\varepsilon) - \varepsilon)}}\right) := u_\alpha. \end{aligned} \tag{2.50}$$

The same approach can be applied to $p_\alpha(1)$, $p_\beta(t)$, and $p_\gamma(t)$. Therefore, the second constraint can be written as

$$\begin{aligned} l_\alpha \sum_{b_2, c_2} p(a_2, b_2, c_2, 0, t_\beta, t_\gamma) - (1 - l_\alpha) \sum_{b_2, c_2} p(a_2, b_2, c_2, 1, t_\beta, t_\gamma) \leq 0, \\ u_\alpha \sum_{b_2, c_2} p(a_2, b_2, c_2, 0, t_\beta, t_\gamma) - (1 - u_\alpha) \sum_{b_2, c_2} p(a_2, b_2, c_2, 1, t_\beta, t_\gamma) \geq 0. \end{aligned} \tag{2.51}$$

Analogous constraints apply to all permutations of the parties.
An important step in determining the bounds in (2.50) is the computation of $E^{\Lambda}_{x_1}$. As mentioned at the beginning of this section, the authors of this publication[14] made an error in this part of the calculation—specifically in evaluating the correlators $E^{\Lambda}_{x_1}$, which are defined in equation (2.41). Note that we can write:

$$\Pr(x = 0) + \Pr(x = 1) = \Pr(\zeta \in \Upsilon). \tag{2.52}$$

However, the mistake occurred here: instead of using $\Pr(\zeta \in \Upsilon)$, the authors incorrectly wrote 1. This is incorrect because the correlators $E^{\Lambda}_{x_1}$ are only defined on the subset Υ, where the PTC condition holds. As a result, the correct expression for the correlator is:

$$E^{\Lambda}_{x_1} = \Pr(\zeta \in \Upsilon) - 2\Pr(x = 1). \tag{2.53}$$

The authors of the PTC method used a generalized version of the RGB4 distribution to demonstrate robustness against white noise. By introducing the noise parameter η, where $\eta = 1$ corresponds to a noiseless distribution, they established that noise-robust nonlocality persists for $\eta \geq 99.52\%$.
Accounting for this mistake, the noise robustness is weakened, yielding noise-robust nonlocality only for $\eta \geq 99.56\%$. This error affects not only the mentioned noise robustness but also any result in the publication[14] that involves the correlators $E^{\Lambda}_{x_1}$.

2.5 Experimental Implementations

Experimental proofs of quantum network nonlocality remain quite rare. The first experiments, conducted in 2017 by Saunders et al.[24] and Carvacho et al.[25], explored the bilocal scenario (entanglement swapping). In 2019, a more rigorous bilocal experiment addressed several loopholes[26]. Extensions to star networks[27 28](with up to four branches) and triangle networks[29 30] followed. However, these studies are closely tied to standard Bell's theorem violations in single-source scenarios and can be realized without requiring entangled measurements, for instance, Polino et al.[30] only one source is entangled and the other two sources are classically correlated.
In the following sections, we present an experiment conducted by Wang et al.[15], demonstrating experimental genuine quantum nonlocality in the triangle network. More precisely, they provide experimental verification of nonlocal correlations having entangled states at each node. Since this thesis is theoretical, the given summary below solely focuses on the most significant aspects of the study, highlighting key results and addressing the loopholes that emerged as a result of the experiment's execution. For a more comprehensive explanation, the reader is referred to the publication.

2.5.1 Experimental Network Nonlocality using the Elegant Distribution

In their publication[15], the authors propose an experimental setup and proof for triangle network nonlocality using the Elegant distribution. There, each of the three parties is connected pairwise via polarization-entangled photon sources, and each party performs an *Elegant Joint Measurements* (EJM). The resulting correlations (see equation (1.6)) are not linked to Standard Bell's nonlocality.
The Elegant distribution $P_E(a, b, c)$[16] is a probability distribution in the triangle network that provides strong evidence for nonlocality, although this has not been rigorously proven. It arises when entangled singlet states are distributed, and the parties perform EJMs in a specific symmetric basis. This distribution is highly structured, characterized by only two independent parameters, making it simple to analyze. For a more detailed discussion, see Gisin[16].
Building on the characterization of the Elegant distribution $P_E(a, b, c)$, we now turn our attention to the experimental implementation. Figure 2.6 depicts the singlet source, using three of them in the entire network $(\rho_\alpha, \rho_\beta, \rho_\gamma)$. They are used to distribute entangled photon pairs in the triangle network. The figure focuses exclusively on the source, while details regarding the setup, including EJMs are provided in the text.

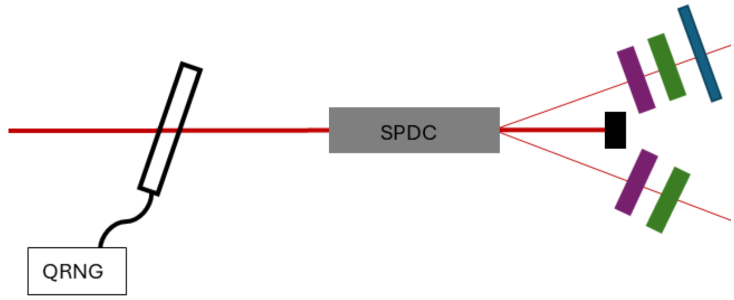

Figure 2.6: Sketch of the source's setup: The laser pump passes through a phase shifter modulated by a quantum random number generator, then a sandwich-like BBO crystal (SPDC), potentially generating two entangled photons. Both photons undergo spatial (purple) and temporal (green) compensation, with the upper photon additionally passing through a half-wave plate (blue). The half-wave plate is needed to adjust the polarization of the upper photon.

Sources: The experiment uses spontaneous parametric down conversion (SPDC) to produce entangled photon pairs, where ultraviolet pump pulses are generated by a laser. The entangled photons are produced through a setup involving two beta barium borate (BBO) crystals and a true-zero-order halfwave plate. The setup generates singlet states by ensuring that the two-photon state becomes indistinguishable after polarization flips and compensation. Three such sources are used, with state tomography performed for characterization. All three sources use the same pump laser. To ensure source independence, random phase shifts are applied to each pump pulse using quantum random number generators (QRNG).
Elegant Joint Measurement: The EJM basis projection setup projects the input state onto one of the four possible entangled bases, one at a time, using optical elements that manipulate the polarization of photons. After each projection, a loss element is introduced to adjust the entanglement, and specialized wave plates are used to convert between the required bases. This process is repeated for each basis, allowing for precise and controlled projection of the input state.
Method and Result: The publication[15] demonstrates quantum nonlocality in the triangle network using two methods. First, violations of conjectured, heuristic inequalities are analyzed by testing whether their experimental data surpasses specific thresholds distinguishing quantum from local models. Significant violations of these inequalities are found, particularly for optimized parameters, highlighting the nonlocal nature of the setup. Second, they use a neural network oracle (see section 1.4.2) to verify if the experimental distribution lies outside the local set by calculating its minimal distance to any local model. The oracle confirmed the experimental distribution lies outside the local set, with a minimal distance of 0.0230 ± 0.0027 from any local model. The results confirm that the observed distribution cannot be explained by local hidden variable models.

2.5.2 Encountering Loopholes

Although the distribution realized in the experiment simulates the Elegant distribution to great accuracy and nonlocal correlations are obtained, the approach from Wang et al.[15] introduces two loopholes. It requires global postprocessing of both the outcomes and the measurement settings to reconstruct the Elegant distribution. Also, the experiment involves renormalizing the data to include only events where all photons successfully arrived at the detectors, adding another layer of global postprocessing. This reliance on global postprocessing presents a theoretical challenge, as unconstrained global postprocessing can, in principle, generate any desired distribution. For example, even if all parties output random bits, selectively keeping only specific outcomes—such as (0,0,0) and (1,1,1)—can artificially produce strong correlations, like those seen in GHZ-type scenarios. As a result, unrestricted postprocessing can fake genuine quantum correlations, making it difficult to determine whether the observed correlations truly reflect nonlocal behavior or are merely artifacts of postprocessed noise.

To address the first loophole, it is essential to implement the measurement directly, without relying on postprocessing that artificially reconstructs the distribution. Using passive optical elements, the photons states are not modified or altered and we do not need measurement settings. Instead, these elements simply guide the paths the photons follow without affecting their intrinsic properties and most importantly, we do not need to change the measurement during experiment. This approach has been proven to work by Abiuso and Krivachy et al.[13], as discussed in section 2.3.

To circumvent the second loophole, it is essential to ensure that no experimental rounds are discarded, even in cases where not all photons are successfully detected. This necessitates a theoretical demonstration that the setup can tolerate a certain level of photon loss—particularly at the sources and along the transmission channels—while still exhibiting nonlocal correlations. Such robustness to noise is a prerequisite for closing the detection loophole in the triangle network. Consequently, implementing a feasible and loophole-free experiment within this network requires resolving this challenge.

3 Noise-Robust Triangle Network Nonlocality

In this chapter, we develop a theoretical framework for network nonlocality in the triangle network using passive optical elements, addressing the fundamental challenge of photon loss in transmission channels—an essential consideration in overcoming the detection loophole. Our approach extends beyond the limitations of the TC method[11], yielding network nonlocal correlations under realistic conditions.
To establish a solid foundation, we begin by examining NOON states, focusing on the case $N = 2$ in an idealized, noise-free setting. Building upon this, we then systematically analyze the effects of photon loss, distinguishing between single-photon loss and full photon loss. For single-photon loss, we further differentiate between scenarios involving photon-number-resolving detectors and click/no-click detectors.
Several of the results presented in this chapter have been published by Krivácht et al.[17]. Overall, this chapter provides an analysis of noise robustness in the presence of photon loss, contributing to a deeper understanding of photon loss effects in the triangle network and marking a step towards closing the detection loophole.

3.1 Multi-Photon Nonlocality

In section 2.3, we explored network nonlocality having balanced quantum states at each source, consisting of a single spatially entangled photon. We now extend this framework to describe tilted quantum states with N spatially entangled photons, referred to as NOON states, which are represented as

$$|\psi\rangle^N = s\,|0N\rangle + r\,|N0\rangle\,, \tag{3.1}$$

where $s, r \in \mathbb{R}$ and $s^2 + r^2 = 1$. It is important to note that the remainder of the setup for the triangle network remains unchanged, as described in section 2.3.
The number of projectors Π_i performed by the parties A, B, and C depend linearly on the number of photons emitted by each source. Since the system involves $3N$ total photons, explicitly defining every individual measurement operator becomes impractical. Instead, we focus on describing the cardinality (number of elements) of the set of projective measurements, $\{\Pi_i\}$, for each party.
The cardinality of the set of projectors can be expressed as

$$\mathrm{Card}(\{\Pi_i\})(N) = 3 \cdot (N + 1). \tag{3.2}$$

This expression follows from considering how photons are distributed between two detectors at each party. If a total of N photons enter a party, the possible combinations of photon distributions are given by the set $\{(0, N), (1, N-1), \ldots, (N, 0)\}$, resulting in $N+1$ possibilities. Similarly, if $2N$ photons enter a party, there are $2N+1$ possible distributions, as the photons can be split across the detectors in all combinations from $(0, 2N)$ to $(2N, 0)$. Additionally, it is important to account for the possibility of 0 photons entering the party, which increases the total cardinality by 1. Thus, the total number of projective measurements is determined by summing over all these possible distributions. The explicit derivation of the POVMs and the corresponding probability distribution $p(a, b, c)$ is provided in section 6.1.

3.1.1 Constructing LHV - Models for tilted NOON States

To initiate the proof of network nonlocality, we first derive the local model for tilted NOON states. As outlined in section 2.3, we make again a distinction between two types of detection schemes: photon-number resolving detectors and click/no-click detectors.

Local Hidden Variable Model for photon-counting distributions

When the distributions involve photon-number resolving detectors at the parties, the TC strategy applies, necessitating theorem 2.1.3[11], as it forms the basis for constructing the local model. Before applying the features of the theorem, we first emphasize the probabilities of obtaining certain outcomes. This can be understood straightforwardly by following the scheme below.
Note that, regardless of whether we consider photon-counting distributions or only click/no-click distributions, on the one hand, the probability that one party obtains 0 photons in the noiseless case is always given by

$$p(a=0) = p(b=0) = p(c=0) = s^2 r^2, \tag{3.3}$$

and a double or triple-zero outcomes are not possible

$$p(a, b=0, c=0) = p(a=0, b, c=0) = p(a=0, b=0, c) = p(a=0, b=0, c=0) = 0. \tag{3.4}$$

With this in mind, we now return to the TC theorem[11]. We observe that the total number of input tokens η_i is equal to the total number of output tokens n_j, satisfying the condition

$$\sum_i \eta_i = \sum_j n_j$$

which implies for the outputs a, b, and c that

$$a + b + c = 3N. \tag{3.5}$$

Furthermore, according to the token-counting theorem, the probability $q_i(t_i^j)$ denotes the likelihood that source S_i distributes a certain number of photons $t_i^j \in \{0, N\}$ to the connected party A_j. Since there are only two possible ways to distribute the photons, using equation (2.3) we write

$$\sum_i \Pr_{s_i}[T_i^j(s_i) = t_i^j] = \sum_i q_i(t_i^j) = q_{s_i}(0) + q_{s_i}(N) = 1, \ \forall s_i \tag{3.6}$$

Now, for each LHV we define a corresponding set, e.g. for α we define the set $X_\alpha := X_\alpha^B \cup X_\alpha^C$, analogously for β and γ. Utilizing equation (3.6), we write

$$\begin{aligned} \alpha \in X_\alpha^B &\Rightarrow T^1(\alpha) = 0, \ T^2(\alpha) = N \\ \alpha \in X_\alpha^C &\Rightarrow T^1(\alpha) = N, \ T^2(\alpha) = 0, \end{aligned} \tag{3.7}$$

with T^1 and T^2 being the token functions, or in our case the response functions b and c for Bob and Charlie, respectively. We employ equation (2.3) and (3.7) to express these probabilities explicitly.

$$\begin{aligned} \Pr_\alpha[b = N] = s^2 =: |X_\alpha^B|, &\quad \Pr_\alpha[b = 0] = r^2 =: |X_\alpha^C| \\ \Pr_\alpha[c = N] = r^2 =: |X_\alpha^C|, &\quad \Pr_\alpha[c = 0] = s^2 =: |X_\alpha^B| \\ \Pr_\beta[c = N] = s^2 =: |Y_\beta^A|, &\quad \Pr_\beta[c = 0] = r^2 =: |Y_\beta^C| \\ \Pr_\beta[a = N] = r^2 =: |Y_\beta^C|, &\quad \Pr_\beta[a = 0] = s^2 =: |Y_\beta^A| \\ \Pr_\gamma[a = N] = s^2 =: |Z_\gamma^A|, &\quad \Pr_\gamma[a = 0] = r^2 =: |Z_\gamma^B| \\ \Pr_\gamma[b = N] = r^2 =: |Z_\gamma^B|, &\quad \Pr_\gamma[b = 0] = s^2 =: |Z_\gamma^A| \end{aligned} \tag{3.8}$$

Using equation (3.6), we obtain the constraints

$$|X_\alpha^B| + |X_\alpha^C| = |Y_\beta^A| + |Y_\beta^C| = |Z_\gamma^A| + |Z_\gamma^B| = 1. \tag{3.9}$$

Given equations (3.8) and (3.9), the local model for a noiseless photon-counting probability distribution can be constructed straightforwardly.

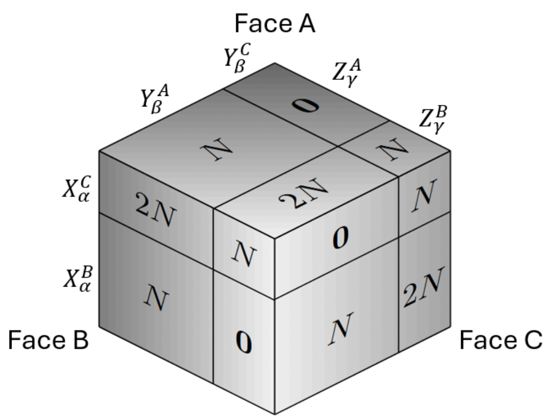

Figure 3.1: Local hidden variable model for the noiseless photon-counting probability distribution with N photons at each source

It is important to emphasize that, regardless of the specific quantum state—such as a generalized state of the form

$$|\psi_G\rangle^N = \sum_{k=0}^{N} w_k \, |N-k, k\rangle \,, \text{ with } \sum_{k=0}^{N} w_k = 1, \tag{3.10}$$

as long as photon number-resolving detectors are used, a LHV model can be constructed by applying the principles of the token-counting approach.
Abiuso and Kriváchy et al.[13] examined the construction of a LHV model for a ring network as well, composed of J sources S_j and J parties A_j considering click/no-click detectors and just a single spatially entangled photon per source. In our setup, each pair of neighboring parties $A_j A_{j+1}$ shares a copy of a tilted NOON state and we solely consider photon number-resolving detectors, thus the resulting probability distribution corresponds to the token-counting one. The local coarse-grained strategy p can be expressed as

$$p(a_1, \dots, a_N) = \int d\alpha_{12} d\alpha_{23} \dots d\alpha_{N1} \, p(a_1|\alpha_{N1}, \alpha_{12}) p(a_2|\alpha_{12}, \alpha_{23}) \dots p(a_N|\alpha_{(N-1)N}, \alpha_{N1}), \tag{3.11}$$

where a_i represents the outcome of party A_i, determined as a local response to the hidden variables $\{\alpha_{i(i-1)}, \alpha_{(i+1)i}\}$, which are shared with its adjacent neighbors.

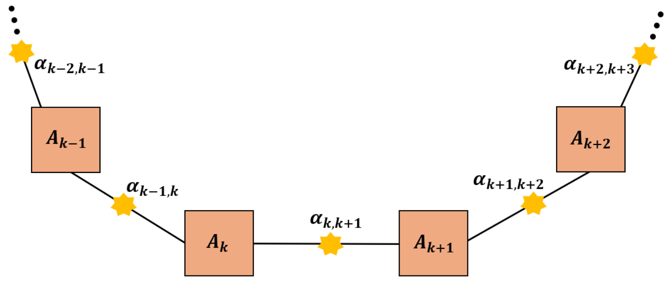

Figure 3.2: Topology of a ring network: a network composed of J sources S_j and J parties A_j and, due to its topology, party A_{J+1} is identified with A_1

Note that the constraints can be constructed similarly as for the triangle network.

Local Hidden Variable Model for click/no-click distributions

In constructing a LHV model for a click/no-click distribution with $N \geq 2$ photons per source, two approaches were considered. The first approach was based on a method similar to that presented in Lemma 1 and section 2.3.2. However, this approach did not yield any successful results. Alternatively, a more straightforward approach is possible due to simplifications arising from high-dimensional NOON states. The measurement outcomes are given by $a, b, c \in \{0, L, R, B\}$, where each value represents a possible detection result: 0 denotes no detection, L and R indicate that the left or right detector clicked, respectively, and B represents both detectors clicking. As discussed in the section on single-photon nonlocality, a global non-zero outcome (χ, χ, χ) only occurs if photons are detected at either the left or right detector. Therefore, coarse-graining the outcomes L and R into a common result χ suffices in that case. However, when considering $N \geq 2$ photons per source, the outcome 2 can also contribute to a global non-zero result. As a consequence, the measurement outcomes can be coarse-grained as follows:

$$a, b, c \in \{0, L, R, 2\} \rightarrow a, b, c \in \{0, \chi\}.$$

This implies that the possible outcomes can be reduced to the coarse-grained results $(a, b, c) = \{(\chi, \chi, \chi), (0, \chi, \chi)\}$. For balanced quantum states, we then have the following probabilities:

$$p(a = 0) = p(b = 0) = p(c = 0) = \frac{1}{4}.$$

Now, assuming we are in the photon-counting regime again, for balanced quantum states, the relation above still holds. If we group $\{N, 2N\} \rightarrow \chi$, the resulting structure is equivalent to a click/no-click distribution, as we cannot move the zero outcomes to other positions on the LHV model without violating equation (3.4). However, this does not hold true for tilted quantum states. In this case, since there are only two coarse-grained outcomes, the zero outcomes must not necessarily appear at fixed positions, as in figure 3.1. As a result, constructing a local model for tilted quantum states in a click/no-click regime is not possible with our method.

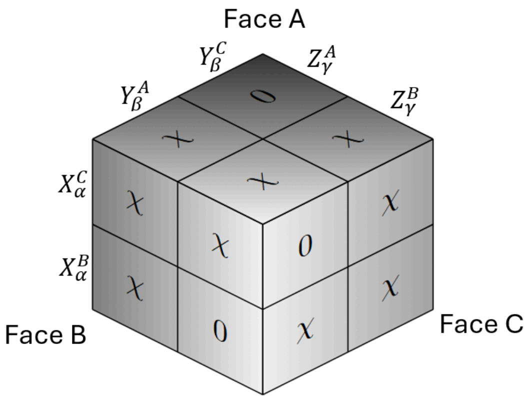

Figure 3.3: Local hidden variable model for the noiseless click/no-click probability distribution with N photons at each source

3.1.2 Proving Network Nonlocality for N=2 photons per Source

In order to prove triangle-network nonlocality for high-dimensional NOON states, we use the approach of section 2.3, although here we only focus on 2 photons per source. We derive the marginals for the constraints in a manner that ensures their validity for both photon-counting and click/no-click distributions. Note that we do the derivations in the photon number-resolving regime. In order to use the constraints for click/no-click detectors, we set $s^2 = r^2 = \frac{1}{2}$. We again start by defining two subsets S_0 and S_1, in which the collective response function of all parties yields $N = 2$ photons, i.e. $p(2, 2, 2)$. When comparing with figure 3.1 and 3.3, these sets are given by

$$\begin{aligned} S_0 &:= X_\alpha^C \times Y_\beta^C \times Z_\gamma^B \\ S_1 &:= X_\alpha^B \times Y_\beta^A \times Z_\gamma^A, \end{aligned} \tag{3.12}$$

with $S_0 \cap S_1 = \emptyset$, $Pr(\zeta \in S_0) = r^6$ and $Pr(\zeta \in S_1) = s^6$, $\zeta = (\alpha, \beta, \gamma)$. Similarly as in the previous chapter, we define

$$\begin{aligned} q(2_i, 2_j, 2_k, \mathrm{o}) &:= p(a = 2_i, b = 2_j, c = 2_k, \zeta \in S_\mathrm{O} \mid \zeta \in S_0 \cup S_1) \\ &= \frac{1}{s^6 + r^6} \cdot p(a = 2_i, b = 2_j, c = 2_k,\, \zeta \in S_\mathrm{O}) \quad \forall i, j, k, \mathrm{o}, \end{aligned} \tag{3.13}$$

with $i, j, k \in \{L, R, B\}$.

0. Constraint (Positivity and Normalization)

$$\begin{gathered} q(2_i, 2_j, 2_k, \mathrm{o}) \geq 0 \quad \forall i, j, k, \mathrm{o} \\ \sum_{i,j,k,\mathrm{O}} q(2_i, 2_j, 2_k, \mathrm{o}) = 1 \end{gathered} \tag{3.14}$$

1. Constraint (Common Photon Cycling Direction)
The first constraint is given by

$$q(2_i, 2_j, 2_k) = \frac{1}{s^6 + r^6} \cdot p(a = 2_i, b = 2_j, c = 2_k) \quad \forall i, j, k. \tag{3.15}$$

It is worth noting that choosing $s^2 = r^2 = \frac{1}{2}$ recovers the same constraint as presented in equation (2.26).

Proof. Summing over o in equation (3.13), leads to the first constraint. □

2. Constraint (No Influence from Unconnected Sources)
The 2. constraint is given by

$$\begin{aligned} q(2_i, \mathrm{o} = 0) - \frac{s^2}{r^2} q(2_i, \mathrm{o} = 1) &= \frac{1}{s^6 + r^6} \cdot \big(\frac{s^2}{r^2} \sum_k p(2_i, 0, k) - \sum_j p(2_i, j, 0)\big) \ \forall i, \\ q(2_j, \mathrm{o} = 0) - \frac{s^2}{r^2} q(2_j, \mathrm{o} = 1) &= \frac{1}{s^6 + r^6} \cdot \big(\frac{s^2}{r^2} \sum_k p(0, 2_j, k) - \sum_i p(i, 2_j, 0)\big) \ \forall j, \\ q(2_k, \mathrm{o} = 0) - \frac{s^2}{r^2} q(2_k, \mathrm{o} = 1) &= \frac{1}{s^6 + r^6} \cdot \big(\frac{s^2}{r^2} \sum_i p(i, 0, 2_k) - \sum_j p(0, j, 2_k)\big) \ \forall k. \end{aligned} \tag{3.16}$$

Note that for photon-number-resolving detectors, the second constraint can potentially be simplified, as discussed in Section 2.2. However, since our analysis includes both detector types, we derive it here in a form that also accommodates click/no-click detectors. Moreover, in the noiseless case, the summation is not required, as each combination of i, j, k corresponds to either a 4 in the case of photon-number-resolving detectors or a χ for click/no-click detectors. We nonetheless leave it, as needed for accounting photon loss.

Proof. We consider the probability that, for example, Alice outputs a non-zero outcome 2_i, $i \in \{L, R, B\}$, while either Bob or Charlie outputs 0. This is captured by the expressions $p(a = 2_i, b = 0, c = k)$ and $p(a = 2_i, b = j, c = 0)$, where $j, k \in \{4\}$ for photon number resolving detectors and $j, k \in \{\chi\}$ for click/no-click detectors. Using figure 3.1 (or 3.3), we write

$$\sum_k p(a = 2_i, b = 0, c = k) = p(2_i, \zeta \in X_\alpha^B \times Y_\beta^A \times Z_\gamma^B) + p(2_i, \zeta \in X_\alpha^B \times Y_\beta^C \times Z_\gamma^B), \tag{3.17}$$

$$\sum_j p(a = 2_i, b = j, c = 0) = p(2_i, \zeta \in X_\alpha^C \times Y_\beta^A \times Z_\gamma^A) + p(2_i, \zeta \in X_\alpha^C \times Y_\beta^A \times Z_\gamma^B). \tag{3.18}$$

Similar as in equation (2.27), we write

$$\sum_k p(2_i, 0, k) - \sum_j p(2_i, j, 0) = \tag{3.19}$$

$$= \underline{\frac{\Pr(X_\alpha^B)}{\Pr(X_\alpha^C)} \cdot p(a = 2_i, \zeta \in X_\alpha^C \times Y_\beta^A \times Z_\gamma^B)} + \frac{\Pr(X_\alpha^B)}{\Pr(X_\alpha^C)} \cdot p(a = 2_i, \zeta \in X_\alpha^C \times Y_\beta^C \times Z_\gamma^B)$$
$$- \frac{\Pr(X_\alpha^C)}{\Pr(X_\alpha^B)} \cdot p(a = 2_i, \zeta \in X_\alpha^B \times Y_\beta^A \times Z_\gamma^A) - \underline{p(a = 2_i, \zeta \in X_\alpha^C \times Y_\beta^A \times Z_\gamma^B)}$$

Since we use tilted quantum states, i.e., $\frac{\Pr(X_\alpha^C)}{\Pr(X_\alpha^B)} = \frac{s^2}{r^2}$, an additional coefficient appears. Moreover, to eliminate the underlined terms, we multiply equation (3.17) by $\frac{\Pr(X_\alpha^C)}{\Pr(X_\alpha^B)}$, yielding:

$$\frac{s^2}{r^2} \sum_k p(2_i, 0, k) - \sum_j p(2_i, j, 0) =$$
$$\underbrace{p(a = 2_i, \zeta \in X_\alpha^C \times Y_\beta^C \times Z_\gamma^B)}_{=(s^6 + r^6) \cdot q(2_i, \mathrm{O}=0)} - \frac{s^2}{r^2} \underbrace{p(a = 2_i, \zeta \in X_\alpha^B \times Y_\beta^A \times Z_\gamma^A)}_{=(s^6 + r^6) \cdot q(2_i, \mathrm{O}=1)}.$$

Thus, we write

$$\sum_{j,k} \big(q(2_i, 2_j, 2_k, 0) - \frac{s^2}{r^2} q(2_i, 2_j, 2_k, 1)\big) = \frac{1}{s^6 + r^6} \cdot \big(\frac{s^2}{r^2} \sum_k p(2_i, 0, k) - \sum_j p(2_i, j, 0)\big). \tag{3.20}$$

Applying this procedure similarly for Bob and Charlie yields the second constraint. □

The linear program, formulated in terms of the variables $q(2_i, 2_j, 2_k, \mathrm{o})$, consisting of 54 variables, and the probability distribution $p(a, b, c)$ derived in section 6.1, yields the following the first result:

Result 1. *The probability distributions $p(a,b,c)$ exhibit nonlocality in the triangle network for the (s,ϕ,t) parameter regime computed in section 6.1. Specifically, for $\phi = \frac{\pi}{2}$ and $s^2 = 0.5$, nonlocality is observed in the interval $0.761 \leq t < 1$. This specific result holds for both photon-counting distributions and click/no-click distributions.*

The results are equivalent to those by Kriváchy et al.[17]
Since we have analyzed all values of s^2, we can visualize the nonlocal regions within a given t interval, resulting in figure 3.4.

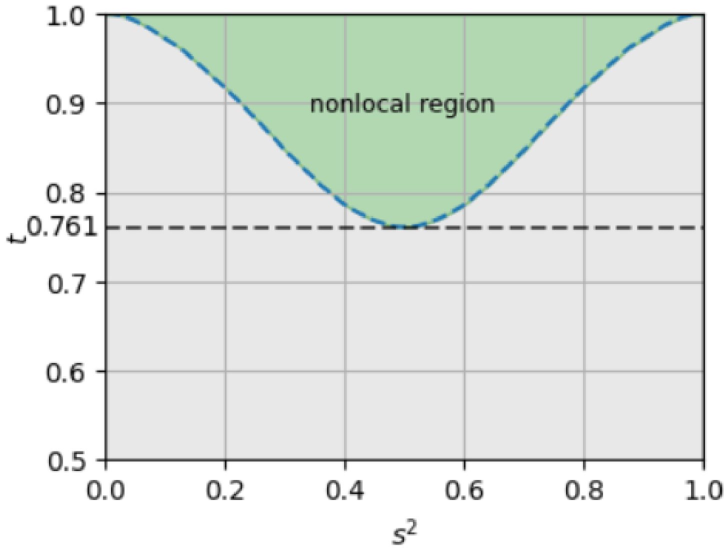

Figure 3.4: Values of t beyond which the probability distribution $p(a,b,c)$ fails to admit a local hidden variable model for a given s^2 [17].

In the noiseless case, high-dimensional quantum states evidently demonstrate an advantage over single-photon sources. Specifically, for balanced quantum states, within the range $t \in (0.761, 0.784]$, nonlocality cannot be proven when using single-photon sources, see figure 3.5. This result highlights the potential of high-dimensional quantum states to enhance nonlocality.

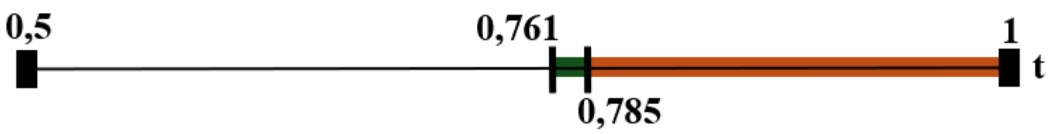

Figure 3.5: The range of nonlocality is extended by $t \in [0.761, 0.784]$ compared to the results by Abiuso et al.[13] and Renou et al.[8]

In principle, the RGB4 method[8] can also be applied to demonstrate nonlocality for higher-dimensional photonic states, as outlined in theorem 2.2.1 and its corresponding proof.

However, the computational complexity increases significantly with the dimensionality of the states. Consequently, it is more practical to employ a LP based on the computed set of probability distributions. This is advantageous because the structure of the constraints remains unchanged, and only the number of variables in the distribution q grows linearly with the number of photons N[1].
We express the total number of variables $V_q(N)$ of q by

$$V_q(N) = 2 \cdot (N+1)^3. \tag{3.21}$$

To compute the needed probability distribution, we follow the method described in section 6.1. The coarse-grained probabilities for the LP can always be expressed in the form:

$$p(N_i, 2N, 0) \propto u_i^2, \quad p(N_i, 0, 2N) \propto v_i^2, \quad p(N_i, N_j, N_k) \propto (u_i u_j u_k + v_i v_j v_k)^2. \tag{3.22}$$

Thus, it suffices to compute the required u and v, as the indices i, j, k carry the same physical meaning in u, v, as in the distribution q.

[1]Note that this is also true for the analytical RGB4 method[8]

3.2 Single-Photon-Loss Nonlocality

The most dominant noise factor in the transmission channels is single photon loss. Throughout this section, we set the number of photons per source to $N = 2$. Using a single photon loss noise model, we describe the noise using Kraus operators[17]:

$$K_0 = |0\rangle\langle 0| + \eta\,|2\rangle\langle 2|, \qquad\qquad K_1 = \sqrt{1-\eta^2}\,|1\rangle\langle 2|, \tag{3.23}$$

where each mode can lose at most one photon, and the probability of successfully transmitting a single photon is η, thus we obtain our noiseless model if $\eta = 1$. The corresponding noisy measurement operators are given by

$$\Pi_{X,\eta}^{(i_1,i_2)} = \sum_{j,j'} K_j^\dagger \otimes K_{j'}^\dagger \Pi_X^{(i_1,i_2)} K_j \otimes K_{j'}, \tag{3.24}$$

where $i_1, i_2 \in \{0, \ldots, 2N \equiv 4\}$ for photon-number-resolving detectors and $i_1, i_2 \in \{0, \chi\}$ for click/no-click detectors. The probability distribution for single photon loss (SPL) is given by

$$p_\eta^{SPL}(a,b,c) = Tr\left(|\psi\rangle^{N=2}\langle\psi|^{N=2} \cdot (\Pi_{A,\eta}^{(i_1,i_2)} \otimes \Pi_{B,\eta}^{(j_1,j_2)} \otimes \Pi_{C,\eta}^{(k_1,k_2)})\right). \tag{3.25}$$

The results are presented here as equivalent to those by Kriváchy et al.[17], although the approach as well as the LP differs.
To derive the LHV model in the context of single photon loss, for a start we begin by considering balanced quantum states. In this model, the probability of obtaining outcome 0 for each party is fixed and given by

$$p_\eta^{SPL}(a=0) = p_\eta^{SPL}(b=0) = p_\eta^{SPL}(c=0) = \frac{1}{4}. \tag{3.26}$$

The structure of the LHV model must therefore reflect this constraint. However, complications arise when considering the post-processed outcomes corresponding to the original coarse-grained outcomes 2 and 4 as in the noiseless scenario. Specifically, in the presence of noise, an original coarse-grained outcome of 2 can lead to an observed outcome of either 1 or 2 in this noise model, and an original outcome of 4 can lead to 2, 3, or 4. We denote these outcome classes as

$$2 \to \tilde{2} = \{1, 2_{\to 2}\}, \qquad 4 \to \tilde{4} = \{2_{\to 4}, 3, 4\}, \tag{3.27}$$

where the subscripts indicate whether the outcome 2 originates from an original 2 or an original 4 outcome in the noiseless case.
This distinction becomes problematic when further analyzing the probability distribution. For instance, when evaluating, e.g. $p_\eta^{\mathrm{SPL}}(2,2,0)$, it is ambiguous whether the two outcome-2 entries stem from original outcome-2 events or from original outcome-4 events. Without access to this information, the LHV model cannot resolve this ambiguity directly.

To address this, we simplify the labeling of outcomes in the LHV model. We redefine the outcome alphabet as

$$\chi = \{1, 2, 3, 4\}, \tag{3.28}$$

treating all outcomes as indistinguishable with respect to their noiseless origin.
Since the TC approach is not applicable in this scenario—since we account for noise in the communication channels—we require to go beyond the TC framework in order to construct a consistent model. Let us focus on the 0 outcomes. Consider Alice's measurement outcomes and let us construct the smallest possible square—aligned with the coordinate axes—that contains all of her outcome-0 events. Let the side lengths of this square be denoted by Y_β^C and Z_γ^A. This square may also enclose outcomes labeled differently. It follows that

$$Y_\beta^C Z_\gamma^A \geq p_\eta^{SPL}(a = 0).$$

Analogous considerations for Bob and Charlie yield the additional constraints:

$$Z_\gamma^B X_\alpha^B \geq p_\eta^{SPL}(b = 0), \quad X_\alpha^C Y_\beta^A \geq p_\eta^{SPL}(c = 0).$$

Furthermore, since $p_\eta^{SPL}(0, 0)$ is impossible, the regions corresponding to 0 outcomes on each face must be mutually exclusive. This implies that the projections of these squares onto the shared axes cannot overlap, resulting in the following conditions:

$$X_\alpha^B + X_\alpha^C \leq 1, \quad Y_\beta^C + Y_\beta^A \leq 1, \quad Z_\gamma^A + Z_\gamma^B \leq 1.$$

Given equation (3.26), the above set of inequalities has a unique solution:

$$X_\alpha^B = X_\alpha^C = Y_\beta^C = Y_\beta^A = Z_\gamma^A = Z_\gamma^B = \frac{1}{2}.$$

Because this solution saturates all the inequalities, we can conclude that the minimal enclosing squares of the 0 outcomes do not contain any other output labels, leaving us with a LHV model as in figure 3.3, with χ labeling all the outcomes except 0, in both photon number resolving and click/no-click regime.
To account for tilted quantum states, it becomes necessary to impose bounds on the hidden variables—analogous to the procedure outlined in the next section (see equation (3.56))—since the previous argument used to construct the LHV model no longer applies. However, introducing such bounds and solving the resulting LP leads to numerical problems and yields only weak results. This highlights the need for developing a more refined LHV model to properly capture the structure of the tilted scenario. We will not further investigate this issue in this work.
Due to the structure of the LHV model, we can apply the same linear program to check for infeasibility as discussed in the previous section. However, special attention must be given to the correct labeling of the terms being summed over in equation 3.16. Additionally, for the noise robustness results we used the coarse-graining scheme {0, (1,0), (0,1), (2,0), (1,1), (0,2), 4}.

Result 2. *When applying the single-photon loss noise model to evaluate noise robustness the following results are obtained (see also figure 3.6): For photon number resolving detectors, for* $t = 0.97$, $s^2 = 0.5$ *and* $\phi = \frac{\pi}{2}$, *the robustness reaches its maximum at* $\eta = 0.897$, *corresponding to a noise tolerance of up to 10.3%. In the case of click/no-click detectors, the maximum robustness with* $\eta = 0.933$, *is achieved for* $t = 0.94$, $s^2 = 0.5$ *and* $\phi = \frac{\pi}{2}$, *resulting in a maximum robustness of 6.7%*[17].

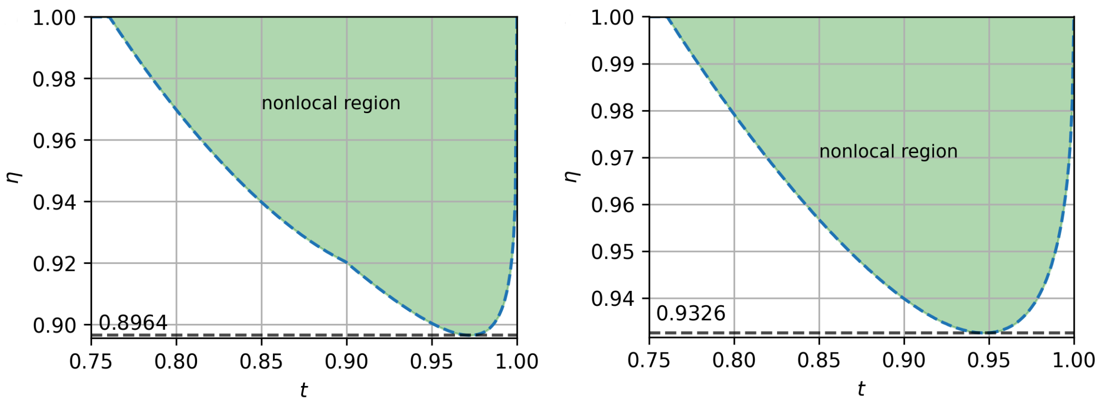

Figure 3.6: Single-Photon Noise Robustness: In the noiseless case, nonlocality was proven above the blue dashed line. However, when s^2 deviates from 0.5, the linear program no longer produces reliable results, and noise robustness could not be proven. The left panel shows the results for the photon-number resolving regime, while the right panel displays the results for the click/no-click regime[17].

A few remarks on our results: We could have applied the PTC method[14], as discussed in section 2.4, but we failed to prove nonlocality for both, balanced or tilted quantum states, we discuss this issue in section 3.4 in greater detail. It is important to note that the PTC method does not work for balanced quantum states in general, whereas our approach provides significant noise robustness. Specifically, their method yields less than 1%, while ours achieves an improvement of more than an order of magnitude. Although we observed no robustness for tilted quantum states, the results remain strong. The observed robustness can be attributed to on the one hand the zero outcomes, since they impose relatively strong constraints, and on the other hand to the fact that the constraints in the LP are mostly equalities, and approximate inequalities are not needed.

3.3 Full Photon Loss Nonlocality via a Geometrical Approach

In this and the next section we study full photon loss occurring in the channels between the sources and the parties. Note that we again focus on NOON states, but considering solely $N = 2$ photons per source and photon number resolving detectors. When using the full photon loss noise model, we again define it by the Kraus operators[17]:

$$\begin{aligned} K_0 &= |0\rangle\langle 0| + \eta\,|2\rangle\langle 2|, \\ K_1 &= \sqrt{2\eta(1-\eta)}\,|1\rangle\langle 2|, \\ K_2 &= (1-\eta)\,|0\rangle\langle 2|, \end{aligned} \tag{3.29}$$

where $1-\eta$ denotes the probability of a single photon being lost. The corresponding noisy measurement operators are given by

$$\widetilde{\Pi}^{(i_1,i_2)}_{X,\eta} = \sum_{j,j'} K_j^\dagger \otimes K_{j'}^\dagger \widetilde{\Pi}^{(i_1,i_2)}_{X} K_j \otimes K_{j'}, \tag{3.30}$$

where $i_1, i_2 \in \{0, \ldots, 2N \equiv 4\}$ for photon-number-resolving detectors. The terms proportional to $|\cdot\rangle\langle 1|$ have been omitted, as we assume that the source state does not contain single-photon components. The probability distribution for full photon loss (FPL) is given by

$$p^{FPL}_{\eta}(a,b,c) = Tr\left(|\psi\rangle^{N=2}\langle\psi|^{N=2} \cdot (\widetilde{\Pi}^{(i_1,i_2)}_{A,\eta} \otimes \widetilde{\Pi}^{(j_1,j_2)}_{B,\eta} \otimes \widetilde{\Pi}^{(k_1,k_2)}_{C,\eta})\right). \tag{3.31}$$

3.3.1 Introducing a new LHV Model accounting for Full Photon Loss

When considering full photon loss, constructing a local hidden variable model presents a challenge, as it allows $p^{FPL}_{\eta}(0,0,0) > 0$. This deviates from the structure of the LHV models discussed in the previous sections of this chapter, where such outcomes were strictly excluded. But in certain subsets λ_i we can still find outcomes that satisfy the condition

$$a(\beta,\gamma) + b(\alpha,\gamma) + c(\alpha,\beta) = 6, \tag{3.32}$$

as well as preserving the intrinsic structure as in figure 3.1. Assume we have M λ_i sets, then they all must fulfill the following definition

$$\lambda_i := \{\zeta | a(\beta,\gamma) + b(\alpha,\gamma) + c(\alpha,\beta) = 6\}. \tag{3.33}$$

Here, each set λ_i consists of all triplets (α,β,γ) such that the sum of $a(\beta,\gamma)$, $b(\alpha,\gamma)$, and $c(\alpha,\beta)$ equals 6 for each triplet. Since we are allowed to rearrange the cubic structure as stated in section 2.3.2, we can create a region Λ, such that

$$\Lambda := \bigcup_i \lambda_i. \tag{3.34}$$

Projecting this set onto the faces F^X of the cubic representation of the LHV model yields, for relatively small noise (i.e., $\eta \lesssim 1$), a comparatively large projection area P^X. The complement of this projection area is referred to as the *Hole Regions*.

Definition 3.3.1 (Hole Regions). *Given the set Λ, then the projection of Λ onto the face F^X of the LHV model is denoted by $P^X := Proj_{F^X}(\Lambda)$. Due to the intrinsic structure of the set Λ, we have four sub-regions on each face for different outputs, we can divide each face F^X into four parts $F^X_{\zeta_i,\zeta_j}$, namely, F^X_{12}, F^X_{11}, F^X_{22} and F^X_{21}, and similar for P^X, we can thus define the hole regions $(h^X_{\zeta_i,\zeta_j})$*

$$h^X_{\zeta_i,\zeta_j} := \{(\zeta_i,\zeta_j)|(\zeta_i,\zeta_j) \in F^X_{\zeta_i,\zeta_j}, (\zeta_i,\zeta_j) \notin P^X_{\zeta_i,\zeta_j}\}. \tag{3.35}$$

$\zeta_i \equiv i$, $\zeta_j \equiv j$ denote a specific segments, e.g. α_1 and β_2 for face C give the notation $h^C_{1,2}$.

Figure 3.7 gives an illustration of the hole region.

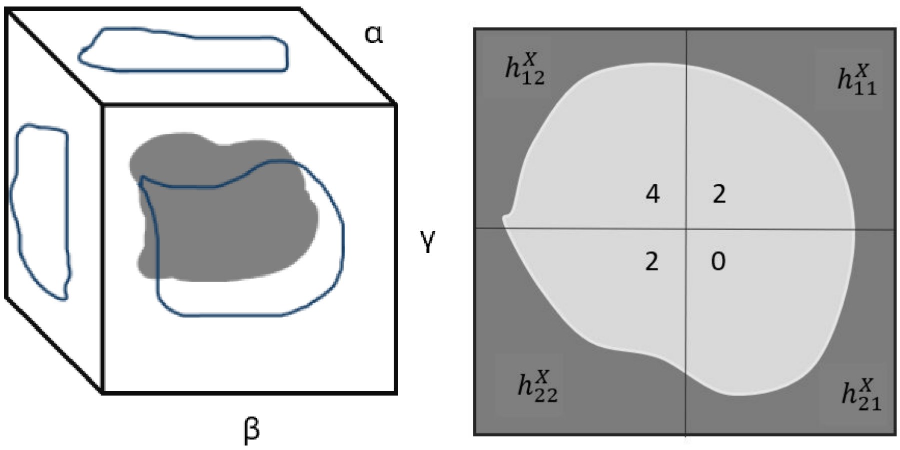

Figure 3.7: Illustration of the Hole Regions: (Left) The dark grey region represents the set Λ, depicted within the cubic representation of the LHV model. The blue contours on the faces of the cube illustrate the projections of Λ along the three hidden variables. (Right) The light grey region indicates the noiseless area where the condition 3.32 is satisfied. The dark grey areas highlight the hole regions $h^X_{\zeta_i,\zeta_j}$.

However, using this LHV model leads to a problem. When rearranging the cubic structure to construct the set Λ, it may occur that certain sets, called λ'_j are included which does not satisfy the condition specified in (3.32), but they do not result from a hole region as well. Therefore, it is necessary to appropriately adjust the set Λ

$$\Lambda \to \Lambda' := \bigcup_i \lambda_i \cup \bigcup_j \lambda'_j \tag{3.36}$$

While we are able to adjust the LHV model geometrically, we did not succeed in finding a fully consistent formulation of the constraints for the adapted LHV model. Nevertheless, we derived the necessary constraints associated with the initially constructed LHV model in the following section, with the hope that the model can either be corrected or utilized in a later work.

3.3.2 Constraints

Since the intrinsic structure of the LHV model is preserved only within the set Λ, it is necessary to derive constraints not only for the LHV model itself but also for all $\alpha_i, \beta_j, \gamma_k$, as well as for the hole regions.

Constraints on the Hidden Variables

To ensure a normalized local model, we write

$$\begin{aligned} \alpha_i, \beta_j, \gamma_k \geq 0, \quad \forall i, j, k, \\ \sum_{i=1}^{2} \alpha_i = \sum_{j=1}^{2} \beta_j = \sum_{k=1}^{2} \gamma_k = 1. \end{aligned} \tag{3.37}$$

In order to derive bounds on each of the hidden variables, we relate them to observable probabilities. Specifically, we consider instances where certain terms, such as $\alpha_1 \cdot \beta_2 \cdot 1$ and $\alpha_2 \cdot \beta_1 \cdot 1$, yield noiseless outputs, see figure 3.7. This effectively corresponds to fixing the outcome e.g. labeled '4' on face C. We write:

$$\alpha_2 \cdot \beta_1 \geq p(024) + p(042) \equiv p(c = 4). \tag{3.38}$$

Furthermore, by examining another part of C, we obtain:

$$(\alpha_2 - 1) \cdot \beta_2 \leq -\left(p(240) + p(420)\right). \tag{3.39}$$

To approximate β_1, we substitute one inequality into the other and make use of equation (3.38), resulting in:

$$\left(\frac{p(c=4)}{\beta_2} - 1\right) \beta_1 \leq -\left(p(240) + p(420)\right) \Leftrightarrow \beta_1^2 - \beta_1 + p(c = 4) \leq 0. \tag{3.40}$$

It is important to note that, within the set Λ, the equality $p(a = 4) = p(b = 4) = p(c = 4)$ holds. However, this symmetry does not persist in the set Λ'. It does not apply to $p(a = 0) = p(b = 0) = p(c = 0)$ within Λ and Λ' as well, since the total probability of obtaining outcome '0' increases under the full photon loss noise model.
The resulting quadratic inequality yields the following bounds on β_1:

$$\underbrace{\frac{1 - \sqrt{1 - 4p(c = 4)}}{2}}_{\geq 0} \leq \beta_1 \leq \underbrace{\frac{1 + \sqrt{1 - 4p(c = 4)}}{2}}_{\geq 0} \quad \Leftrightarrow \quad \left|\beta_1 - \frac{1}{2}\right| \leq \frac{1}{2}\sqrt{1 - 4p(c = 4)}. \tag{3.41}$$

Since β_1 must remain non-negative, the derived bounds hold as long as $1 - 4p(c = 4) \geq 0$. This condition is however satisfied because, by construction of the LHV model, $p(c = 4) \leq \frac{1}{4}$. This procedure can be applied to all variables ζ_i, where $i \in \{1, 2\}$, by considering analogous conditions that fix the outcome '4' on each face. The general result is then:

$$\left|\zeta_i - \frac{1}{2}\right| \leq \frac{1}{2}\sqrt{1 - 4p(x = 4)}, \quad \forall \zeta_i, x. \tag{3.42}$$

Constraints on the Hole Regions

The constraints are given by

$$0 \leq \sum_{i,j} h^X_{\zeta_i,\zeta_j} \leq 1 - Proj_{F^X}(\Lambda), \quad \forall X, \zeta_i, \zeta_j \tag{3.43}$$

$$0 \leq h^X_{\zeta_i,\zeta_j} \leq \zeta_i \cdot \zeta_j, \quad \forall X, \zeta_i, \zeta_j \tag{3.44}$$

It is worth noting that if we consider the adapted set Λ', the resulting constraints remain identical, except that in equation (3.43), one must account for the projection of Λ'. Moreover, when working with Λ', it becomes necessary to also impose bounds on the subsets λ'_j. However, due to the intricate structure of λ', only trivial bounds can be formulated, which would additionally require the introduction of a new variable without providing significant analytical insight.

Constraints on the LHV Model - LP Constraints

Due to the structural modifications of the LHV model and the additional constraints, deriving suitable conditions to demonstrate non-locality, becomes considerably more challenging than in the original framework. The definition of the distribution $q(2_i, 2_j, 2_k, \mathrm{o})$ remains consistent with the previous sections and is explicitly given by:

$$q(2_i, 2_j, 2_k, \mathrm{o}) := p(a = 2_i, b = 2_j, c = 2_k, \zeta \in S_\mathrm{O} \,|\, \zeta \in S_0 \cup S_1).$$

Here, $i, j, k \in \{L, R, B\}$ as before. The sets S_0 and S_1 are defined by $\alpha_1\beta_1\gamma_1$ and $\alpha_2\beta_2\gamma_2$ respectively.

0. Constraint (Positivity and Normalization)

$$q(2_i, 2_j, 2_k, \mathrm{o}) \geq 0 \quad \forall i, j, k, \mathrm{o} \tag{3.45}$$

$$\sum_{i,j,k,\mathrm{O}} q(2_i, 2_j, 2_k, \mathrm{o}) = \frac{p(222)}{\alpha_1\beta_1\gamma_1 + \alpha_2\beta_2\gamma_2}$$

It is important to note that this constraint is non-linear. To express it in linear form, we need to bound the hidden variables $\alpha_i, \beta_j, \gamma_k$ by applying equation (3.42). This procedure yields bounds that are linear.

Proof. The first part is due to the definition of $q(2_i, 2_j, 2_k, \mathrm{o})$. The second part is computed as follows

$$\sum_{i,j,k,\mathrm{O}} q(2_i, 2_j, 2_k, \mathrm{o}) = \sum_{i,j,k} \sum_{\mathrm{O}} \frac{p(a = 2_i, b = 2_j, c = 2_k, \zeta \in S_{\mathrm{O}})}{p(\zeta \in S_0 \cup S_1)} = \\ = \sum_{i,j,k} \frac{p(a = 2_i, b = 2_j, c = 2_k)}{\alpha_1\beta_1\gamma_1 + \alpha_2\beta_2\gamma_2} = \frac{p(222)}{\alpha_1\beta_1\gamma_1 + \alpha_2\beta_2\gamma_2}. \quad (3.46)$$

□

1. Constraint (Common Photon Cycling Direction)
The 1. constraint is given by

$$\sum_{\mathrm{O}} q(2_i, 2_j, 2_k, \mathrm{o}) = \frac{p(2_i, 2_j, 2_k)}{\alpha_1\beta_1\gamma_1 + \alpha_2\beta_2\gamma_2} \quad (3.47)$$

As before, we need to bound the hidden variables in order to obtain a linear constraint. For the proof, we proceed as follows:

Proof.

$$\sum_{\mathrm{O}} q(2_i, 2_j, 2_k, \mathrm{o}) = \sum_{\mathrm{O}} \frac{p(a = 2_i, b = 2_j, c = 2_k, \zeta \in S_{\mathrm{O}})}{p(\zeta \in S_0 \cup S_1)} = \frac{p(2_i, 2_j, 2_k)}{\alpha_1\beta_1\gamma_1 + \alpha_2\beta_2\gamma_2}. \quad (3.48)$$

□

These two constraints hold equivalently even when the set Λ' is considered for the LHV model. However, for the second constraint, this is not the case.
2. Constraint (No Influence from Unconnected Sources)
The 2. constraint is given by

$$l_\kappa \frac{l_{\alpha_1}}{u_{\alpha_2}} p(2_i, 0, 4) \leq q(2_i, \mathrm{o} = 0) \leq u_\kappa \frac{u_{\alpha_1}}{l_{\alpha_2}} \left(u_{\alpha_2} u_{\beta_2} u_{\gamma_1} - h^A_{12} l_{\alpha_2} - p(2, 0, 4) + p(2_i, 0, 4) \right), \quad (3.49)$$

$$l_\kappa \frac{l_{\alpha_2}}{u_{\alpha_1}} p(2_i, 4, 0) \leq q(2_i, \mathrm{o} = 1) \leq u_\kappa \frac{u_{\alpha_2}}{l_{\alpha_1}} \left(u_{\alpha_1} u_{\beta_1} u_{\gamma_2} - h^A_{21} l_{\alpha_1} - p(2, 4, 0) + p(2_i, 4, 0) \right), \quad (3.50)$$

$$l_\kappa \frac{l_{\beta_2}}{u_{\beta_1}} p(4, 2_j, 0) \leq q(2_j, \mathrm{o} = 0) \leq u_\kappa \frac{u_{\beta_2}}{l_{\beta_1}} \left(u_{\alpha_2} u_{\beta_2} u_{\gamma_2} - h^B_{11} l_{\beta_1} - p(4, 2, 0) + p(4, 2_j, 0) \right), \quad (3.51)$$

$$l_\kappa \frac{l_{\beta_1}}{u_{\beta_2}} p(0, 2_j, 4) \leq q(2_j, \mathrm{o} = 1) \leq u_\kappa \frac{u_{\beta_1}}{l_{\beta_2}} \left(u_{\alpha_1} u_{\beta_1} u_{\gamma_1} - h^B_{22} l_{\beta_2} - p(0, 2, 4) + p(0, 2_j, 4) \right), \quad (3.52)$$

$$l_\kappa \frac{l_{\gamma_1}}{u_{\gamma_2}} p(4, 0, 2_k) \leq q(2_k, \mathrm{o} = 0) \leq u_\kappa \frac{u_{\gamma_1}}{l_{\gamma_2}} \left(u_{\alpha_1} u_{\beta_2} u_{\gamma_2} - h^C_{12} l_{\gamma_1} - p(4, 0, 2) + p(4, 0, 2_k) \right), \quad (3.53)$$

$$l_\kappa \frac{l_{\gamma_2}}{u_{\gamma_1}} p(0,4,2_k) \leq q(2_k, \mathrm{o}=1) \leq u_\kappa \frac{u_{\gamma_2}}{l_{\gamma_1}} \left(u_{\alpha_2} u_{\beta_1} u_{\gamma_1} - h^C_{21} l_{\gamma_2} - p(0,4,2) + p(0,4,2_k) \right). \tag{3.54}$$

$l_\cdot$ and $u_\cdot$ are bounds on the hidden variables, the full notation is given in the following proof.

Proof. As in previous sections, we consider that, e.g. Alice outputs a non-zero outcome 2_i, with $i \in \{L, R, B\}$, while one of the other parties outputs 0. We take the marginal of the q-distribution, i.e. $q(2_i, \mathrm{o}=1) = \kappa \cdot p(2_i, \zeta \in S_1)$. We write $\kappa := \frac{1}{\alpha_1\beta_1\gamma_1 + \alpha_2\beta_2\gamma_2}$ for brevity. We use the following notation for the lower and upper bound of κ and ζ_i, respectively:

$$l_\kappa \leq \kappa \leq u_\kappa. \tag{3.55}$$

$$l_{\zeta_i} \leq \zeta_i \leq u_{\zeta_i} \ \forall i \tag{3.56}$$

We calculate those bounds using equation (3.42). We derive the constraints as in section 2.2 and afterwards properly bound them, since we leave out the need to explain this constraint for click/no-click detectors. We can swap the subsets of X without changing the subset Y and Z, thus if S_1 is given by the S_1 in equation 3.12, we define a set $C := X^C_\alpha \times Y^A_\beta \times Z^A_\gamma$, with $p(X^B_\alpha) \equiv \alpha_2$ such that

$$q(2_i, \mathrm{o}=1) = \kappa \cdot \frac{\alpha_2}{\alpha_1} p(2_i, \zeta \in C), \tag{3.57}$$

with $p(X^C_\alpha) \equiv \alpha_1$. Now we run into a problem, normally if we project from one subcuboid to another, we know the probability output, but since we must also consider the hole regions, it might happen, although in S_1 we initially had $p(i,2,2)$ for some given i, that in the subset C we might not get for b and c values from the projections of the set Λ, but obtain values from the hole regions. Thus we write

$$p(2_i, \zeta \in C) \equiv p_H(2_i, \zeta \in C) + p_{\not{H}}(2_i, 4, 0), \tag{3.58}$$

with the subscript H and $\not{H}$ denoting the hole region and the region of $Proj_{F^A}(\Lambda)$, respectively. To establish an lower and upper bound for the term $p_H(2_i, \zeta \in C)$, we analyze its properties.

Considering no noise, this term would vanish, setting the lower bound to 0. As for the upper bound, we can simply take $Pr(\zeta \in C) = \alpha_1\beta_1\gamma_2$ and subtract everything unrelated to p_H, we write

$$0 \leq p_H(2_i, \zeta \in C) \leq \alpha_1\beta_1\gamma_2 - h^A_{12} \cdot \alpha_1 - \sum_i p(2_i, 4, 0). \tag{3.59}$$

We thus obtain the following bound for $q(2_i, s=1)$

$$l_\kappa \frac{l_{\alpha_2}}{u_{\alpha_1}} p(2_i,4,0) \leq q(2_i, \mathrm{o}=1) \leq u_\kappa \frac{u_{\alpha_2}}{l_{\alpha_1}} \left(u_{\alpha_1} u_{\beta_1} u_{\gamma_2} - h^A_{21} l_{\alpha_1} - p(2,4,0) + p(2_i,4,0) \right). \tag{3.60}$$

The other constraints are derived similarly. □

When considering the adapted set Λ', the derivation of the second constraint remains incomplete. This is because the subsets λ'_j introduce additional regions that include noise contributions. Consequently, equation (3.58) must be adjusted to account for these effects. Moreover, appropriate bounds are required to avoid introducing an additional variable, which is necessary to preserve linearity. However, we have not identified a suitable approach.

3.4 Full Photon Loss Nonlocality via PTC Method

Although our initial approach proving noise robustness against full-photon loss was not successful, we can apply the Parity Token Counting (PTC) method instead, introduced in section 2.4, utilizing its associated constraints (2.48) and (2.51). To this end, we followed the same strategy as by Boreiri el at.[14], by directly implementing the constraints in the general defined form for a LP, see (3.61). There, they use the standard definition of a linear program.

$$\begin{aligned} \text{minimize:} \quad & c^\top x \\ \text{subject to:} \quad & Ax \leq b \\ & x \geq 0 \end{aligned} \tag{3.61}$$

b is a vector of dimension $\mathbb{R}^m$ containing the information of the probability distribution and A is a matrix of dimension $\mathbb{R}^{m\times n}$ containing all the information of the in section 2.4.2 stated constraints. For our noise model, introduced in the previous section 3.3, we need to adjust the dimensions correctly. For the first constraint (see equation (2.48)), we define three matrices

$$A_{p\,\rightarrow\,\tilde{p}}(i,j) \in \mathbb{R}^{13824\times 41472},\ A_{norm}(i,j) \in \mathbb{R}^{1\times 41472},\ A_{x_2=y_2}(i,j) \in \mathbb{R}^{1728\times 41472}. \tag{3.62}$$

These three matrices are vertically concatenated, obtaining

$$A_{\text{eq}} = \begin{bmatrix} A_{p\,\rightarrow\,\tilde{p}} \\ A_{norm} \\ A_{x_2=y_2} \end{bmatrix} \in \mathbb{R}^{(13824+1+1728)\times 41472}. \tag{3.63}$$

The second constraint (see equation (2.51)) is given by six submatrices,

$$A^x_{up}(i,j) \in \mathbb{R}^{48\times 41472},\ A^x_{down}(i,j) \in \mathbb{R}^{48\times 41472} \quad \forall x \in \{a,b,c\}. \tag{3.64}$$

Again, these matrices are vertically concatenated

$$A_{\text{ineq}} = \begin{bmatrix} A^a_{up}(i,j) \\ A^a_{down}(i,j) \\ \vdots \\ A^c_{down}(i,j) \end{bmatrix} \in \mathbb{R}^{(48\cdot 6)\times 41472}. \tag{3.65}$$

Each submatrix is associated with a corresponding vector b. The vector $b_{p\rightarrow\tilde{p}}(i) \in \mathbb{R}^{13824}$ encodes the computed probability distribution $p^{FPL}_\eta(a,b,c)$. $b_{\text{norm}} = [1]$ enforces the normalization condition, while all other b-vectors

$$b_{x_2=y_2}(i) \in \mathbb{R}^{1728},\ b^x_{up}(i), b^x_{up}(i) \in \mathbb{R}^{48} \tag{3.66}$$

consist solely of zeros. In section 6.2, we outline the calculation of the components needed to construct the LP.

Furthermore, recall that we relabeled the indices from $p(a_i, b_j, c_k) \rightarrow p(a_1, a_2, b_1, b_2, c_1, c_2) \equiv p(x_1, x_2)$, while $x_1 \in \{0, 1\}$ represents the tokens (number of photons), i.e., $a, b, c \in \{0, 4\} \rightarrow x_1 = 0$ and $a, b, c \in \{2\} \rightarrow x_1 = 1$. $x_2 \in \{0, 1, 2, ..., 11\}$ represents the additional information, i.e, which and how many photons go either to the left, the right or both detectors, leading to twelve possible outcomes.
Using the linear program, we obtain an unintuitive result (see Figure 3.8): as the degree of tilt increases, the robustness of nonlocality appears to increase as well. In particular, for $s^2 = 0.95$, the maximum robustness is reached at $\eta = 3.3\%$. Even for $s^2 = 1$, which corresponds to a product state without entanglement, the result suggests some level of noise robustness—an evidently incorrect outcome, as quantum correlations should vanish in the absence of entanglement.

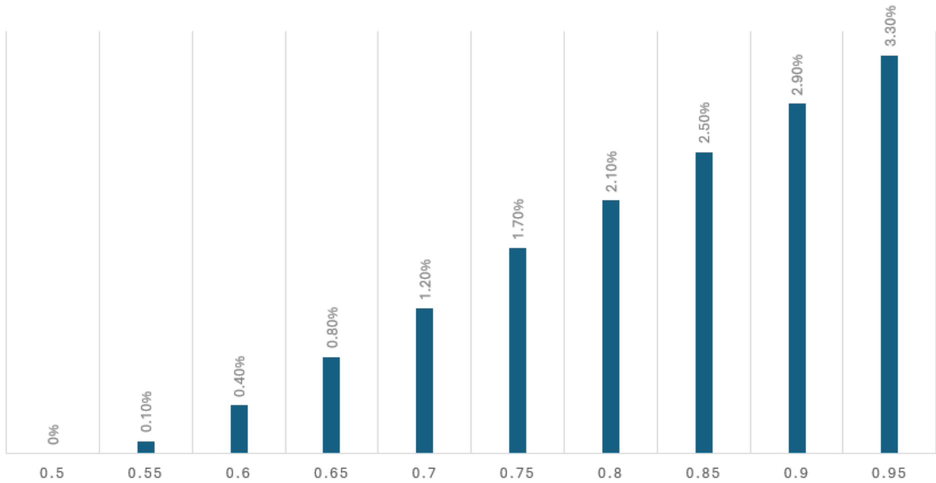

Figure 3.8: Estimated noise robustness η for different values of the tilt parameter s^2, obtained from the linear program. The result suggests that nonlocality becomes more robust as the state approaches a product state ($s^2 \rightarrow 1$). However, this behavior is nonphysical, as no quantum nonlocality should exist without entanglement.

Furthermore, it is important to note that the PTC method was also unsuccessful when applied to the noise model involving single-photon loss.
Various approaches were explored in an attempt to obtain correct results. These included adapting the code implementation, applying different coarse-graining strategies, and recalculating the probability distributions. Furthermore, the linear program was reformulated to use $p(x_2, t)$ as variables, in accordance with the constraints given in equations (2.48) and (2.51). Despite extensive efforts, no reasonable infeasible solution could be identified, although using this formulation is expected to be viable.

4 Noise-Robustness under Source Imperfection

In this chapter, we extend our analysis of network nonlocality by addressing the impact of source imperfection, building upon our previous results concerning photon loss in transmission channels. Specifically, we aim to close the detection loophole by considering spontaneous parametric down-conversion (SPDC) sources. Unlike the approach taken by Kriváchy et al.[17], which presents a more generalized framework, our analysis remains focused on the probability distribution relevant to our setup.
A similar investigation was recently published by Boreiri et al.[31]; however, our work goes beyond theoretical considerations by providing a concrete proposal for an experimental realization. In particular, we first establish a theorem demonstrating that network nonlocality can persist despite source imperfections and extend our findings to a generalized ring network with J parties. Additionally, we outline a detailed protocol for generating quantum states with two spatially entangled photons and discuss the key experimental challenges associated with such an implementation. Finally, we present a complete experimental setup for realizing a network nonlocality test within the triangle network, bridging the gap between theoretical predictions and practical feasibility.

4.1 Loophole-Free Analysis of Quantum Networks with Imperfect Sources

4.1.1 Persistence of Nonlocality in the Triangle Network

We consider the triangle network with realistic sources, allowing for the possibility that a source may fail to produce the desired NOON state. In this scenario, we focus on the case where either the intended state, a tilted NOON quantum state, is successfully created, or no photons are generated at all, corresponding to the vacuum state $|00\rangle$. We assume that the source can certify that the state generation was successful. The probability of successfully generating the desired state

$$|\psi\rangle^N = s\,|0N\rangle + r\,|N0\rangle\,,$$

is denoted by Ξ, with the probability of failure given by $1-\Xi$, where $\Xi \in [0,1]$.
For our analysis, we demand our distribution to be a TC distribution,

$$p = \{p((n_1,\alpha_1,\beta_1),(n_2,\alpha_2,\beta_2),(n_3,\alpha_3,\beta_3))\},$$

with its properties characterized in theorem 2.1.3. Here, n_j denotes the number of tokens, α_j represents additional information indicating in which of the two detectors the photons has been detected, and β_j indicates successful state generation.
To account for potential losses, we introduce classical bits that the parties count without affecting the additional information α_j. This adjustment ensures adherence to a TC strategy. The resulting density matrix, incorporating both successful state generation and failure events, is expressed as

$$\rho_\Xi = (1-\Xi)\cdot |00\rangle \langle 00|_P \otimes |\phi\rangle \langle\phi|_B + \Xi \cdot |\psi\rangle^N \langle\psi|_P^N \otimes |00\rangle \langle 00|_B \,, \tag{4.1}$$

where the subscript P refers to the photonic state, and B represents the classical bits. The state $|\phi\rangle$ is purely classical and acts as a compensation for the quantum state. For an even number of photons, each source distributes $\frac{N}{2}$ classical bits to the parties it is connected to. In the case of an odd photon number, a different strategy is needed: each source sends a fixed number of bits (N in total) to the right with probability, e.g. $p_{\text{source}} \equiv s^2$ and to the left with probability $1 - p_{\text{source}} \equiv r^2$. The number of bits and the probability values must be identical across all sources; otherwise, misalignment in the local model would prevent a proper construction.
The measurement performed by each party are given by the POVM's $\{\Pi_X^{x,\delta(\zeta_i),\delta(\zeta_j)}\}$. We define

$$\{\Pi_X^{x,\delta(\zeta_i),\delta(\zeta_j)}\} := \{\Pi_{X,P}^{x} \otimes \Pi_{X,B}^{\delta(\zeta_i),\delta(\zeta_j)}\}_{x,\delta}, \tag{4.2}$$

as the tensor product of the computational basis for the photonic and bit compensation POVM's, respectively. $\delta(\zeta) \in \{0,1\}$ denotes if the source fails ($\delta(\zeta)=1$) to generate the state $|\psi\rangle$ or succeeded ($\delta(\zeta)=0$), with $\zeta \in (\alpha,\beta,\gamma)$. The probability distribution is given by

$$p_{noise}^{\Xi}(\tilde{a},\tilde{b},\tilde{c}) = Tr\left(\rho_\Xi^{\otimes 3}\cdot \Pi_A^{a,\delta(\beta),\delta(\gamma)} \otimes \Pi_B^{b,\delta(\alpha),\delta(\gamma)} \otimes \Pi_C^{c,\delta(\alpha),\delta(\beta)}\right). \tag{4.3}$$

To construct the LHV model, we use the following approach. Let us denote the set of local hidden variables as Q. Since there is a nonzero probability that all three sources generate the desired state $|\psi\rangle$, we define the corresponding subset of Q as

$$K := \{\zeta \mid \delta(\alpha)=\delta(\beta)=\delta(\gamma)=0\}, \tag{4.4}$$

with $\Pr(\zeta\in K) = \Xi^3$ and $K \subseteq Q$. This subset retains all additional information α_j, while outside of it, we consider only the tokens.
Conversely, there is also a possibility that all three sources fail, leading to the subset

$$F := \{\zeta \mid \delta(\alpha)=\delta(\beta)=\delta(\gamma)=1\} \tag{4.5}$$

, which occurs with probability $\Pr(\zeta\in F) = (1-\Xi)^3$. Given $K \cap F = \emptyset$ and utilizing a TC strategy, the LHV model is constructed similarly as in chapter 3. Figure 4.1 provides an example for $N=2$ photons per source.

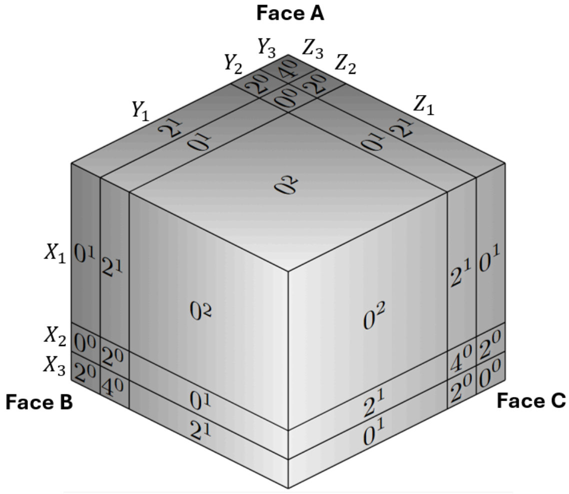

Figure 4.1: Due to TC strategy, the LHV model can be easily constructed. When setting $\Xi = 1$, we attain again the original LHV model as in figure 3.1, otherwise it remains a subcube ($K \subseteq Q$). As an example, we chose balanced quantum states, with $N = 2$ photons. The notation of the superscript $(0, 1, 2)$ to denote the addition of classical bits to the amount of photons, arriving at the parties.

For further computation, we will further describe the hidden variables α, β, γ using sets. E.g., α will be replaced by X_1, X_2 and X_3, with $\sum_i X_i = 1$, $Pr(X_1) = 1 - \Xi$, $Pr(X_2) = \Xi \cdot s^2$ and $Pr(X_3) = \Xi \cdot r^2$, where each $Pr(X_i)$ represents a segment in the model. This definition is similar for β and γ, having $P(Y_i)$ and $P(Z_i)$ respectively.
Based on this information, we present the following theorem concerning a loophole-free analysis of the triangle network in the presence of imperfect sources.

Theorem 4.1.1 (Network Nonlocality having Imperfect Sources)**.** *Consider a triangle network in which each source — α, β, and γ — distributes the mixed state given in equation* (4.1)*, while using a TC strategy. Each source is designed to generate a state, characterized by the same number of photons and the same degree of tilt. Under these conditions, the network exhibits nonlocal correlations for the same values of t and ϕ as those corresponding to the pure state $\rho_\psi = |\psi\rangle\langle\psi|$, $\forall\ \Xi \in (0, 1]$.*

Proof. We begin with the noisy probability distribution $p^{\Xi}_{\text{noise}}(\tilde{a}, \tilde{b}, \tilde{c})$, where $\tilde{a}, \tilde{b}, \tilde{c}$ are coarse-grained variables representing the photons with the additional information β_j.
When fine-graining $p^{\Xi}_{noise}(\tilde{a}, \tilde{b}, \tilde{c})$ with respect to the success/failure of each source, we write

$$\begin{aligned} p^{\Xi}_{\text{noise}}(\tilde{a}, \tilde{b}, \tilde{c}) &\equiv p^{\Xi}_{\text{noise}}(a, b, c, \delta(\alpha), \delta(\beta), \delta(\gamma)) \\ &= p_{\text{noise}}(a, b, c|\delta(\alpha), \delta(\beta), \delta(\gamma)) \cdot p^{\Xi}(\delta(\alpha), \delta(\beta), \delta(\gamma)) \end{aligned} \tag{4.6}$$

with $(\tilde{a}) = (a, \delta(\beta), \delta(\gamma))$, and respectively for $\tilde{b}$ and $\tilde{c}$. Additionally, note that if

$\delta(\alpha) = \delta(\beta) = \delta(\gamma) = 0$, then

$$p^{\Xi}(\delta(\alpha) = 0, \delta(\beta) = 0, \delta(\gamma) = 0) = \Xi^3$$

and we obtain for $p_{noise}(a, b, c|0, 0, 0)$, the original probability distribution $p(a, b, c)$, independent of Ξ.
With these definitions and the help of the LHV-model, we consider the two sets $\widetilde{S}_0 := X_3 \times Y_2 \times Z_3$ and $\widetilde{S}_1 := X_2 \times Y_3 \times Z_2$, with $\widetilde{S}_0 \cap \widetilde{S}_1 = \emptyset$ and

$$\begin{aligned} Pr(X_3) = Pr(Y_2) = Pr(Z_3) = \Xi \cdot s^2, \\ Pr(X_2) = Pr(Y_3) = Pr(Z_2) = \Xi \cdot r^2. \end{aligned} \tag{4.7}$$

All (NNN) events only happen iff $\zeta \in \widetilde{S}_0 \cup \widetilde{S}_1$. We define

$$q(N_i, N_j, N_k, \mathrm{o}) := p^{\Xi}_{noise}(a = N_i, b = N_j, c = N_k, \zeta \in \widetilde{S}_{\mathrm{O}} | \zeta \in \widetilde{S}_0 \cup \widetilde{S}_1)$$

$$= \frac{1}{\Xi^3 \cdot (s^6 + r^6)} \cdot p^{\Xi}_{noise}(a = N_i, b = N_j, c = N_k, \zeta \in \widetilde{S}_{\mathrm{O}}), \quad i, j, k \in \{L, R, B\} \tag{4.8}$$

The transformation step utilizes the probabilities $Pr(\zeta \in \widetilde{S}_0)$ and $Pr(\zeta \in \widetilde{S}_1)$, which are defined by the equations (4.7). Consequently, we obtain the probability for the union of the sets $\widetilde{S}_0$ and $\widetilde{S}_1$

$$Pr(\zeta \in \widetilde{S}_0 \cup \widetilde{S}_1) = \Xi^3 \cdot (s^6 + r^6).$$

Using equation (4.6), we sum over s, thus obtaining the first constraint

$$\sum_{\mathrm{O}} q(N_i, N_j, N_k, \mathrm{o}) = \frac{1}{\Xi^3 \cdot (s^6 + r^6)} \cdot p^{\Xi}_{\text{noise}}(N_i, N_j, N_k)$$

$$= \frac{1}{\Xi^3 \cdot (s^6 + r^6)} \cdot p_{\text{noise}}(N_i, N_j, N_k | 0, 0, 0) \cdot p^{\Xi}(\delta(\alpha) = 0, \delta(\beta) = 0, \delta(\gamma) = 0) \tag{4.9}$$

$$= \frac{1}{s^6 + r^6} \cdot p(N_i, N_j, N_k), \quad \forall i, j, k.$$

For the second constraint, we write

$$\sum_{j,k} q(N_i, N_j, N_k, \mathrm{o} = 0) = q(N_i, \mathrm{o} = 0) = \frac{1}{\Xi^3 \cdot (s^6 + r^6)} p^{\Xi}_{noise}(a = N_i, \zeta \in S_0) \tag{4.10}$$

Assume, we fix some specific i on the face of Alice. Extending along, e.g. $\widetilde{S}_0$, this probability can be expressed as a volume V_1, with $V_1 \subset \widetilde{S}_0$. We want to find relation to the volume (V_2) underneath it, that still is in K. Since the area of the chosen i on the face of Alice is the same, only the height of the volume V_2 might change, thus we write

$$\frac{1}{\Xi^3 \cdot (s^6 + r^6)} \cdot p^{\Xi}_{noise}(a = N_i, \zeta \in \widetilde{S}_0) = \frac{1}{\Xi^3 \cdot (s^6 + r^6)} \cdot \frac{Pr(X_2)}{Pr(X_3)} \cdot p^{\Xi}_{noise}(a = N_i, \zeta \in C). \tag{4.11}$$

, with $C := X_3 \times Y_3 \times Z_2$ ($V_2 \subset C \subset K$) denoting the subcube with the output $p^{\Xi}_{noise}(N, 2N, 0)$. We know that $Pr(X_2) = \Xi \cdot s^2$ and $Pr(X_3) = \Xi \cdot r^2$ and since the probability in (4.11) has again the prefactor Ξ^3, we obtain

$$q(N_i, \mathrm{o} = 0) = \frac{1}{s^6 + r^6} \cdot \frac{s^2}{r^2} \cdot p(a = N_i, \zeta \in C) \quad \forall i. \tag{4.12}$$

Note that this procedure holds also for all j, k and for $\mathrm{o} = 1$. Thus, all constraints are independent of Ξ, and thus we have the same constraint structure as we would have for $\Xi = 1$. We can conclude that we obtain non-locality for all Ξ beside 0 as long as we have non-locality for specific t and ϕ values. $\square$

Remark 1: Intuitively, this can be understood as follows: Any nonlocality region within Q must originate from the subset K. This is because only within K can the faces be distinguished based on the additional information α_j. Outside of K, such information does not exist, as we solely count the tokens n_j.
Remark 2: Note that this theorem only is correct for $N \geq 2$ photons per source. For one photon, it is not possible to well-define equation 4.1, due to $|\phi\rangle\langle\phi|$, since the token counting theorem does not allow sending non-integer tokens into the network.

4.1.2 Generalization to a Ring Network with J Parties

Theorem 4.1.1 can be extended to a ring network consisting of J sources S_j and J parties A_j. Those J parties share a copy of the tilted NOON state for each couple of neighboring parties $A_j A_{j+1}$.The measurement basis $\{\Pi_X^{x,\delta(\zeta_i),\delta(\zeta_j)}\}$ is identical as in equation 4.2. Additionally note that this distribution is again a TC distribution, $p = \{p((n_1, \alpha_1, \beta_1), ..., (n_J, \alpha_J, \beta_J))\}$. Since we employ a TC strategy, constructing the LHV model becomes straightforward, as discussed in section 3.1.

Proof. Due to these constraints, we define a set K', which is a subset of the set of the local hidden variables Q':

$$K' := \{\zeta' | \delta(\alpha_{12}) = \delta(\alpha_{23}) = ... = \delta(\alpha_{J1}) = 0\}, \tag{4.13}$$

where $\zeta' = (\alpha_{12}, \alpha_{23}, ..., \alpha_{J1})$, with $Pr(\zeta' \in K') = \Xi^J$ and $K' \subseteq Q'$. Again, the subset K' retains exclusively all the additional information α_j. Similarly as before, each source defines again a set. We denote them as P_i^{μ}, with $\mu = \{1, 2, ..., J\}$ and $i \in \{1, 2, 3\}$. These sets have equivalent properties as in the previous section:

$$\begin{aligned}
&\mathrm{Pr}(P_1^{\mu}) = \Xi \cdot s^2, \quad \forall \mu, \\
&\mathrm{Pr}(P_2^{\mu}) = \Xi \cdot r^2, \quad \forall \mu, \\
&\mathrm{Pr}(P_3^{\mu}) = 1 - \Xi, \quad \forall \mu, \\
&\sum_i P_i^{\mu} = 1, \quad \forall \mu.
\end{aligned} \tag{4.14}$$

Similarly, we denote the noisy probability distribution as $p^{\Xi}_{noise}(\tilde{a_1}, \tilde{a_2}, ..., \tilde{a_J})$. When fine-graining with respect to the success/failure of each source, we write

$$\begin{aligned} p^{\Xi}_{\text{noise}}(\tilde{a_1}, ..., \tilde{a_J}) &\equiv p^{\Xi}_{\text{noise}}(a_1, ..., a_J, \delta(\alpha_{12}), ..., \delta(\alpha_{J1})) \\ &= p_{\text{noise}}(a_1, , ..., a_J | \delta(\alpha_{12}), ..., \delta(\alpha_{J1})) \cdot p^{\Xi}(\delta(\alpha_{12}), ..., \delta(\alpha_{J1})). \end{aligned} \tag{4.15}$$

Hereby, note that $p^{\Xi}(\delta(\alpha_{12}) = ... = \delta(\alpha_{J1}) = 0) = \Xi^J$.
In the ring network the $(a_1 = N, a_2 = N, .., a_J = N)$ event is again only possible, if either all photons move to the left or to the right. We define the sets S'_0 and S'_1 as follows

$$S'_0 := \bigtimes_{\mu=1}^{J} P^{\mu}_1, \tag{4.16}$$

$$S'_1 := \bigtimes_{\mu=1}^{J} P^{\mu}_2. \tag{4.17}$$

Subscripts 1 and 2 are simply chosen for simplicity. We define

$$q(i_1, i_2, ..., i_N, \mathrm{o}') = p(a_1 = i_1, a_2 = i_2, ..., a_N = i_N, \zeta' \in S'_{\mathrm{O}'} | \zeta' \in S'_0 \cup S'_1). \tag{4.18}$$

Simplifying equation (4.18) using $Pr(\zeta' \in K') = \Xi^J \cdot (s^{2J} + r^{2J})$, leads to

$$q(i_1, i_2, ..., i_N, \mathrm{o}') = \frac{1}{\Xi^J \cdot (s^{2J} + r^{2J})} \cdot p(a_1 = i_1, a_2 = i_2, ..., a_N = i_N, \zeta' \in S'_{\mathrm{O}'}). \tag{4.19}$$

When summing over o', we obtain

$$\begin{aligned} \sum_{\mathrm{O}'} q(i_1, ..., i_J, \mathrm{o}') &= \frac{1}{\Xi^J \cdot (s^{2J} + r^{2J})} \cdot p^{\Xi}_{\text{noise}}(i_1, ..., i_J) \\ &= \frac{1}{\Xi^J \cdot (s^{2J} + r^{2J})} \cdot p_{\text{noise}}(i_1, ..., i_J | 0, ..., 0) \cdot p^{\Xi}(\delta(\alpha_{12}) = ... = \delta(\alpha_{J1}) = 0) \\ &= \frac{1}{s^{2J} + r^{2J}} \cdot p(i_1, ..., i_J), \quad \forall i_1, ..., i_J. \end{aligned} \tag{4.20}$$

For the second constraint, we sum over all i_j except for i_k, yielding

$$\begin{aligned} \sum_{i_1,...,i_{k-1},i_{k+1},...,i_J} q(i_1, \ldots, i_k, \ldots, i_N, \mathrm{o}' = 0) &= q(i_k, \mathrm{o}' = 0) \\ &= \frac{1}{\Xi^J \cdot (s^{2J} + r^{2J})} p^{\Xi}_{\text{noise}}(a_k = i_k, \zeta' \in S_0). \end{aligned} \tag{4.21}$$

Now, we define a set

$$\mathcal{Y} := \left\{ \zeta' \mid \delta(\alpha_{12}) = \cdots = \delta(\alpha_{J1}) = 0, \ \zeta' \in K' \setminus (S'_0 \cup S'_1) \right\}.$$

This set is defined to include all possible outcomes in which all sources successfully generate the desired quantum state, while not all of the parties necessarily receive N photons as an outcome.
We transition from the subset S_0 to an element in $\mathcal{Y}$, denoted as Y $(Y \subset \mathcal{Y})$. We write

$$\frac{1}{\Xi^J \cdot (s^{2J} + r^{2J})} \cdot p^{\Xi}_{noise}(a_k = i_k, \zeta' \in S_0) = \frac{1}{\Xi^J \cdot (s^{2J} + r^{2J})} \cdot \frac{Pr(P_1^k)}{Pr(P_2^k)} \cdot p^{\Xi}_{noise}(a_k = i_k, \zeta' \in Y), \tag{4.22}$$

with $Y := P_1^1 \times ... \times P_2^k \times ... \times P_1^J$. With equations (4.14) we can simplify the term on the right side, obtaining

$$q(i_k, \mathrm{o}' = 0) = \frac{1}{s^{2J} + r^{2J}} \cdot \frac{s^2}{r^2} \cdot p(a_k = i_k, \zeta' \in Y). \tag{4.23}$$

This procedure holds for all $i_1, ..., i_J$ and $\mathrm{o}' = 1$. Once again both constraints are independent of Ξ, leading to the same constraints necessary to have in order to prove potential nonlocality in a ring network with J parties and with perfect sources. $\square$

4.2 Quantum State Generation

Based on theorem 4.1.1, we presents in this following section an experimental setup in order to generate NOON states. Building upon the analysis conducted in chapter 3, we consider the case of $N = 2$ photons per source. However, we also allow the quantum state to be tilted, thereby introducing two distinct setups: one for balanced quantum states and another for tilted quantum states. In addition to the theoretical analysis, we address the practical challenges that may arise when implementing the quantum state generation setup. These include potential issues such as photon loss, detector efficiency, and the required independence of the three sources for the setup.
It is important to highlight that while the proposed setup is a concrete example, other setups could also be considered as long as they align with the principles outlined in theorem 4.1.1.
Section 4.2.1 contains the same content as the publication by Krivác̆hy et al.[17]

4.2.1 Setup for Generating Balanced and Tilted Quantum States

In this section we propose a setup using heralded single-photon sources at each node of the triangle network in order to generate spatially-entangled quantum states of the form

$$|\psi\rangle \propto |02\rangle + |20\rangle \,. \tag{4.24}$$

Figure 4.2 illustrates the fundamental setup for generating spatially entangled photon pairs.

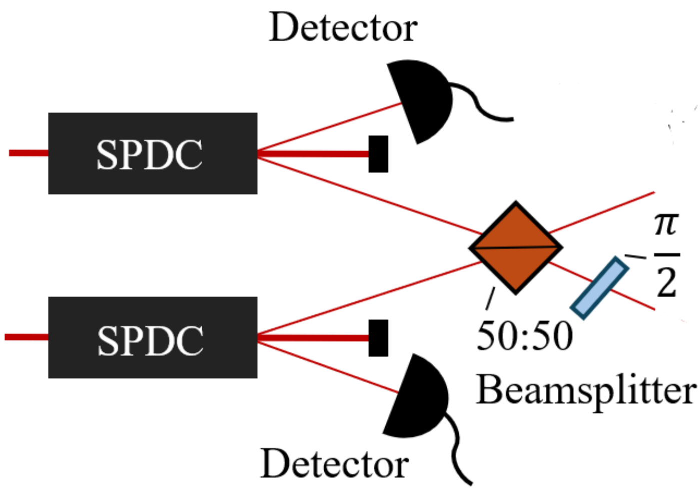

Figure 4.2: Generating balanced quantum states: two SPDC sources generate photon pairs, of which two interfere at a 50:50 beamsplitter, harnessing the Hong-Ou-Mandel effect. The detectors measure the remaining two photons to ensure a classical communication channel to those parties the source is connected with[17].

In this setup, each source is equipped with two heralded single-photon emitters (SPDC crystals). Each of them has a probability of ξ to create a pair of photons. When two photons are successfully created at a given source, they can be used to generate the state. While a naive implementation would still require global post-selection to ensure simultaneous photon generation across all sources, we exploit the theorems 2.1.3 and 4.1.1 to eliminate this need.

The key insight is that each source can locally communicate its heralding information to the two parties it is connected with. This ensures that the resulting distribution adheres to a token-counting structure, where the presence of photons in specific modes follows strict combinatorial constraints. As a result, the experiment remains robust against imperfect sources while maintaining triangle network nonlocality. Crucially, due to theorem 4.1.1 this approach preserves the integrity of the nonlocal correlations without introducing experimental loopholes arising from global post-processing.

To ensure consistency between the experimental setup and the underlying theoretical framework, we address the following key aspects: Firstly, the noise parameter Ξ is now denoted by ξ, since two SPDC crystals are involved and as they may not have identical probabilities of heralding a photon pair, we refine the noise parameters' definition as

$$\Xi \rightarrow \xi_1 \cdot \xi_2. \tag{4.25}$$

Secondly, since each source is assumed to communicate with its connected parties, it is essential that one photon per pair is detected by a photon detector. This detector classically transmits information about whether a photon pair has been generated. Only if both detectors—one for each crystal—register a photon, we can confirm that the state $|\psi\rangle$ has been created. In all other cases, no photons are allowed to reach the parties, as each source is equipped with a shutter that blocks the photonic paths. Nevertheless, each party then receives a classical bit, thereby ensuring the conservation of the total number of tokens.

Finally, we emphasize that the photons produced by the two SPDC sources and but not measured by the detectors must be indistinguishable. This requirement allows us to direct them to a balanced 50:50 beam splitter, where, due to the Hong-Ou-Mandel effect, the resulting state is given by

$$|\psi_{bal}\rangle = \frac{1}{\sqrt{2}}(|02\rangle + |20\rangle).$$

Note that a phase shifter must be applied in the second mode to obtain the desired state. To generate tilted quantum states, we modify the setup to allow for controlled variation of a tilt parameter. Figure 4.3 depicts the setup for generating tilted quantum states.

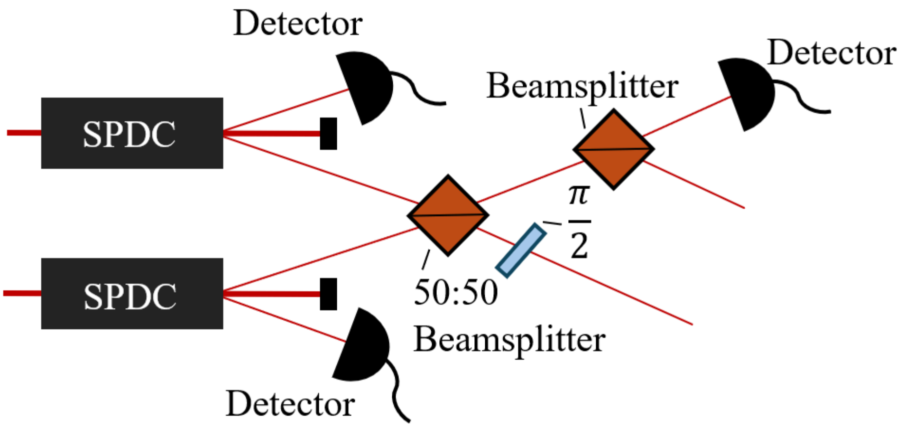

Figure 4.3: Generating tilted quantum states: an additional beam splitter is introduced in one of the output modes, while the third mode is measured to post-select the desired outcome, providing control over the degree of tilt[17].

Specifically, we introduce an additional beam splitter after the first one in e.g. the left mode.
Initially, the system produces the state:

$$\frac{1}{\sqrt{2}}|020\rangle + \frac{1}{\sqrt{2}}|200\rangle.$$

By adding an extra beam splitter, an additional degree of freedom is introduced, leading to the transformed state

$$\frac{1}{\sqrt{2}}(a|011\rangle + b|002\rangle + c|020\rangle) + \frac{1}{\sqrt{2}}|200\rangle.$$

We then measure the newly introduced third mode. If the measurement outcome is 0, we consider the process to be successful. However, if the measurement yields 1 or 2, the attempt is discarded. This post-selection results in the state

$$\frac{1}{\sqrt{2}}c|020\rangle + \frac{1}{\sqrt{2}}|200\rangle.$$

After discarding the now-trivial third mode and renormalizing the coefficients, we obtain a tilted quantum state

$$|\psi_{tilt}\rangle = \frac{c}{\sqrt{c^2+1}} \cdot |02\rangle + \frac{1}{\sqrt{c^2+1}} \cdot |20\rangle . \tag{4.26}$$

The degree of tilt can be adjusted by altering the transmissivity of the second beam splitter, which is effectively controlled by the coefficient c in the final expression.

4.2.2 Experimental Setup and its Practical Challenges

Given the results of this and the previous chapter, we can now propose an experimental setup that eliminates the need for global postprocessing and, consequently, the associated loopholes. In particular, we note that two of the three noise parameters—detector efficiency (ν) and source imperfections (Ξ)—are not expected to pose fundamental obstacles to a realistic experimental implementation. The assessment concerning detector efficiency is supported by several experimental studies[20 21 22]. While photon loss in the transmission channel remains a significant challenge, our analysis nonetheless indicates a certain degree of robustness against the dominant form of noise.

By utilizing our source setup into the triangle framework introduced in chapter 2 (see figure 2.3), we arrive at the following experimental configuration:

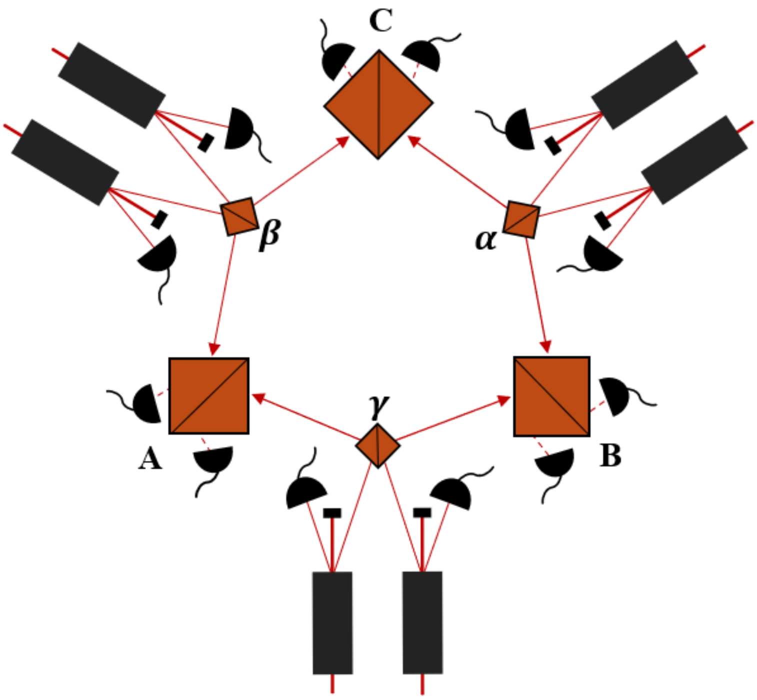

Figure 4.4: Triangle Network Experimental Setup with Refined Source Implementation: The experimental setup considered here is based on the proposal by Abiuso and Kriváchy et al.[13], with an important refinement regarding the implementation of the sources. We introduce the setup shown in figure 4.2, in which each source α, β, γ generates balanced quantum states. This choice is motivated by two main factors: balanced quantum states have been shown to offer the best robustness to noise in the channels, and their experimental realization is more straightforward. For simplicity and clarity of presentation, we omit the phase shifter from the sketch, as it plays no essential role in this schematic setup. The figure shown is intended as a conceptual illustration.

Although the generation of the quantum state appears promising, several theoretical challenges must still be addressed. These include photon loss at the sources, detector failures, the production of additional photons, and the independence of the sources. In the following, we will discuss five potential issues from a theoretical perspective and present corresponding solutions.

Issue I: Detector Efficiency
Although modern detectors achieve very high efficiencies —- up to 99%[20 21 22] – a small possibility of photon loss during detection still remains. Given that each source may involve up to three detectors, this issue must be taken into account. Fortunately, there is a simple solution: whenever a photon is not detected, the underlying mechanism informs the parties that state generation was unsuccessful, even when it actually succeeded. We note that this introduces an additional probability $p_{\text{loss,det}}$ into equation (4.25), accounting for potential photon loss at the detectors.

Issue II: Generation of two-photon Pairs
When using a nonlinear crystal to herald a photon pair, there remains a very small probability of generating two-photon pairs, occurring with probability ξ_1^2 (and ξ_2^2). Since our protocol strictly requires an equal number of photons at each source α, β, γ, this issue must be addressed. A solution is to use photon-number-resolving detectors: whenever a detector registers more than one photon, the connected parties are informed that state generation was unsuccessful. To account for higher-order photon generation, we introduce another additional probability p_{ξ^2} into our analysis.

Issue III: Independence of the Sources
In the context of the triangle network, a fundamental requirement is that the sources must be independent, ensuring there is no hidden coordination or correlation between them. To achieve this independence, one potential method is to employ a technique similar to that used by Wang et al.[15] Specifically, they utilized a Quantum Random Number Generator (QRNG) to produce random numbers. Each QRNG generates values between 0 and 1, which are then mapped to specific angles, with a precision of 0.01°. These angles are used to tilt an optical window in the system. This random variation in the optical window's tilt results in random phase shifts being applied to the pump beam, with phase shifts ranging from 0 to 2π. By employing such a method, the sources' actions remain statistically independent, ensuring that the network operates without any unintended correlations between the source elements.

Issue IV: Using Hong-Ou-Mandel Effect (Creating Spatially-entangled Photons)
In the context of our current understanding and the ability to generate spatially entangled photons, we can affirm that the state $|\psi\rangle$ is achievable, as demonstrated by several experimental works[32 33 34 35]. These studies confirm that the generation of spatially entangled photons is nowadays experimentally feasible.

Issue V: Photon Loss during Quantum State Generation
Photon loss at the sources can occur both during transmission to the detectors and in

the process of generating the quantum state $|\psi\rangle$. In order to distinguish these cases, we define two types of photons: the heralding photons, which travel to the detectors, and state-photons, which are the actual entangled state. In both scenarios, photon loss is a potential concern. Therefore, the photons are emitted into free space at the point of state generation, as there are no further interactions.
To minimize photon loss in free space, we consider the probability of photon loss:

$$p_{\text{loss}} = 1 - T_{\text{optical}} \cdot T_{\text{medium}} \tag{4.27}$$

where T_{optical} accounts for diffraction and aperture losses, and T_{medium} represents transmission efficiency in the medium. Since the photons move in free space, we can set $T_{\text{medium}} \approx 1$. To maximize T_{optical} to 1, diffraction must be minimized, alignment needs to be optimized, and proper mode matching must be ensured.
For detector-photons, occasional loss is inconsequential since undetected photons simply result in the detectors informing the parties that state generation was unsuccessful. In this case, no photons enter the connected parties, ensuring that lost detections do not disrupt the experiment.
A more critical issue arises in rare cases where one SPDC crystal produces an unwanted 2-2 photon pair. If one of the detector-photons is lost when entering the fiber, the detector register only a single photon instead of both. This results in the source generating a three-photon state, and since the first two detectors confirm detection, the remaining photons are allowed to enter the system. This scenario violates theorem 4.1.1. While this event is unlikely, it remains possible over many experimental rounds. Unfortunately, we have not found a solution to resolve this issue.
Thus, most of these issues can be resolved or ruled out, but the probability of successful state creation, decreases

$$\Xi \to \xi_1 \cdot \xi_2 \cdot p_{\text{loss,det}} \cdot p_{\xi^2} \cdot (1 - p_{loss}) \sim \xi_1 \cdot \xi_2 \cdot p_{\text{loss,det}} \cdot p_{\xi^2} \cdot T_{\text{optical}}. \tag{4.28}$$

5 Summary and Discussion

In this work, we investigate network nonlocality in the triangle scenario from the single- to the multi-photon regime by constructing a local hidden variable model for generalized NOON states and demonstrating nonlocality for two photons per source. We analyze the effect of single-photon loss in transmission channels and show robustness to noise up to 10.3% in the photon number resolving and up to 6.7% in the click/no-click regime. Although our initial attempt to address full photon loss is not successful, it provides valuable insights into constructing such models. We also address source imperfections and show that, even when the sources fail to produce the desired states, nonlocality can still be observed, independent of the amount of noise. Together with the noise-robustness, we manage to resolve the detection loophole. Moreover, we show the same results for a ring network with J parties. Furthermore, we propose an experimental scheme based on heralded spatial entanglement via SPDC, which circumvents the need for global post-processing by using failure bits to certify unsuccessful events. These results advance the feasibility of a loophole-free experimental demonstration of triangle network nonlocality.

As mentioned in section 1.4.4, the content of this work has been prepared simultaneously with the publication *Closing the detection loophole in the triangle network with high-dimensional photonic states* by Kriváchy et al.[17] It is important to note that the results formulated in this thesis are included in this publication if they have led to new significant insights. In the publication[17], the authors demonstrate noise robustness by introducing a critical output, defined as a specific measurement outcome—either 0 or 4 photons—that plays a crucial role for constructing a LHV model. While in this thesis, except for section 3.3 and 3.4, we consider scenarios in which the probability of the critical output appearing simultaneously for any two parties in a given round is always zero, the authors show that nonlocality can still be certified without imposing such constraints. In particular, they demonstrate this for tilted quantum states under single-photon loss, as well as in the regime of full photon loss. Notably, in the case of full photon loss, they achieve maximum noise robustness at $\eta = 99.86\%$. Moreover, using the method briefly discussed in section 1.4.2, it is shown that for a realistic noise model, neural network-based heuristics give approximately 50% robustness. Furthermore, theorem 2.1.3 has been generalized to apply to any distribution in the publication by Kriváchy et al.[17], collectively reinforcing the results of this thesis.

To extend the findings of this work, we could explore the possibility of detecting nonlocality for higher orders of N, and evaluate this within the context of our single-photon noise model, or perhaps an $N-1$ photon noise model, which on the one hand preserve the probabilities of the zero outcome while on the other hand potentially increases nonlocality.

Additionally, we could apply the inflation technique as described by Pozas-Kerstjens et al.[9] to extend or enhance the range of nonlocality for $N = 2$ photons per source.

Although we are able to close the detection loophole, several other issues remain unresolved, leaving room for future investigation. For instance, throughout this work, we consistently assume independent and identically distributed (i.i.d.) behavior across each experimental round. However, in realistic scenarios, this assumption may not hold. Deviations from the i.i.d. assumption give rise to so-called memory attacks, in which hidden internal memory introduces correlations between rounds. As a result, the observed correlations can no longer be reliably interpreted as genuine nonlocality, as they could potentially be mimicked by classical mechanisms that exploit these inter-round dependencies[36].

Finally, demonstrating such robustness to photon loss would be valuable not only for the specific distribution studied here, but also for the implementation of other types of distributions. While source imperfection has already been addressed in recent works[31,17], it would be interesting to explore the impact of other loss parameters. In light of the rapid advancement of quantum technologies, it remains an open and compelling question whether analogous robustness can be achieved.

6 Appendix

In this chapter, we present supplementary discussions that are not included in the main text to maintain readability. Section 6.1 covers the computation of the probability distribution, based on Kriváchy et al.[17] Section 6.2 discusses the fundamental components required to construct the linear program used in the publication by Boreiri et al.[14]

6.1 Computing Probability Distribution

We present the method used to compute the noiseless output distribution $p(a, b, c)$ for NOON states, where $a, b, c \in \{0, N, 2N\}$ (or $a, b, c \in \{0, L, R, 2\}$ in the case of click/no-click detectors). The transformation of a beamsplitter with transmissivity t and phase ϕ is described in terms of the creation operators $a^\dagger$ as follows:

$$\begin{pmatrix} a_2^\dagger \\ a_1^\dagger \end{pmatrix}_i = \begin{pmatrix} \sqrt{t} & -e^{-i\phi}\sqrt{1-t} \\ e^{i\phi}\sqrt{1-t} & \sqrt{t} \end{pmatrix}_B \begin{pmatrix} a_2^\dagger \\ a_1^\dagger \end{pmatrix}_o . \tag{6.1}$$

Using this transformation, we express the state transformation as

$$|mn\rangle = \frac{1}{\sqrt{m!n!}} \left[\sqrt{t}a_2^\dagger - e^{-i\phi}\sqrt{1-t}a_1^\dagger\right]^m \left[e^{i\phi}\sqrt{1-t}a_2^\dagger + \sqrt{t}a_1^\dagger\right]^n |00\rangle. \tag{6.2}$$

For practical convenience, we define $u := \sqrt{t}$, $l^* := e^{-i\phi}\sqrt{1-t}$ and $l^* := e^{i\phi}\sqrt{1-t}$, and rewrite the equation using the binomial theorem:

$$\begin{aligned} |mn\rangle_i = \sum_{k=0}^{m}\sum_{q=0}^{n} \frac{m!}{k!(m-k)!}\frac{n!}{q!(n-q)!}\sqrt{(m+n-(k+q))!}\frac{\sqrt{(k+q)!}}{\sqrt{m!n!}}(-1)^{m-k} \\ \cdot\, u^{k+n-q}\, l^{m-k}\, l^{*q}\, |k+q, m+n-(k+q)\rangle_o. \end{aligned} \tag{6.3}$$

The output state $|.\rangle_o$ represents the photon number distribution at the output ports. To obtain the relevant POVMs $\{\Pi_x^X\}$ for $N = 2$ photons per source, we derive equations (6.4) - (6.7).

$$|00\rangle_i = |00\rangle_o, \tag{6.4}$$

$$|02\rangle_i = t|02\rangle_o + \sqrt{2t\tau}e^{i\phi}|11\rangle_o + \tau e^{2i\phi}|20\rangle_o, \tag{6.5}$$

$$|20\rangle_i = \tau|02\rangle_o - \sqrt{2t\tau}e^{-i\phi}|11\rangle_o + te^{-2i\phi}|20\rangle_o, \tag{6.6}$$

$$\begin{aligned} |22\rangle_i = \sqrt{6}t\tau\left(e^{-2i\phi}|04\rangle_o + e^{2i\phi}|40\rangle_o\right) + \sqrt{6}\left(\sqrt{t}\tau^{\frac{3}{2}} - t^{\frac{3}{2}}\sqrt{\tau}\right)e^{-i\phi}|13\rangle_o + \\ \left(t^2 - 4t\tau + \tau^2\right)|22\rangle_o + \sqrt{6}\left(t^{\frac{3}{2}}\sqrt{\tau} - \sqrt{t}\tau^{\frac{3}{2}}\right)e^{i\phi}|31\rangle_o. \end{aligned} \tag{6.7}$$

Those equations allow us to construct the POVMs $\{\Pi_X^x\}$. As initial state we write tilted NOON-state as

$$|\psi\rangle^N = s\,|0N\rangle + r\,|N0\rangle\,, \tag{6.8}$$

with $s^2 + r^2 = 1$ and $s, r \in \mathbb{R}$. The global initial state is given by

$$|\Psi\rangle^N_{A_1A_2B_1B_2C_1C_2} \equiv |\psi\rangle^N_{A_2B_1} \otimes |\psi\rangle^N_{B_2C_1} \otimes |\psi\rangle^N_{C_2A_1}.$$

The distribution $p(a,b,c)$ is given by

$$p(a,b,c) = Tr\left(|\Psi\rangle^N \langle\Psi|^N \cdot \left(\Pi^a_{A_1,A_2} \otimes \Pi^b_{B_1,B_2} \otimes \Pi^c_{C_1,C_2}\right)\right). \tag{6.9}$$

By applying equations (6.4)–(6.7) for $N = 2$ photons per source, in conjunction with equation (6.9), we obtain the probability distribution $p(a,b,c)$:

$$p(2_L,2_L,2_L) = s^6t^6 + r^6\tau^6 + 2s^3r^3t^3\tau^3\cos(6\phi)$$

$$p(2_R,2_R,2_R) = s^6\tau^6 + r^6t^6 + 2s^3r^3t^3\tau^3\cos(6\phi)$$

$$p(2_L,2_R,2_R) = t^2\tau^2\left(s^6\tau^2 + r^6t^2 + 2s^3r^3t\tau\cos(6\phi)\right)$$

$$p(2_L,2_R,2_L) = t^2\tau^2\left(s^6t^2 + r^6\tau^2 + 2s^3r^3t\tau\cos(6\phi)\right)$$

$$p(2_B,2_R,2_R) = 2t\tau\left(r^6t^4 + s^6\tau^4 - 2s^3r^3t^2\tau^2\cos(6\phi)\right)$$

$$p(2_B,2_L,2_L) = 2t\tau\left(r^6\tau^4 + s^6t^4 - 2s^3r^3t^2\tau^2\cos(6\phi)\right)$$

$$p(2_B,2_B,2_L) = 4t^2\tau^2\left(r^6\tau^2 + s^6t^2 + 2s^3r^3t\tau\cos(6\phi)\right)$$

$$p(2_B,2_B,2_R) = 4t^2\tau^2\left(r^6t^2 + s^6\tau^2 + 2s^3r^3t\tau\cos(6\phi)\right)$$

$$p(2_B,2_L,2_R) = p(2_B,2_R,2_L) = 2t^3\tau^3\left(r^6 + s^6 - 2s^3r^3\cos(6\phi)\right)$$

$$p(2_B,2_B,2_B) = 8t^3\tau^3\left(r^6 + s^6 - 2s^3r^3\cos(6\phi)\right)$$

$$p(2_B,0,4) = 2s^2r^4t\tau \quad p(2_B,4,0) = 2s^4r^2t\tau$$

$$p(2_L,4,0) = s^4r^2t^2 \quad p(2_L,0,4) = s^2r^4\tau^2 \quad p(2_R,0,4) = s^2r^4t^2 \quad p(2_R,4,0) = s^4r^2\tau^2$$

Note that we coarse-grain $p(a,b,c)$ into the outcome set $\{0, 2_L, 2_R, 2_B, 4\}$. Furthermore, when formulating the LP, we can further simplify the notation and the calculation of the probability distribution by utilizing equations (2.9) and (2.10). Specifically, by deriving the corresponding u_i and v_i values as in equations (6.5) and (6.6), we recover the same probability structure as in (2.9) and (2.10).

By incorporating the noise parameter η through the Kraus operators into the calculation of the probability distribution, it suffices to modify equations (6.4)–(6.7), while the remaining procedure remains unchanged.

6.2 Construction of the LP using PTC Method

In this section we define the exact construction of the matrices and the vector $b_{p \to \tilde{p}}$ introduced in section 3.4. Recall that $x_i \equiv \{a_i, b_i, c_i\}$, with $x_1 \in \{0, 1\}$ and $x_2 \in \{0, 1, ..., 11\}$. Note that $|a_1| \cdot |a_2| \cdot |b_1| \cdot |b_2| \cdot |c_1| \cdot |c_2| = 13824$.

$$A_{p \to \tilde{p}}(i,j) := \begin{cases} 1 & \text{if } j = 1152a_2 + 96b_2 + 8c_2 + 4t_a + 2t_b + t_c, \\ & \quad i = 6912a_1 + 576a_2 + 288b_1 + 24b_2 + 12c_1 + c_2, \\ & \quad \text{and parity conditions hold;} \\ f(\varepsilon) & \text{if } j = i + 13824; \\ -f(\varepsilon) & \text{if } j = i + 13824 \cdot 2; \\ 0 & \text{otherwise.} \end{cases}$$

$$A_{norm}(1,j) := \begin{cases} 1 & \text{if } \ j = 6912a_1 + 576a_2 + 288b_1 + 24b_2 + 12c_1 + c_2 + 13824, \\ 1 & \quad j = 6912a_1 + 576a_2 + 288b_1 + 24b_2 + 12c_1 + c_2 + 13824 \cdot 2 \text{ and} \\ & \quad i = 0, \\ 0 & \text{otherwise.} \end{cases}$$

$$A_{x_2 = y_2}(i,j) := \begin{cases} 1 & \text{if } j = 6912a_1 + 576a_2 + 288b_1 + 24b_2 + 12c_1 + c_2 + 13824, \\ & \quad i = 144a_2 + 12b_2 + c_2, \\ -1 & \text{if } j = 6912a_1 + 576a_2 + 288b_1 + 24b_2 + 12c_1 + c_2 + 13824 \cdot 2, \\ & \quad i = 144a_2 + 12b_2 + c_2, \\ 0 & \text{otherwise.} \end{cases}$$

$$A^a_{up}(i,j) := \begin{cases} -q^{(a)}_{\text{up}} & \text{if } j = 1152a_2 + 96b_2 + 8c_2 + 4 \times 0 + 2t_b + t_c, \quad i = 4a_2 + 2t_b + t_c; \\ 1 - q^{(a)}_{\text{up}} & \text{if } j = 1152a_2 + 96b_2 + 8c_2 + 4 \times 1 + 2t_b + t_c, \quad i = 4a_2 + 2t_b + t_c; \\ 0 & \text{otherwise.} \end{cases}$$

$$A^a_{down}(i,j) := \begin{cases} q^{(a)}_{\text{down}} & \text{if } j = 1152a_2 + 96b_2 + 8c_2 + 4 \times 0 + 2tb + tc, \quad i = 4a_2 + 2t_b + t_c; \\ -(1 - q^{(a)}_{\text{down}}) & \text{if } j = 1152a_2 + 96b_2 + 8c_2 + 4 \times 1 + 2tb + tc, \quad i = 4a_2 + 2t_b + t_c; \\ 0 & \text{otherwise.} \end{cases}$$

$$A^b_{up}(i,j) := \begin{cases} -q^{(b)}_{\text{up}} & \text{if } j = 1152a_2 + 96b_2 + 8c_2 + 4t_a + 2\times 0 + tc, \quad i = 4b_2 + 2t_a + t_c; \\ 1 - q^{(b)}_{\text{up}} & \text{if } j = 1152a_2 + 96b_2 + 8c_2 + 4t_a + 2\times 1 + t_c, \quad i = 4b_2 + 2t_a + t_c; \\ 0 & \text{otherwise.} \end{cases}$$

$$A^b_{down}(i,j) := \begin{cases} q^{(b)}_{\text{down}} & \text{if } j = 1152a_2 + 96b_2 + 8c_2 + 4t_a + 2\times 0 + tc, \quad i = 4b_2 + 2t_a + t_c; \\ -(1 - q^{(b)}_{\text{down}}) & \text{if } j = 1152a_2 + 96b_2 + 8c_2 + 4t_a + 2\times 1 + tc, \quad i = 4b_2 + 2t_a + t_c; \\ 0 & \text{otherwise.} \end{cases}$$

$$A^c_{up}(i,j) := \begin{cases} -q^{(c)}_{\text{up}} & \text{if } j = 1152a_2 + 96b_2 + 8c_2 + 4t_a + 2t_b + 0, \quad i = 4b_2 + 2t_a + t_b; \\ 1 - q^{(c)}_{\text{up}} & \text{if } j = 1152a_2 + 96b_2 + 8c_2 + 4t_a + 2t_b + 1, \quad i = 4b_2 + 2t_a + t_b; \\ 0 & \text{otherwise.} \end{cases}$$

$$A^c_{down}(i,j) := \begin{cases} q^{(c)}_{\text{down}} & \text{if } j = 1152a_2 + 96b_2 + 8c_2 + 4t_a + 2t_b + 0, \quad i = 4b_2 + 2t_a + t_b; \\ -(1 - q^{(c)}_{\text{down}}) & \text{if } j = 1152a_2 + 96b_2 + 8c_2 + 4t_a + 2t_b + 1, \quad i = 4b_2 + 2t_a + t_b; \\ 0 & \text{otherwise.} \end{cases}$$

$q^{(a)}_{\text{up}}$, $q^{(b)}_{\text{up}}$, $q^{(c)}_{\text{up}}$, $q^{(a)}_{\text{down}}$, $q^{(b)}_{\text{down}}$ and $q^{(c)}_{\text{down}}$ are calculated using equations (2.42) and (2.50). Lastly we define $b_{p\to\tilde{p}}(i)$.

$$b_{p\to\tilde{p}}(i) = p(a_1, a_2, b_1, b_2, c_1, c_2), \quad \text{where} \quad i = 6912a_1 + 576a_2 + 288b_1 + 24b_2 + 12c_1 + c_2.$$

6.3 Code and Data Availability

A reference implementation for setting up and solving the linear program is available at GitHub Repository: Master's Thesis LP Code. All necessary data can be reproduced using the information provided in this thesis, together with the accompanying code.

List of Figures

Bibliography

[1] Bell, J. S. On the einstein podolsky rosen paradox **1**. URL `https://cds.cern.ch/record/111654/files/vol1p195-200_001.pdf`.

[2] Einstein, A., Podolsky, B. & Rosen, N. Can quantum-mechanical description of physical reality be considered complete? **47**, 777–780. URL `https://link.aps.org/doi/10.1103/PhysRev.47.777`.

[3] Tavakoli, A., Pozas-Kerstjens, A., Luo, M.-X. & Renou, M.-O. Bell nonlocality in networks **85**, 056001. URL `https://iopscience.iop.org/article/10.1088/1361-6633/ac41bb`.

[4] Pironio, S. All CHSH polytopes **47**, 424020. URL `http://arxiv.org/abs/1402.6914`.

[5] Clauser, J. F., Horne, M. A., Shimony, A. & Holt, R. A. Proposed experiment to test local hidden-variable theories **23**, 880–884. URL `https://link.aps.org/doi/10.1103/PhysRevLett.23.880`.

[6] Branciard, C., Gisin, N. & Pironio, S. Characterizing the nonlocal correlations of particles that never interacted **104**, 170401. URL `http://arxiv.org/abs/0911.1314`.

[7] Fritz, T. Beyond bell's theorem: Correlation scenarios **14**, 103001. URL `https://iopscience.iop.org/article/10.1088/1367-2630/14/10/103001/pdf`.

[8] Renou, M.-O. *et al.* Genuine quantum nonlocality in the triangle network **123**, 140401. URL `https://doi.org/10.1103/PhysRevLett.123.140401`.

[9] Pozas-Kerstjens, A., Gisin, N. & Renou, M.-O. Proofs of network quantum nonlocality in continuous families of distributions **130**, 090201. URL `https://doi.org/10.1103/PhysRevLett.130.090201`.

[10] Wolfe, E., Spekkens, R. W. & Fritz, T. The inflation technique for causal inference with latent variables **7**, 20170020. URL `https://www.degruyterbrill.com/document/doi/10.1515/jci-2017-0020/html`.

[11] Renou, M.-O. & Beigi, S. Network nonlocality via rigidity of token-counting and color-matching **105**, 022408. URL `https://doi.org/10.1103/PhysRevA.105.022408`.

[12] Kriváchy, T. *et al.* A neural network oracle for quantum nonlocality problems in networks **6**, 70. URL `https://www.nature.com/articles/s41534-020-00305-x`.

[13] Abiuso, P. *et al.* Single-photon nonlocality in quantum networks **4**, L012041. URL https://link.aps.org/doi/10.1103/PhysRevResearch.4.L012041.

[14] Boreiri, S., Ulu, B., Brunner, N. & Sekatski, P. Noise-robust proofs of quantum network nonlocality. URL http://arxiv.org/abs/2311.02182.

[15] Wang, N.-N. *et al.* Experimental genuine quantum nonlocality in the triangle network. URL http://arxiv.org/abs/2401.15428.

[16] Gisin, N. Entanglement 25 years after quantum teleportation: testing joint measurements in quantum networks **21**, 325. URL https://doi.org/10.3390/e21030325.

[17] KrivácHy, T. & Kerschbaumer, M. Closing the detection loophole in the triangle network with high-dimensional photonic states. URL http://arxiv.org/abs/2503.24213.

[18] Bibak, F., Santo, F. D. & Dakić, B. Quantum coherence in networks **133**, 230201. URL http://arxiv.org/abs/2407.11122.

[19] Rosset, D., Gisin, N. & Wolfe, E. Universal bound on the cardinality of local hidden variables in networks **18**. URL http://arxiv.org/abs/1709.00707.

[20] Lita, A. E., Miller, A. J. & Nam, S. W. Counting near-infrared single-photons with 95% efficiency **16**, 3032. URL https://opg.optica.org/oe/abstract.cfm?uri=oe-16-5-3032.

[21] Natarajan, C. M., Tanner, M. G. & Hadfield, R. H. Superconducting nanowire single-photon detectors: physics and applications **25**, 063001. URL https://iopscience.iop.org/article/10.1088/0953-2048/25/6/063001.

[22] Fukuda, D. *et al.* Titanium-based transition-edge photon number resolving detector with 98% detection efficiency with index-matched small-gap fiber coupling **19**, 870. URL https://opg.optica.org/oe/abstract.cfm?uri=oe-19-2-870.

[23] Boreiri, S. *et al.* Towards a minimal example of quantum nonlocality without inputs **107**, 062413. URL https://doi.org/10.1103/PhysRevA.107.062413.

[24] Saunders, D. J., Bennet, A. J., Branciard, C. & Pryde, G. J. Experimental demonstration of non-bilocal quantum correlations **3**, e1602743. URL https://www.science.org/doi/epdf/10.1126/sciadv.1602743.

[25] Carvacho, G. *et al.* Experimental violation of local causality in a quantum network **8**, 14775. URL https://www.nature.com/articles/ncomms14775.

[26] Sun, Q.-C. *et al.* Experimental demonstration of nonbilocality with truly independent sources and strict locality constraints **13**, 687–691. URL https://www.nature.com/articles/s41566-019-0502-7.

[27] Poderini, D. *et al.* Experimental violation of n-locality in a star quantum network **11**, 2467. URL `https://www.nature.com/articles/s41467-020-16189-6`.

[28] Zhang, C. *et al.* Experimental observation of quantum nonlocality in general networks with different topologies **1**, 22–26. URL `https://linkinghub.elsevier.com/retrieve/pii/S2667325820300029`.

[29] Suprano, A. *et al.* Experimental genuine tripartite nonlocality in a quantum triangle network. URL `https://doi.org/10.1103/PRXQuantum.3.030342`.

[30] Polino, E. *et al.* Experimental nonclassicality in a causal network without assuming freedom of choice **14**, 909. URL `https://www.nature.com/articles/s41467-023-36428-w`.

[31] Boreiri, S., Brunner, N. & Sekatski, P. Bell nonlocality in quantum networks with unreliable sources: Loophole-free postelection via self-testing. URL `http://arxiv.org/abs/2501.14027`.

[32] Gao, X., Zhang, Y., D'Errico, A., Heshami, K. & Karimi, E. High-speed imaging of spatiotemporal correlations in hong-ou-mandel interference **30**, 19456–19464. URL `https://doi.org/10.1364/OE.456433`.

[33] Ferreri, A., Ansari, V., Brecht, B., Silberhorn, C. & Sharapova, P. R. Spatial entanglement and state engineering via four-photon hong-ou-mandel interference **5**, 045020. URL `https://iopscience.iop.org/article/10.1088/2058-9565/abb411`.

[34] Devaux, F., Mosset, A., Moreau, P.-A. & Lantz, E. Imaging spatiotemporal hong-ou-mandel interference of biphoton states of extremely high schmidt number **10**, 031031. URL `https://link.aps.org/doi/10.1103/PhysRevX.10.031031`.

[35] Ferreri, A., Ansari, V., Silberhorn, C. & Sharapova, P. R. The multimode four-photon hong-ou-mandel interference **100**, 053829. URL `https://doi.org/10.1103/PhysRevA.100.053829`.

[36] Weilenmann, M., Budroni, C. & Navascues, M. Memory attacks in network nonlocality and self-testing. URL `http://arxiv.org/abs/2402.12318`.